

*** 83-30166**

NASA Contractor Report 166101

(NASA-CR-166101) DEVELOPMENT OF ROTORCRAFT
INTERIOR NOISE CONTROL CONCEPTS. Phase 1:
DEFINITION STUDY (Sikorsky Aircraft,
Stratford, Conn.) 211 p HC A10/MP A01

N83-30166

Unclass
28213

CSCC 20A G3/71

**Development of Rotorcraft Interior
Noise Control Concepts**

Phase 1: Definition Study

C.A. Yoerkie

UNITED TECHNOLOGIES CORPORATION
Sikorsky Aircraft Division
Stratford, CT 06601

J.A. Moore

J.E. Manning

CAMBRIDGE COLLABORATIVE, INC.
Cambridge, MA 02142

Contract NAS1-16932
May 1983



National Aeronautics and
Space Administration

Langley Research Center
Hampton, Virginia 23665

Figures 3, 4, 6, 7, 8A, 8B, 9A, 9B, 10, 11 and 12 were originally prepared by Mr. Joseph I. Smullin. They are included in the report to illustrate the approach used for noise control on the Agusta A-109 helicopter.

The material on pages 32-41 is an edited version of material prepared by Joseph I. Smullin for J & A Enterprises, Inc., under purchase order from Cambridge Collaborative, Inc.

Mr. Smullin can be reached at J & A Enterprises, Inc., 22 Woodbine Avenue, Swampscott, Massachusetts 01907.

Inside
front cover

NASA Contractor Report 166101

**Development of Rotorcraft Interior
Noise Control Concepts**

Phase 1: Definition Study

C.A. Yoerkie

**UNITED TECHNOLOGIES CORPORATION
Sikorsky Aircraft Division
Stratford, CT 06601**

J.A. Moore

J.E. Manning

**CAMBRIDGE COLLABORATIVE, INC.
Cambridge, MA 02142**

**Contract NAS1-16932
May 1983**

NASA

**National Aeronautics and
Space Administration**

**Langley Research Center
Hampton Virginia 23665**

1. Report No. NASA CR-166101		2. Government Accession No.		3. Recipient's Catalog No.	
4. Title and Subtitle Development of Rotorcraft Interior Noise Control Concepts, Phase I: Definition Study				5. Report Date May 1983	
				6. Performing Organization Code 78286	
7. Author(s) C.A. Yoerker, J.A. Moore and J.E. Manning				8. Performing Organization Report No. SER-510126	
9. Performing Organization Name and Address Sikorsky Aircraft Division United Technologies Corporation Stratford, Ct. 06601				10. Work Unit No.	
				11. Contract or Grant No. NAS1-16932	
12. Sponsoring Agency Name and Address National Aeronautics and Space Administration Langley Research Center Hampton, VA 23665				13. Type of Report and Period Covered Contractor Report	
				14. Sponsoring Agency Code	
15. Supplementary Notes Langley Technical Monitor: William H. Mayes					
16. Abstract A review of information relevant to rotorcraft interior noise was performed with emphasis on the dominant acoustic and vibration noise sources and the transmission paths responsible for noise in the passenger compartment (cabin). A rank ordering of these noise sources established the main rotor gearbox as the primary contributor to cabin noise levels. In addition, current noise control methods were found inadequate for development of general noise control concepts. The major portion of this Phase I effort involved the development of a detailed analytic modeling approach with capabilities for evaluating a variety of noise control concepts (exclusive of source modification). This required a model containing details of the energy transfer from various sources, via a multitude of paths, to the cabin acoustic space. Since the number of structural and acoustic resonances in the frequency range of interest is large, a statistical approach (Statistical Energy Analysis - or SEA as it is commonly called) was applied. Included in the model are many airframe parameters, such as coupling and damping loss factors and source attachment point impedances. A comprehensive measurement program was devised to validate the entire model during the Phase II effort. Ground test measurements will be used to evaluate the airframe parameters and energy path transfer functions. Flight test measurements will determine source levels for input to the model.					
17. Key Words (Suggested by Author(s)) Helicopter Cabin Noise Statistical Energy Analysis Modeling Structureborne Noise Helicopters, Acoustics, Vibration			18. Distribution Statement Unclassified - Unlimited		
19. Security Classif. (of this report) Unclassified		20. Security Classif. (of this page) Unclassified		21. No. of Pages 210	22. Price

TABLE OF CONTENTS

	<u>PAGE</u>
SUMMARY	1
INTRODUCTION	2
DESCRIPTION OF HELICOPTER NOISE	5
Commercial Helicopters in General	5
Noise Sources for Two Specific Helicopters	5
Detailed case study of Augusta A-109 Noise Sources.	6
Noise source identification	11
Noise transmission paths	14
Rank order for sources	20
Source identification for Sikorsky S-76	24
DIAGNOSTIC TECHNIQUES FOR SOURCE AND PATH IDENTIFICATION	30
Review of Existing Case Studies	30
Experimental Techniques	32
General approach	33
Engineering methods for source identification	34
Contribution of source/path combinations to the cabin noise environment	35
Acoustic excitation	36
Vibration excitation	37
Signal Processing Techniques	39
Source identification	40
Transmission path identification.	41
INTERIOR NOISE PREDICTION MODEL.	43
Sources of Cabin Noise	43
Acoustic/aerodynamic sources	43
Vibration sources	49
Statistical Energy Analysis (SEA) Model of Vibration and Acoustic Transmission in Helicopter Airframes.	53
Introduction to SEA	56
The SEA matrix equation	61
SEA parameters	63
Mode count for acoustical and structural subsystems	63
Damping loss factor	69
Coupling loss factor	72
Power input evaluation	76
System response evaluation	84
SEA Model of the Sikorsky S-76	87
Description of the S-76 airframe	88

TABLE OF CONTENTS (Cont'd)

	<u>PAGE</u>
Selection of SEA subsystems for the S-76 model	90
Evaluation of SEA parameters for the S-76 model	100
Mode density for the S-76	100
Damping loss factor for the S-76	108
Coupling loss factors for the S-76	111
Frame junction coupling loss factor evaluation for the S-76	113
Frame-panel coupling loss factor evaluation for the S-76	113
Panel-acoustic space coupling loss factor evaluation for the S-76	116
Direct coupling between acoustic spaces for the S-76	118
Input power evaluation for the S-76 model	121
The SEA matrix equation for the S-76 model	121
 MEASUREMENT PROGRAM FOR MODEL VALIDATION	 122
Objectives	122
Ground Test Measurement Program	124
Vibration level distribution measurements	125
Vibration source coherence measurements	125
Acoustic level distribution measurements	125
SEA parameter estimation measurements	125
Attachment point impedances	126
Damping loss factors	126
Coupling loss factors	128
Preliminary Airframe Vibration Transmission Measurements	133
Flight Test Measurement Program	145
Statement of Work for Ground and Flight Test Measurements	152
Task 1.0 ground test measurements	152
Task 2.0 flight test measurements	153
Model Comparisons and Refinements	153
 SUMMARY AND CONCLUDING REMARKS	 154
 APPENDIXES	
 A - Details of Source/Path Identification Techniques	 156
Path identification by temporal discrimination	156
Temporal discrimination: correlation analysis	156
Temporal discrimination: the frequency domain	159
Path identification for dispersive systems	164
Cross-correlation analysis for a dispersive system	164
Cepstral analysis	167

TABLE OF CONTENTS (Cont'd)

APPENDIXES (Cont'd)	<u>PAGE</u>
B - Frame Junction Transmission Model	173
Frame junction geometry	173
Transmission coefficient description of junction dynamics	175
Junction impedance matrix	176
Incident and transmitted power	177
Sample evaluation of transmission coefficient	179
S-76 frame junction vibration transmission characteristics	186
C - Acoustic Intensity Method	193
REFERENCES	199

LIST OF FIGURES

<u>Figure No.</u>		<u>Page</u>
1	Internal Noise Sources and Paths . . .	4
2	Sikorsky S-76 Structural Cutaway . . .	7
3	Agusta A-109 Gearbox Installation . .	8
4	Flow Chart of A-109 Interior Noise Reduction Program	9
5	A-109 Interior Noise Levels at 72 m/s - Stripped vs. "Silent" Treatment	10
6	Narrow Bandwidth (6.2 Hz) Spectrum of A-109A Cabin Noise Stripped Interior - Speed 72 m/s	12
7	SPL vs Speed - Center of A-109 Cabin Stripped Interior	13
8A	Relative Panel Contribution to A-109 Cabin SPL - 72 m/s, Stripped Interior (Area Weighted Panel Vibration)	15
8B	Relative Panel Contribution to A-109 Cabin SPL - 72 m/s, Stripped Interior (Area Weighted Panel Vibration)	16
9A	Reduction of Sound Radiated from Major Surfaces Required to Achieve Target Noise Level for "Silent" Interior (83 dBA Based on .5, 1, 2 kHz) (Noise Reductions are Referenced to Stripped Interior) . . .	18
9B	Reduction of Sound Radiated from Major Surfaces Required to Achieve Target Noise Level for "Silent" Interior (83 dBA Based on .5, 1, 2 kHz) (Noise Reductions are Referenced to Stripped Interior) . . .	19

LIST OF FIGURES (Cont'd)

<u>Figure No.</u>		<u>Page</u>
10	Noise Source Contributions to Cabin SPL at Rear Passenger Location	21
11	A-109 Gearbox Struts	22
12	Contribution of Gearbox Mounts to Vibration of the Cabin Overhead Panel	23
13	S-76 Bare Cabin SPL-75 m/s LFO 100% N_R	26
14	S-76 Treated Cabin SPL vs Location . .	27
15A	S-76 Acceleration - Center Copilot Windshield 75 m/s LFO	28
15B	S-76 SPL - .03m Away from Center of Copilot Windshield	28
16	Variation of S-76 Bare Cabin SPL for Three Aircraft - Rear Center Seat, 75 m/s LFO	29
17	Frequency Spectrum of Wall-Pressure Fluctuations	48
18	A Typical SEA Model	57
19	Block Diagram for SEA System Response Evaluation	89
20	S-76 Cabin Dimensions	91
21	Dynamic Behavior of Composite Honeycomb Panel	106
22	S-76 Plate and Skin Materials	109
23	Typical Crossed Frame Junction	112
24	Flow of Activities	123

LIST OF FIGURES (Cont'd)

<u>Figure No.</u>		<u>Page</u>
25	Typical Transfer and Coherence Function Measurement	136
26	Variation of Coherence Function Levels for Overhead Panels vs. RAL Excitation	137
27	Variation of Transfer Function Levels for Overhead Panels vs. FAR Excitation	138
28	Effect of Excitation Point on Panel Transfer Function	140
29	Effect of Excitation Point on Drip Pan Transfer Function	141
30	Effect of Excitation Point on Rear Bulkhead Transfer Function	142
31	Web Transfer Functions for RAL Excitation	143
32	Web Transfer Functions for FAR Excitation	144
33	Transfer Function at Frame Section 1 for RAL Excitation	146
34	Variation of Vertical Transfer Function Along the Main Longitudinal Frame for RAL Excitation	147
35	Variation of Vertical Transfer Function Along the Main Longitudinal Frame for FAR Excitation	148
36	Effect of Excitation Point on Window Post Center Transfer Function	149

LIST OF FIGURES (Cont'd)

<u>Figure No.</u>		<u>Page</u>
37	Cross Correlation in Multiple-Path System	158
38	Cross Correlation of Dispersive Waves	160
39	Normalized SCOT	163
40	Application of the Cepstrum Method in the Removal of Ground Reflection	172
41	Sketch of Frame Junction Showing Coordinate System	174
42	S-76 Frame Junction: Transmission Coefficients for Out-of-Plane Bending	189
43	S-76 Frame Junction: Coupling Loss Factors for Out-of-Plane Bending.	190
44	S-76 Frame Junction: Coupling Loss Factors for Torsional Motion	191
45	S-76 Frame Junction: Coupling Loss Factors for In-Plane Bending	192
46	Typical Intensity Probe Schematic	197
47	Typical Intensity Measurement Instrumentation	198

LIST OF TABLES

<u>Table No.</u>		<u>Page</u>
1	Structural Subsections for the S-76 SEA Model	96
2	Acoustical Subsections for the S-76 SEA Model	99
3	Summary of Parameter Requirements for Frame and Acoustical Sub- systems	101
4	Summary of Parameter Requirements for Single Layer Panel Subsystems. .	104
5	Blocked and Radiated Cases for Frame Junction Vibration Transmission	182
6	Blocked Force/Moment Expressions . .	183
7	Impedance Expressions for Torsional and Bending Motions	184
8	Dynamics Parameters for Torsion and Bending of Frame	185
9	Representative S-76 Frame Parameter Values	188

SUMMARY

This report covers work performed during Phase I of a four phase, aggressive analytic/development program whose goal is to reduce helicopter passenger noise exposure to the levels experienced in fixed-wing commercial jet aircraft. The following is a brief summary of the Phase I effort.

A review of information relevant to rotorcraft interior noise was performed with emphasis on the dominant acoustic and vibration noise sources and the transmission paths responsible for noise in the passenger compartment (cabin). A rank ordering of these noise sources established the main rotor gearbox as the primary contributor to cabin noise levels. In addition, current noise control methods were found inadequate for development of general noise control concepts.

The major portion of this Phase I effort involved the development of a detailed analytic modeling approach with capabilities for evaluating a variety of noise control concepts (exclusive of source modification). This required a model containing details of the energy transfer from various sources, via a multitude of paths, to the cabin acoustic space. Since the number of structural and acoustic resonances in the frequency range of interest is large, a statistical approach (Statistical Energy Analysis - or SEA as it is commonly called) was applied. Included in the model are many airframe parameters, such as coupling and damping loss factors and source attachment point impedances.

A comprehensive measurement program was devised to validate the entire model during the Phase II effort. Ground test measurements will be used to evaluate the airframe parameters and energy path transfer functions. Flight test measurements will determine source levels for input to the model.

ORIGINAL PAGE IS
OF POOR QUALITY

INTRODUCTION

The control of interior noise is a continuing problem in aircraft, particularly rotary-wing aircraft. The interior noise levels in rotorcraft are higher than in fixed wing aircraft because the propulsion system components are in close proximity to the cabin and are rigidly connected to the airframe. The higher noise levels cause speech interference and increased vocal output required for communication. The result is a decrease in passenger and crew comfort.

The primary noise sources in rotorcraft are the main rotor gearbox and hydraulic systems; while the engines, turbulent boundary layer, main rotor, tail rotor, and Environmental Control Units (ECU) are secondary sources. Figure 1 shows schematically these sources and the paths to the cabin acoustic space.

Within the gearbox, vibratory excitations are produced as part of the gear meshing process and these excitations result in vibration of the transmission housing and airframe which ultimately radiate noise inside the cabin. Hydraulic system noise exists in some aircraft such as the S-76, and is a function of pump selection and attachment of the hydraulic lines to the structure.

Boundary layer noise is of an aerodynamic origin and becomes apparent at high flight speeds. The boundary layer noise is primarily radiated into the cabin by the cockpit windshield and through the cabin windows. In other areas the aircraft skin has sufficient transmission loss to attenuate the boundary noise. Engine noise depends on the choice of the power plant and its location relative to the cabin. Casing radiated noise, inlet, and exhaust noise are mainly coupled to the cabin via airborne paths. ECU noise is generated by the air-cycle machine or blowers and is generally conducted to the cabin via ducts. Noise may also be generated by the grills at the point where the air is exhausted into the cabin.

For a goal of 60 to 65 dB SIL in the cabin, which is typical of that achieved in fixed wing commercial aircraft, each of the above sources must be subjected to noise control. Literature review has shown that many noise control measures for rotorcraft have been developed and applied; however, noise prediction techniques so far have been limited to empirical relationships that are valid only for the craft from which they were derived. The procedures developed for predicting noise levels inside the cabin cannot handle certain types of noise control measures such as vibration

isolation, structure-borne noise propagation in the airframe, and structural damping. In most instances (for example: Levine and DeFelice [1]) the complex problem of modeling structureborne noise paths is acknowledged, but these paths are then quickly replaced with a uniform intensity distribution over the dominant radiating surfaces. Thus limitations were placed on trade-off studies involving structural and source/path modifications. Advances in technology now allow for modeling of structureborne vibration in these complex helicopter airframe structures.

The main thrust of the present work task is the application of these advanced modeling techniques (SEA) to the reduction of cabin noise resulting from the dynamic coupling of the gearbox to the airframe and the interior cabin space. To achieve reduced cabin noise levels, refinement of existing noise control methods as well as improved predictive methods are required. Additionally, the approach to reducing the noise must be attacked on a systems basis since past experience has indicated that methods used to alleviate one noise source may enhance the noise from another source. Also, it is necessary that the methods be developed on a firm analytical basis to insure that developed noise control techniques will be beneficial to a wide range of rotorcraft designs and can be incorporated in the early stage of aircraft design for economic trade-off studies.

It is not the intent of the present effort to work the source noise reduction problem with respect to gear tooth profile design, etc., since other research efforts are underway in this area. Rather the intent is to focus on the vibratory/acoustic energy paths exterior to the gearbox or other sources through and into the cabin, to modify the paths of the cabin sidewall and to develop vibration isolation systems to reduce the cabin noise levels.

The objective of the present research is to develop and demonstrate minimum weight techniques of reducing the interior cabin noise levels of a rotorcraft with a goal of achieving the subjective equivalent noise levels of current subsonic jet transports. The emphasis of the present task is to develop vibration suppression and other noise control techniques to be applied on the paths of the gearbox/airframe/cabin space which are within the framework of the physical and operational constraints of a typical rotorcraft and its flight environment. Analyses of the noise control concepts shall be developed and validated by experimental tests in order to understand the basic physical mechanism involved and to apply the techniques to future systems.

ORIGINAL PAGE IS
OF POOR QUALITY

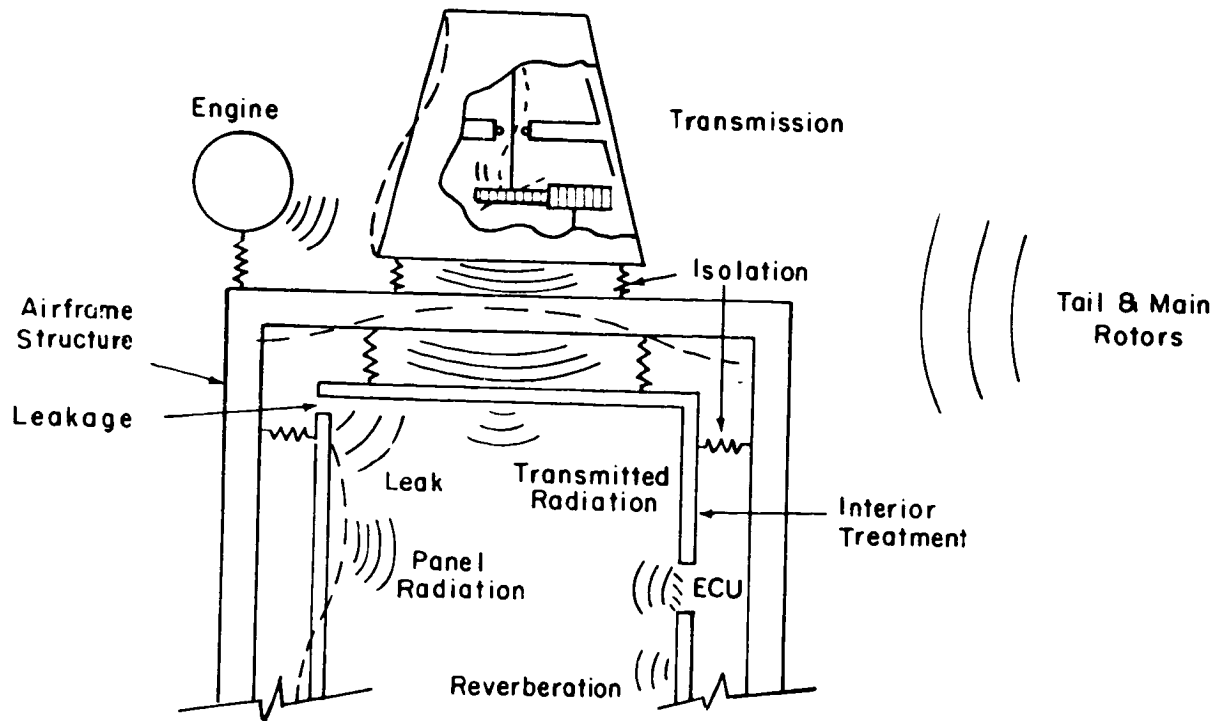


Figure 1. Internal Noise Sources and Paths

DESCRIPTION OF HELICOPTER NOISE

Commercial Helicopters in General

It is an accepted fact that both passengers and crew members in current commercial helicopters are exposed to high noise levels [2, 3, 4] relative to other forms of transportation. These high cabin noise levels are, in general, dominated by gearbox, hydraulics, and engine noise sources [3, 4, 5, 6, 7, 8]. This conclusion covered a broad range of gearbox types and mount configurations (pad, strut, strut and torque plate, etc.) and the major helicopter manufacturers (both national and international).

There are growing concerns amongst manufacturers, operators, and governments regarding the reduction and control of cabin noise. These concerns about high cabin noise levels are compromised by the economic realities of payload and component weight reductions. It has been shown that as gearbox weight is reduced, the total of gearbox and cabin soundproofing weight has increased [7]. Thus, the weight benefit achieved by higher horsepower density designs is often more than offset by the weight of added cabin treatment.

This points out the need for a more comprehensive study and an analytic model of the entire aircraft so that a variety of noise control measures can be evaluated. These evaluations would involve weight, noise reduction, cost, safety, and other trade-off considerations. This can only be accomplished if the model contains information on the sources, the multitude of structure-borne and airborne paths from each source to the cabin, and the cabin acoustic properties.

Noise Sources for Two Specific Helicopters

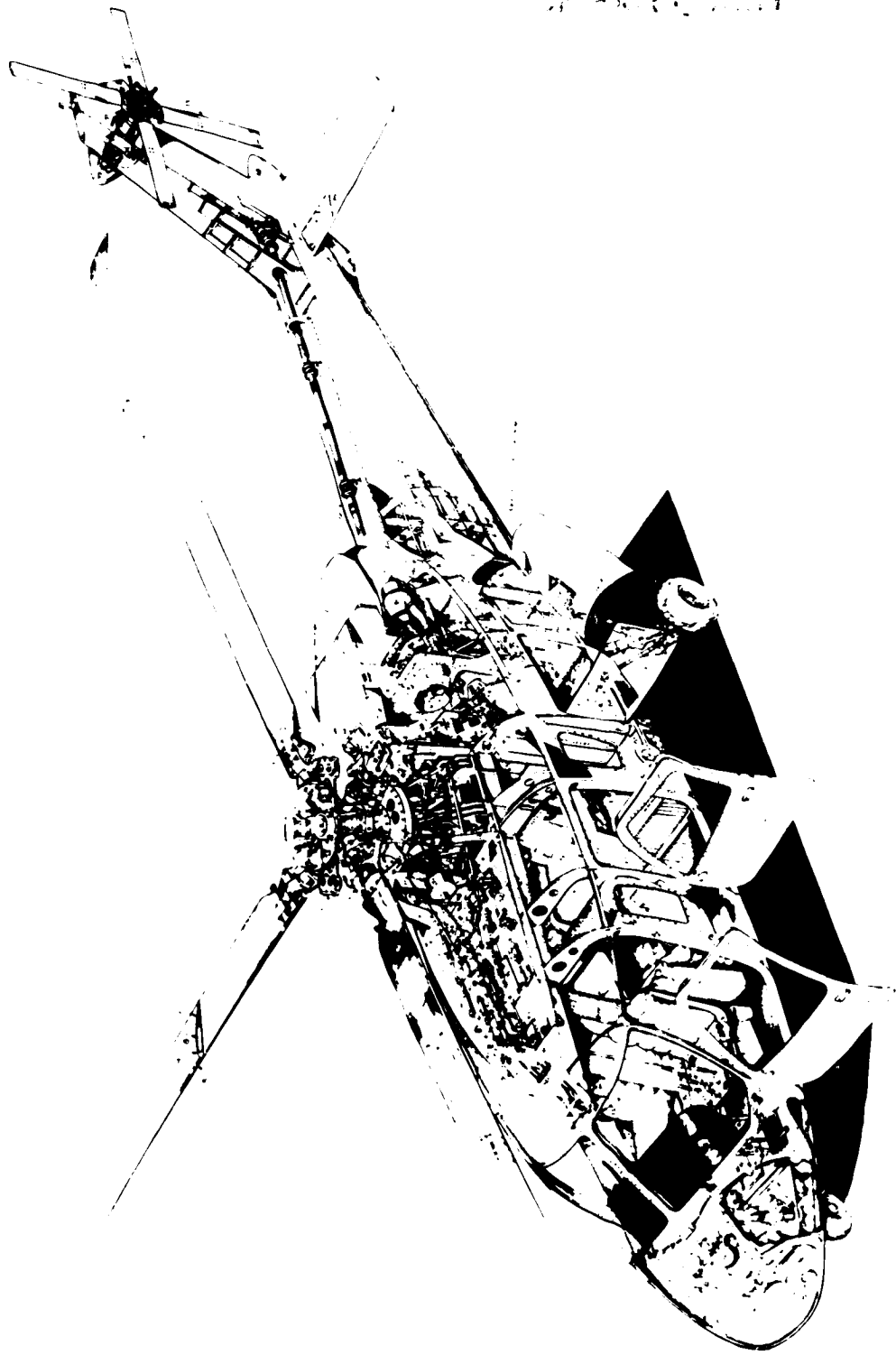
The major features of the S-76 and A-109 are shown in Figures 2 and 3. Both aircraft are similar in that the main gearbox (the dominant cabin noise source) is directly mounted to the frame; the S-76 by relatively short feet and the A-109 by a torque plate and struts. In each aircraft the frame structure, which is quite stiff relative to the skin panels, forms an efficient three-dimensional vibration transmission path. A major structural ceiling element extends from the gearbox mounts to the windshield, which is a substantial radiation surface for cockpit no

Detailed case study of Agusta A-109 noise sources. - The Agusta A-109 is designed to provide high performance rotary-wing aircraft for the business and commercial aviation market. The manufacturer recognized that some reduction in cabin noise was necessary to provide maximum customer acceptance. Therefore, the company embarked on a noise reduction R&D program in 1976. A flow chart for this program is shown in Figure 4. Figures and information for this section are based on data published in Reference [8]. The goal of the program was to reduce the cabin noise to a Speech Interference Level (PSIL_{0.5, 1, 2}) of 84 dB for a "Quiet" interior and 76 dB for a "Silent" interior. An A-weighted sound pressure level of 83 dBA was set as a target for the silent interior. For typical cabin noise spectra, achievement of the 83 dBA target also achieves the 76 dB PSIL goal.

The goals of the noise reduction program were substantially met without structural modifications. The resulting treatment is commonly referred to as a "carpet hanging" treatment and includes: (a) covering all non-window surfaces above the seat cushions with plastic trim or upholstery, (b) use of "double wall" construction for trim panels, (c) use of vibration isolation to prevent vibration transmission to the trim panels and air conditioning/heating ducts and additionally on the "Silent" interior, (d) use of a clear plastic divider between the pilot and passenger compartments, and (e) use of double windows in the passenger compartments. In addition to these basic carpet hanging treatments, it was necessary to improve door gasketing and use heavier door hinges, and to use air conditioning/heating unit silencers.

The weight of the overall "Silent" treatment is approximately 115 pounds. A one-third octave band spectrum for the cabin noise in the "Silent" interior is shown in Figure 5 and compared to levels on the stripped interior.

SIKORSKY S-76



0577000 00 02 19
02 00 00 00 00 00

Figure 2. Sikorsky S-76 Structural Cutaway

ORIGINAL PAGE IS
OF POOR QUALITY

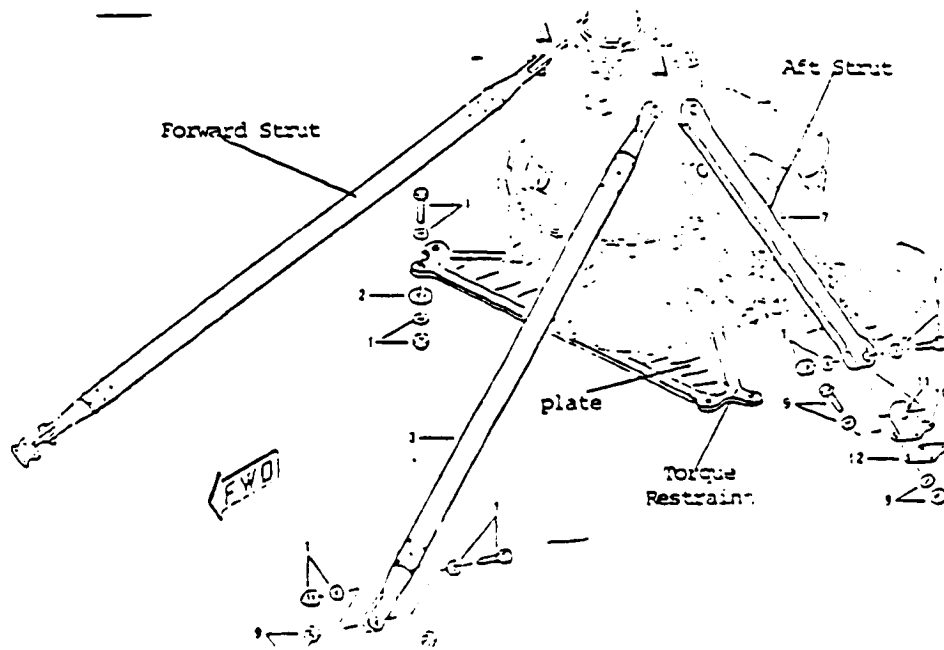
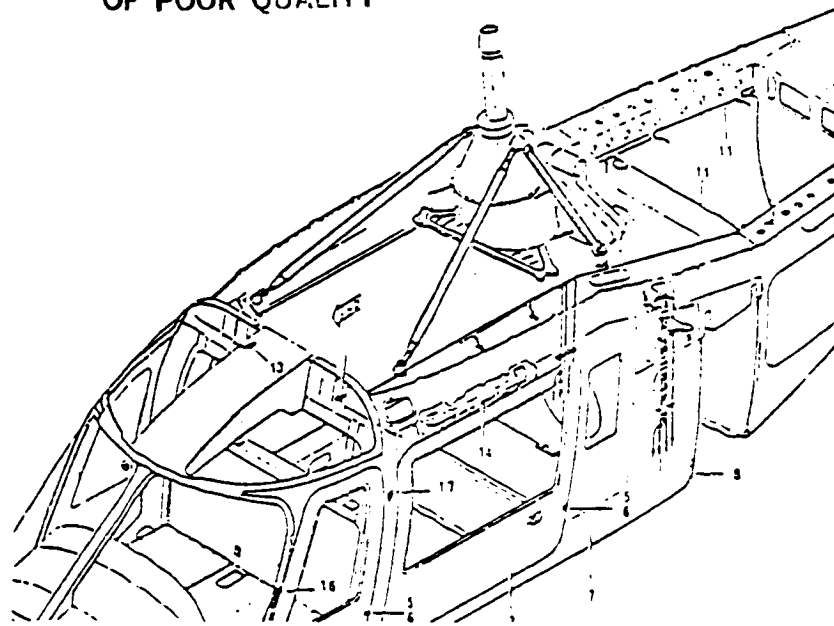


Figure 3. Agusta A-109 Gearbox Installation.

ORIGINAL TITLE OF POOR QUALITY

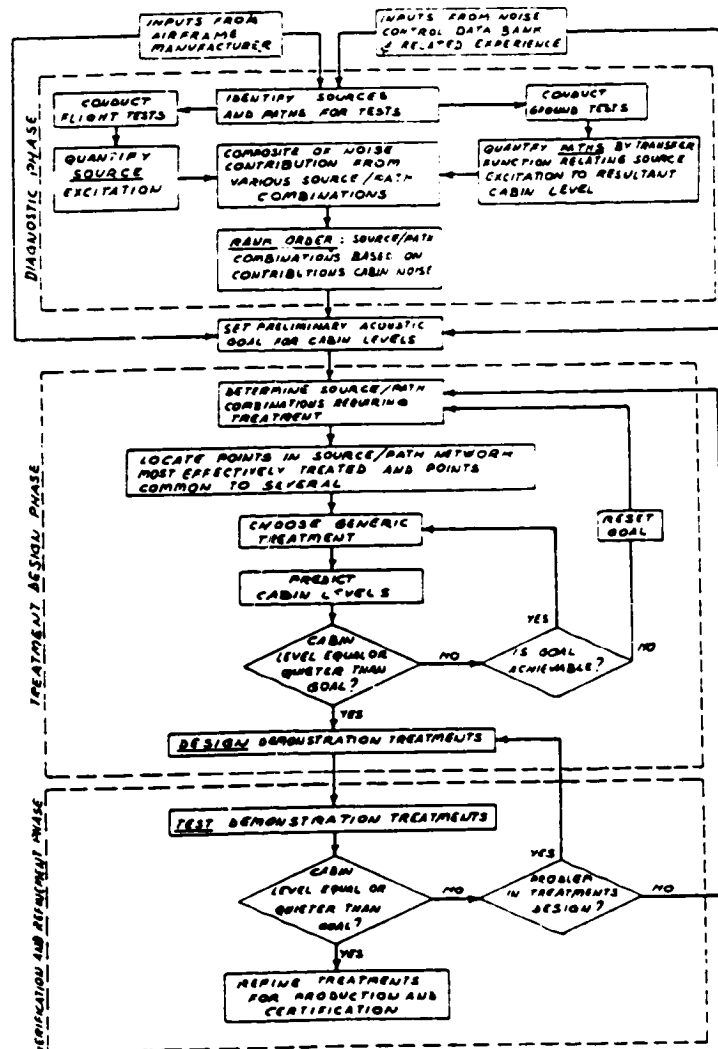


Figure 4. Flow Chart of A-109 Interior Noise Reduction Program

Figure from Reference 8

ORIGINAL PAGE IS
OF POOR QUALITY

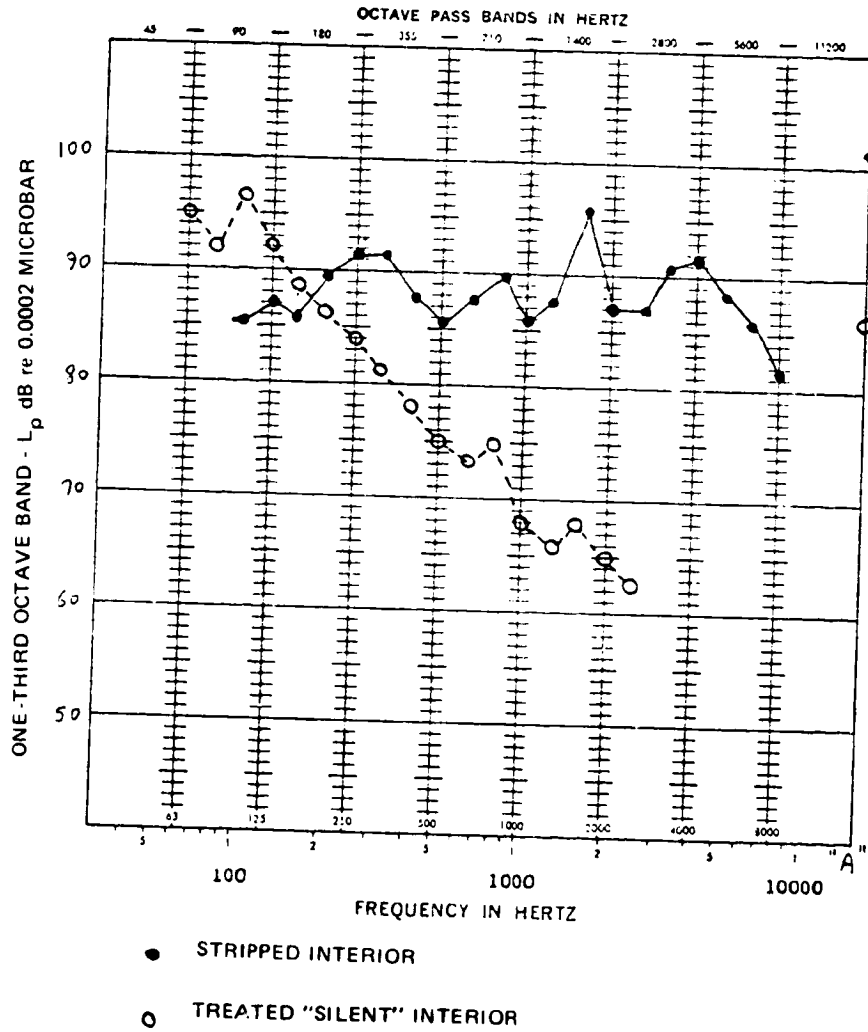


Figure 5. A-109 Interior Noise Levels at 72 m/s
Stripped vs. "Silent" Treatment

Figure from Reference 8

Noise source identification. - The first phase of the A-109 noise reduction program was to identify the noise sources and vibration/sound transmission paths. Toward this end, measurements of cabin noise were taken for a stripped interior [8].

A narrow band spectrum of the interior noise is shown in Figure 6. The correspondence of lines in the noise spectrum with fundamental and harmonic frequencies of the different rotating machinery serves to identify these components as major noise sources. The primary source is the main gearbox. Tail rotor noise is significant in the frequency range from 100 to 500 Hz but is not a major component of the A-weighted noise. The main rotor noise contributes to the spectrum below 100 Hz and it can be ignored as a source of A-weighted noise. Although the lines in the narrow band spectrum make the major contribution to the A-weighted cabin noise level, the broadband sources are also important. These sources are associated with the fluctuating pressures in the boundary layer, broadband components of rotor noise, and combustion noise in the turbines. It is difficult to separate the relative contributions of these broadband sources.

Measurements of cabin noise for different flight speeds are shown in Figure 7. Note that peaks in the one-third octave spectrum at 800, 1600, and 4000 Hz correspond to the lines in the narrow band spectrum and dominate the overall levels. Analysis of the narrow band spectra for the different speeds shows that the line components decrease with increasing flight speed while the broadband components increase with increasing flight speed. These counter-acting effects are not unexpected, but make a quantitative identification of the relative strength of the broadband sources impossible.

Intermittent sources were also identified for the A-109. The dominant source in this category was the compressor bleed-air for cabin heating.

ORIGINAL FIGURE
OF POOR QUALITY

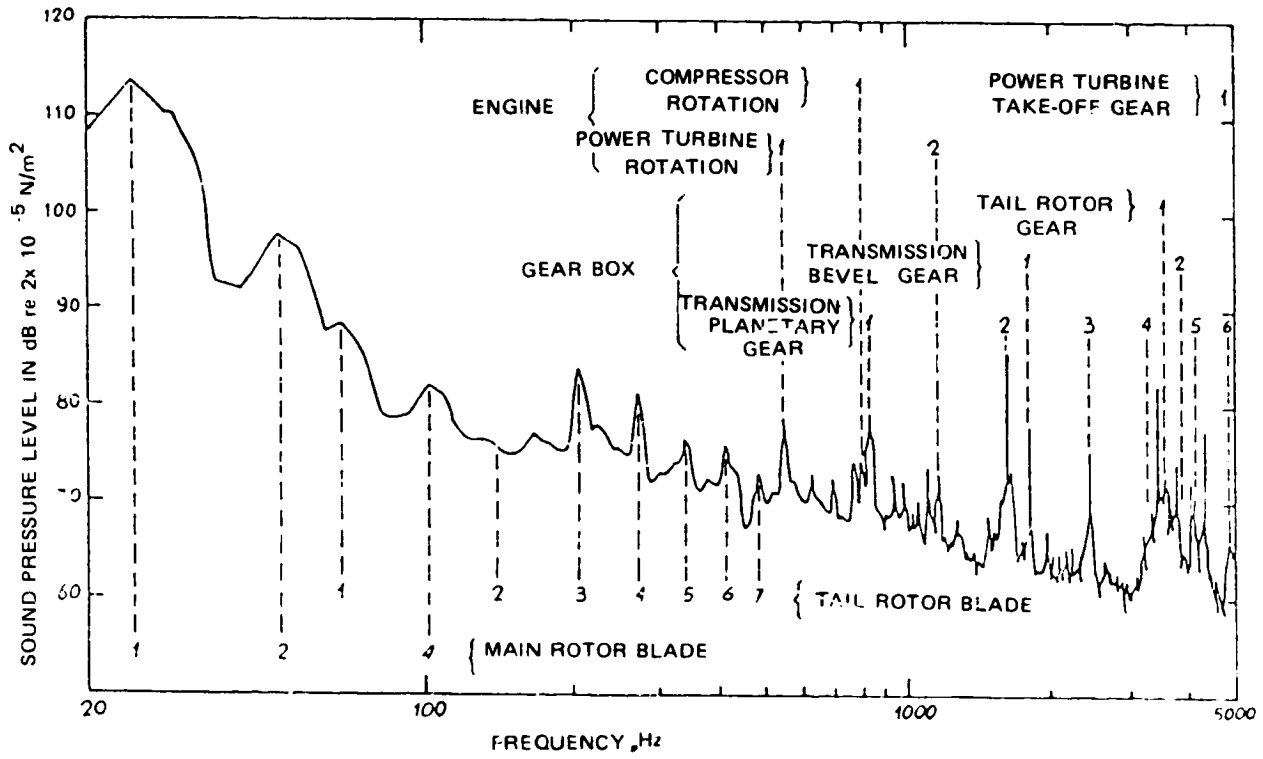


Figure 6. Narrow Bandwidth (6.2 Hz) Spectrum of A-109A Cabin Noise Stripped Interior - Speed 72 m/s

Figure from Reference 8

ORIGINAL QUALITY
OF PAPER QUALITY

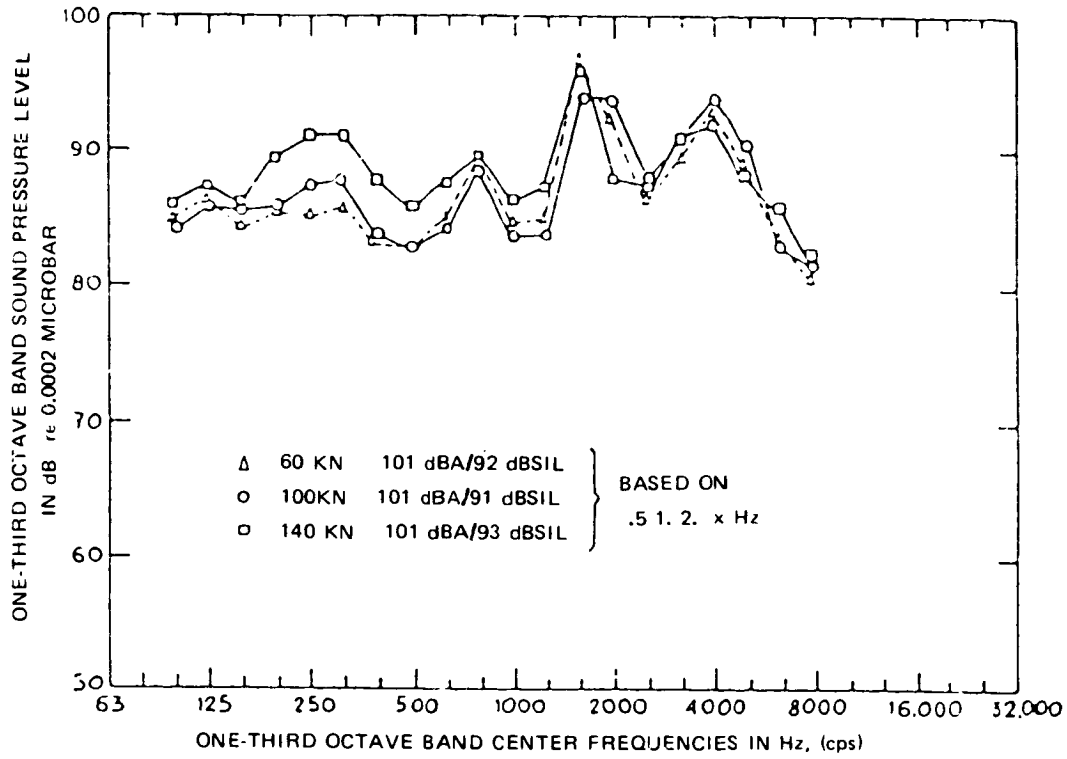


Figure 7. SPL vs Speed - Center of A-109 Cabin Stripped Interior

Figure from Reference 8

Noise transmission paths. - The correspondence of the lines in the narrow band spectrum with harmonics of the rotational frequencies serve to identify the sources of noise, but do not indicate the path by which the noise is transmitted to the cabin. The path identification for the A-109 was carried out in two steps. Since the objective of the noise reduction program was to reduce cabin noise by treatment of the radiating surfaces in the cabin, the first step was to obtain average vibration levels for each surface in order to identify their relative contribution to the cabin noise.

The time-average acoustic power radiated by a surface can be written as:

$$W_{\text{rad}} = (\rho_0 c_0) A \langle v^2 \rangle \sigma_{\text{rad}} \quad (1)$$

where W_{rad} is the radiated power, $\rho_0 c_0$ is the characteristic impedance of the cabin acoustic space, A is the surface area of the radiating surface, $\langle v^2 \rangle$ is the mean-square vibration averaged over the surface, and σ_{rad} is the radiation efficiency. If σ_{rad} is the same for all surfaces, then the area-weighted vibration level can be used to rank order the radiating surfaces.

Measured results are shown in Figures 8a and 8b for the stripped interior. The major sources are the aft bulkhead and the overhead panel. The windows are not a major source of noise in the stripped interior. However, they can become a major source when the other radiating surfaces are treated to reduce their noise radiation.

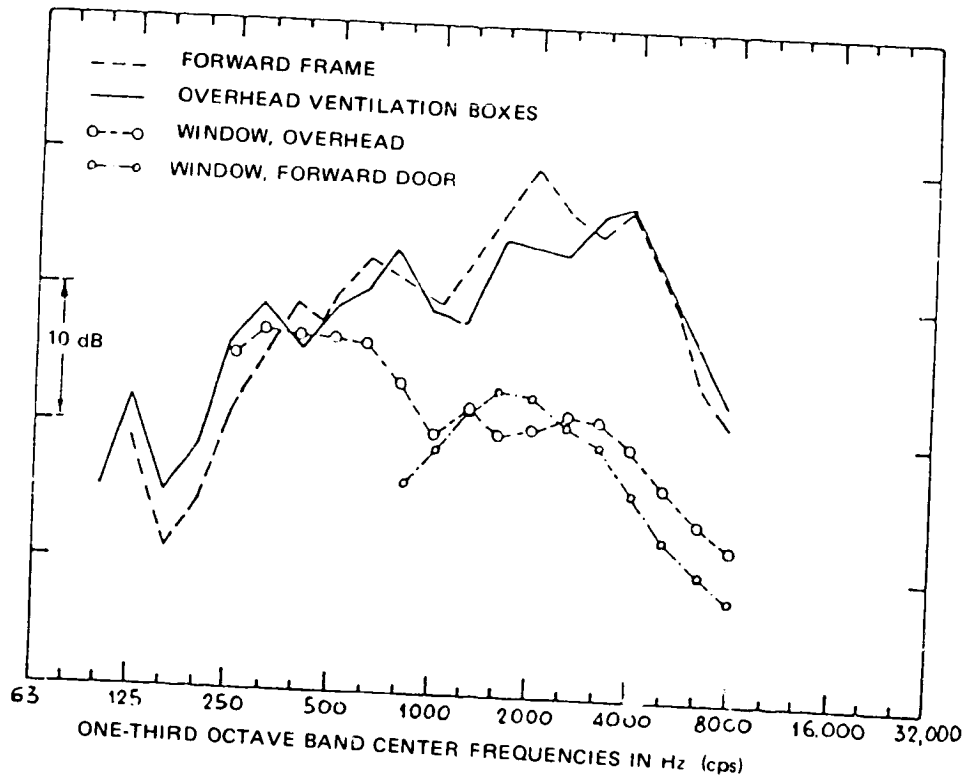


Figure 8A. Relative Panel Contribution to A-109 Cabin SPL - 72 m/s, Stripped Interior (Area Weighted Panel Vibration)

Figure from Reference 8

ORIGINAL PAGE
OF POOR QUALITY

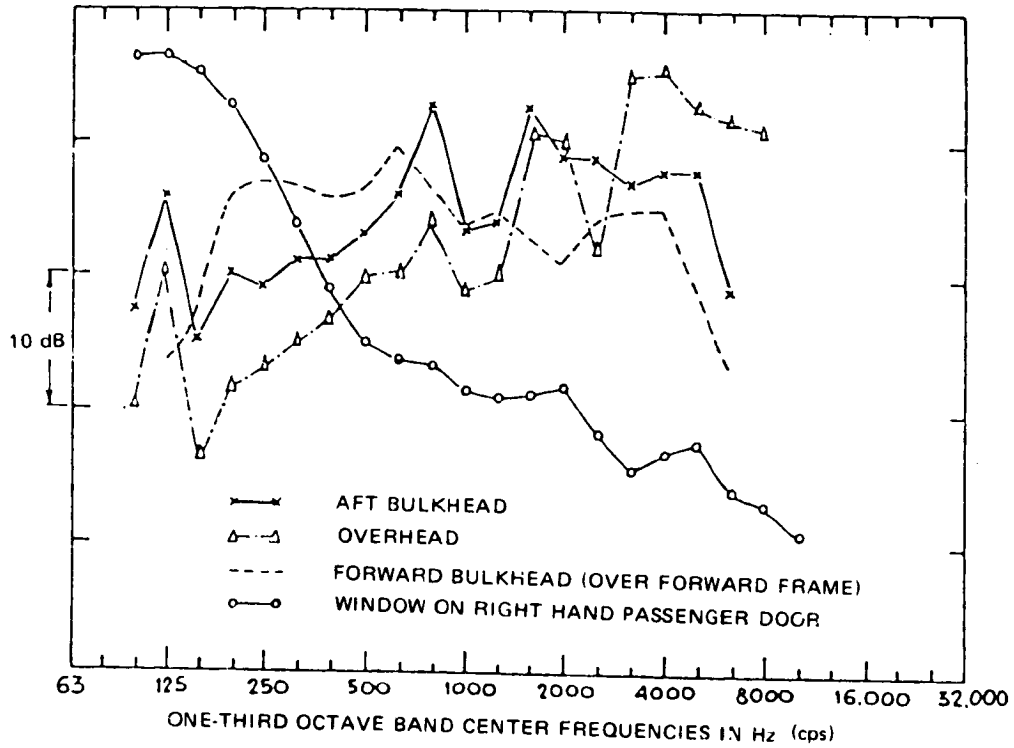


Figure 8B. Relative Panel Contribution to A-109 Cabin SPL - 72 m/s, Stripped Interior (Area Weighted Panel Vibration)

Figure from Reference 8

The measured contribution to the cabin noise by the various surfaces can be used to calculate the noise reduction needed to meet a given overall objective. This is done in Figures 9a and 9b. The procedure used was to assign a noise reduction target for each surface such that the contribution by each surface to the overall noise is equal. Note that the goal of 83 dBA requires that the noise radiated by the windows be reduced.

The second step in the path identification was to determine the contribution of various source/transmission path combinations to the cabin noise. A transfer function technique was used. In this technique measurements were carried out on the ground using artificial sources - loudspeakers and shakers. The artificial source is used to excite the structure at a point corresponding to an input location for one of the sources. The cabin noise is then measured and the ratio of rms noise to rms input vibration is obtained as a measured transfer function. For example, to measure the contribution by airborne gearbox noise, a loudspeaker is used to excite the acoustic space surrounding the gearbox and the acoustic level in the space is measured as the input to the transfer function. The resulting noise at several points in the cabin is measured as the output and a transfer function is determined as a function of frequency. To measure the contribution by structureborne noise from the gearbox, a shaker is used to excite the frame at a point where the gearbox attaches. The vibration level is measured at the attachment point as an input to the transfer function and the cabin acoustic level is measured as an output. The process can be repeated to determine transfer functions for each gearbox attachment point.

After the transfer functions have been determined in a ground test, measurements are made in flight to determine source levels. The rms source level is multiplied by the approximate transfer function to determine the contribution of the particular source/path combination being considered. The contribution from all sources and paths is summed incoherently (addition of mean-square sound pressures) to obtain the overall sound pressure level. This summed level can then be compared with the measured overall level to determine the adequacy of the transfer function analysis. If important source/path combinations are left out, the measured level will be significantly higher than the predicted level.

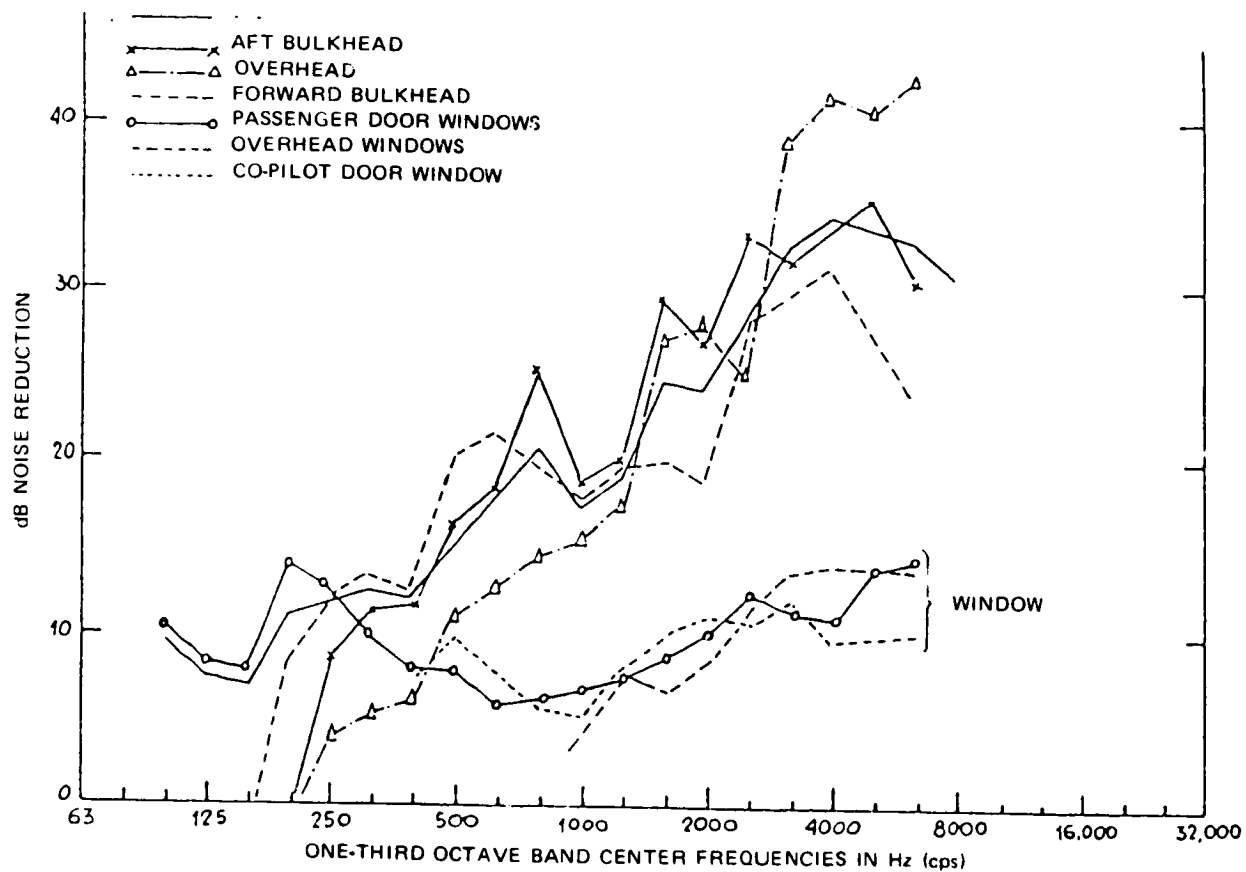


Figure 9A. Reduction of Sound Radiated from Major Surfaces Required to Achieve Target Noise Level for "Silent" Interior (83 dBA Based on .5, 1, 2 kHz) (Noise Reductions are Referenced to Stripped Interior)

Figure from Reference 8

ORIGINAL FIGURE
OF POOR QUALITY

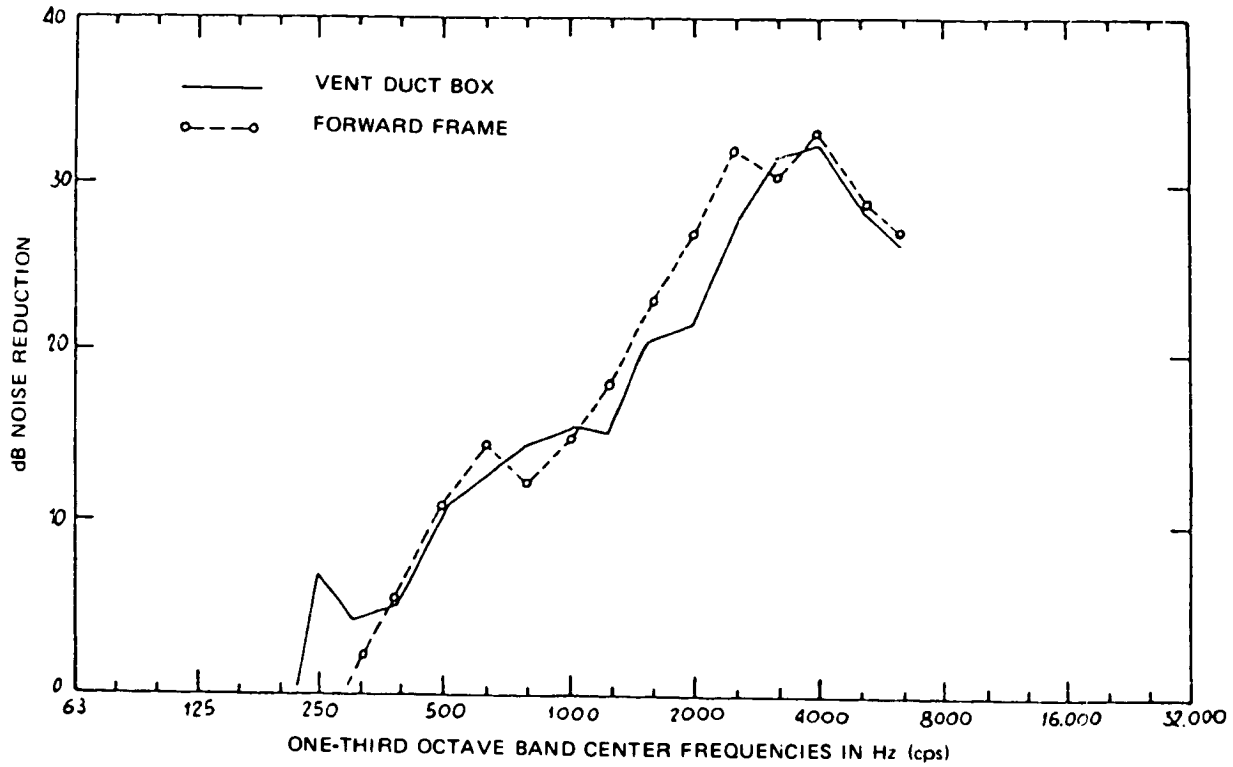


Figure 9B. Reduction of Sound Radiated from Major Surfaces Required to Achieve Target Noise Level for "Silent" Interior (83 dBA Based on .5, 1, 2 kHz) (Noise Reductions are Referenced to Stripped Interior)

Figure from Reference 8

For the two examples described above, gearbox airborne noise and gearbox structureborne noise source levels would be measured during flight with a microphone in the gearbox acoustic space and accelerometers at the gearbox attachment points.

Results of the source/path identification for the A-109 are shown in Figure 10. The dominant contribution to the A-weighted noise is from the gearbox structureborne noise. The gearbox airborne and engine structureborne are also seen to be important sources and paths.

The transfer function technique can also be used to study the relative contribution to the overhead panel vibration by the different gearbox supporting struts. Figures 3 and 11 show the gearbox and its supporting struts. Results from the transfer function analysis are shown in Figure 12. The rear strut is seen to be a less important path than the other struts.

Rank order for sources. - The major source of noise in the A-109 with a stripped interior is the gearbox. The dominant path by which noise is transmitted is structureborne from the gearbox through the forward mounting struts and torque restraints to the overhead panel and aft bulkhead.

The airborne engine noise is not of major importance except with regard to the bleed-air used for cabin heating. However, engine structureborne noise is an important secondary source.

The windows are not a major source of noise for the stripped interior. However, as the other radiating surfaces are treated, the windows can become an important source.

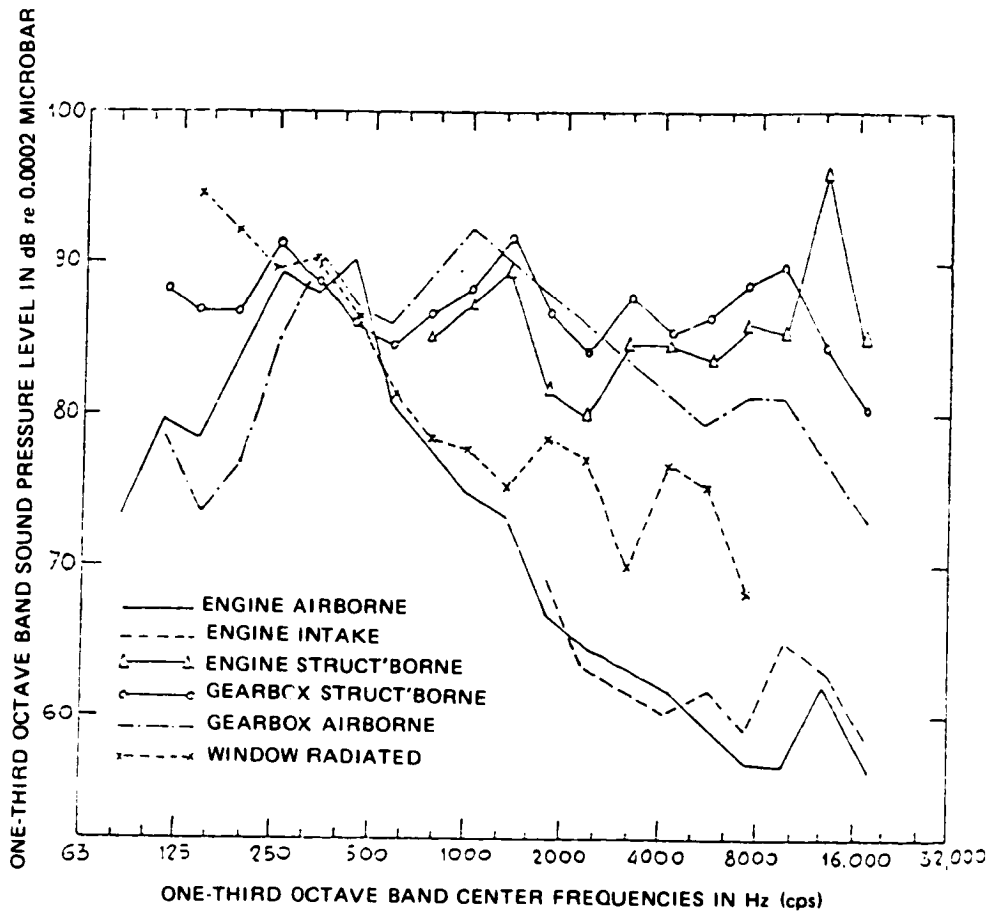


Figure 10 Noise Source Contributions to Cabin SPL at Rear Passenger Location

Figure from Reference 8

ORIGINAL PAGE IS
OF POOR QUALITY

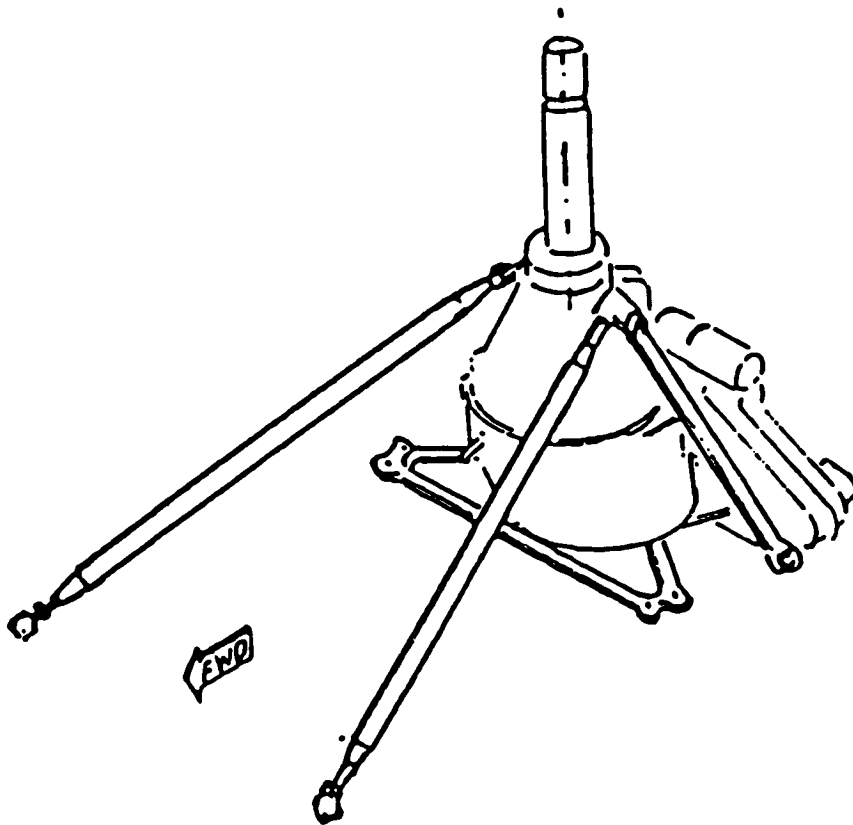


Figure 11. A-109 Gearbox Struts.

Figure from Reference 8

ORIGINAL SOURCE
OF POOR QUALITY

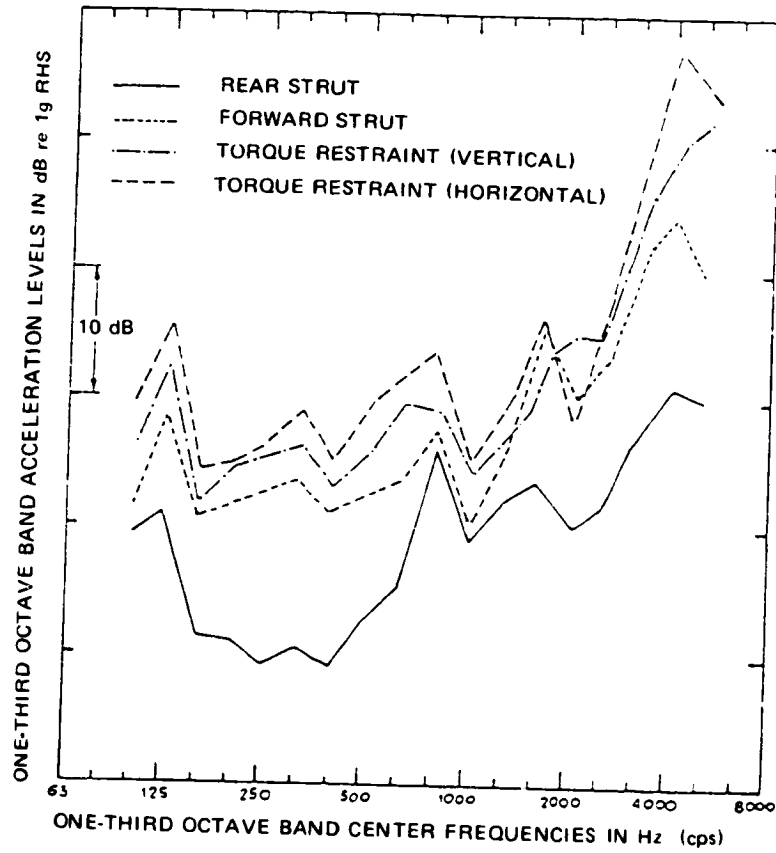


Figure 12. Contribution of Gearbox Mounts to Vibration of the Cabin Overhead Panel.

Figure from Reference 8

The tail rotor is a major source of noise over the frequency range from 100 to 500 Hz. It does not contribute significantly to the A-weighted noise. The main rotor is important only at frequencies below 100 Hz and makes a negligible contribution to the A-weighted noise.

Aerodynamic sources associated with the turbulent boundary layer are important only with regard to window vibration and door leaks. As other surfaces are treated these sources become more important.

The source and path identification and rank ordering were not repeated for the treated A-109 helicopter. However, it was found that a cabin noise level of 86 dBA could be achieved by addition of a "carpet hanging" treatment without reducing the source levels of the gearbox. During assembly and testing it was found that the assembly technique had considerable effect on the cabin noise levels due to acoustic leakage at trim panel joints and the shorting of isolators. Door leaks and air conditioning/heating noise also became important sources and required some treatment.

Source identification for Sikorsky S-76. - The Sikorsky S-76 structural configuration, as depicted in Figure 2, shows several potentially dominant vibration paths. The gearbox feet are directly mounted to main fore/aft structural beams. In the base cabin configuration many tones are present in the acoustic spectrum shown in Figure 13. At this point in time source identification has involved picking out lines on a narrowband spectrum. These narrowband tones clearly indicate the gearbox and hydraulics as primary sources.

The paths by which energy is transferred from these sources to the cabin are a matter of conjecture. Since the data in Figure 13 were taken in the aft cabin passenger location directly below the gearbox, one might expect the major path to be radiation from the drip pan. While this may be true for the untreated case, it is certainly not the case for the treated configuration. Figure 14 indicates that the major gearbox noise (1 kHz Octave Band) is lowest under the gearbox and highest near the pilot/copilot locations. This implies an energy path along the main fore/aft beams to the front windshield and then radiation into the cockpit acoustic space. The effect of windshield radiation for an S-76 is shown in Figure 15. The windshield acceleration (Figure 15a) is dominated by main gearbox, hydraulics and accessory vibration sources. These vibrations are radiated into the cockpit as acoustic energy as shown in Figure 15b. It is apparent that the cockpit noise is dominated by these same sources. Although more

investigation and testing would be required to make a correlation between windshield vibration and cockpit noise, this preliminary data seems to indicate the windshield is a significant contributor to cockpit noise levels.

Thus the postulation is made that the windows and panels are coupled to the framing and energy transmits primarily through the framing into the various panels where it radiates into the cabin.

Since a major portion of the cabin noise is created by gear tooth manufacturing inaccuracies, aircraft-to-aircraft variations in noise levels are to be expected. Figure 16 contains acoustic spectra for three S-76's manufactured several years apart. Aircraft A and C have more tonal qualities, whereas aircraft B contains more sideband activity.

ORIGINAL
OF POC...

ACOUSTIC DATA - OCTAVE SPECTRUM

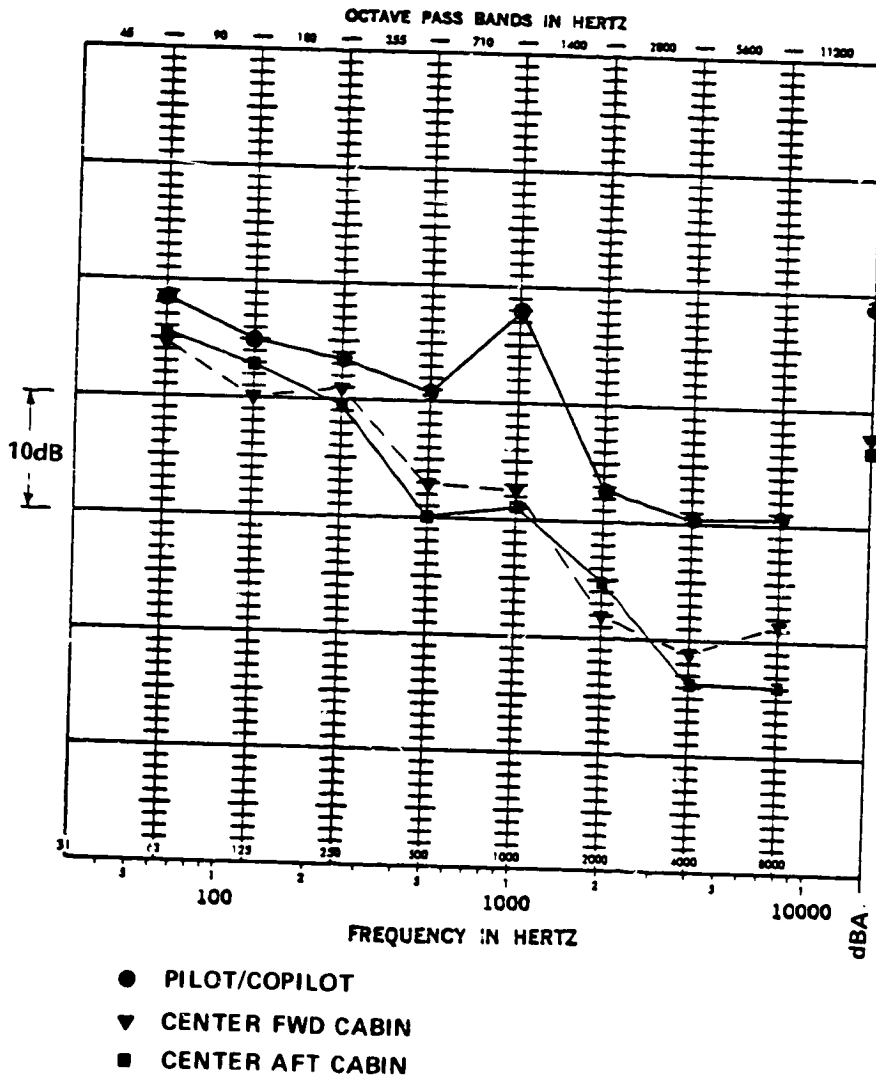


Figure 14. S-76 Treated Cabin SPL vs Location.

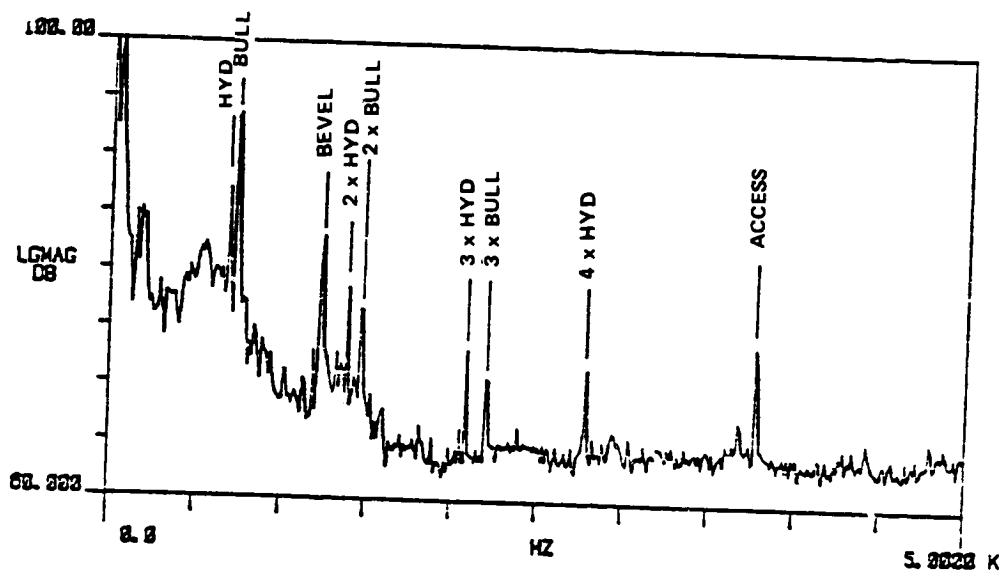


Figure 15A. S-76 Acceleration - Center Copilot Windshield 75 m/s LFO.

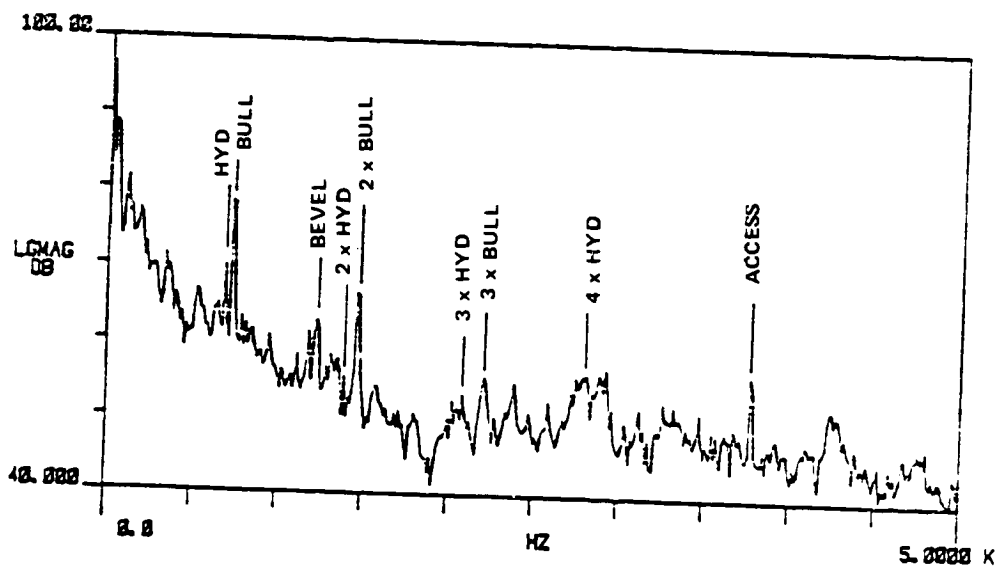


Figure 15B S-76 SPL - .03m Away from Center of Copilot Windshield.

VARIATION OF SPL
OF POS. QUALITY

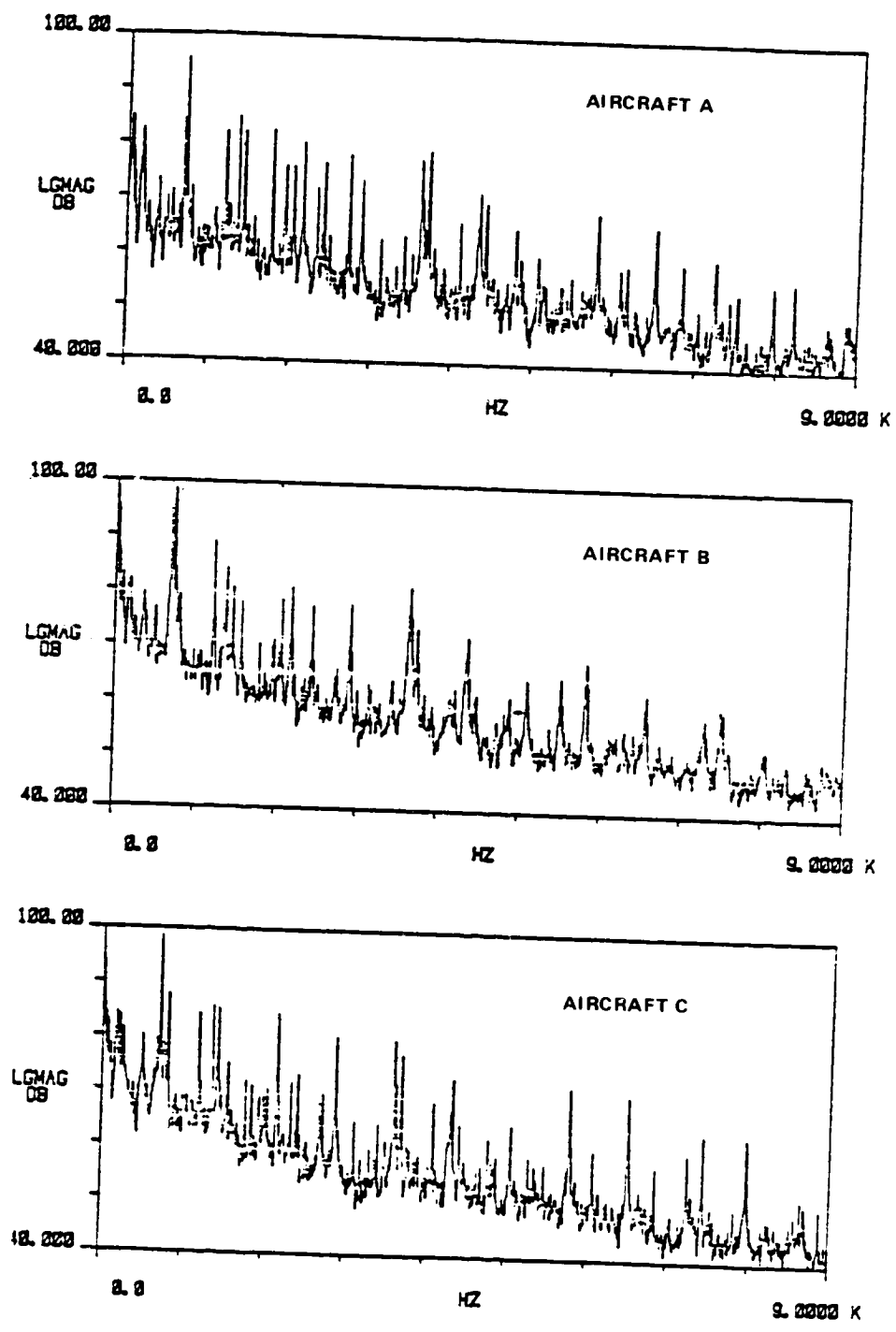


Figure 16. Variation of S-76 Bare Cabin SPL for Three Aircraft - Rear Center Seat, 75 m/s LFO.

DIAGNOSTIC TECHNIQUES FOR SOURCE AND PATH IDENTIFICATION

Review of Existing Case Studies

The techniques for source and path identification used in the existing case studies have been predominantly experimental in nature. Measurements are performed in flight for different operating conditions. Acoustic and vibration sensors are placed at appropriate locations near the sources, along the transmission paths, on the interior surfaces of the cabin, and at passenger locations. The selection of sensor locations is based on past experience and understanding of the cabin noise environment.

Source identification is often crudely based on the highly tonal character of the cabin noise spectrum. The gearbox is an important source of distinct tones where the tonal frequencies are straightforwardly related to gear tooth mesh rates. Other mechanical occurrences producing distinct tones include turbine blade passage, shaft rotation, rotor blade rate, hydraulic pump piston rate, etc. In identifying sources the observed tones in the cabin noise spectrum are matched with the known mechanical processes that produce tones. It is not possible to do the same for broadband sources, neither is it possible to identify the transmission path(s) for such sources once they have been identified.

When the source contributions are not distinctly identifiable in the cabin noise spectrum, then the identification is often made based on a relatively simple modeling of the system. Source levels are either measured directly or estimated analytically and combined with a transfer function for the transmission path in estimating the contribution to the cabin noise level.

Measured acoustic source levels are generally combined with a transmission loss model for the intervening skin panel, window, or bulkhead separating the source from the cabin interior. Differing levels of sophistication are used in characterizing the source based on its spatial characteristics [9]. Often an attempt is made to characterize the directivity of the main or tail rotor noise in quantifying the exterior levels over the cabin skin panels. The spatial correlation of the exterior pressure field exciting the skin panels is also important in estimating the acoustic transmission into the cabin.

This is particularly true for flow noise due to the turbulent boundary layer over the exterior surfaces. The exciting pressure fluctuations are non-acoustic in nature and it is therefore not strictly appropriate to use acoustic transmission loss information for the skin panels in estimating the transmission, although this is often done for simplicity.

Transmission loss information for light aircraft and helicopter fuselage structures is typically based on extensions of results for simple panels to the case where the skin is sectioned by frames and stringers [10, 11]. Different regions arise based on frequency and spacings between the frames or stringers. Radiation into the cabin is generally evaluated from expressions for the radiation efficiencies of flat plates. Some studies have modeled interactions and coupling between resonant modes of the skin panels and the acoustic resonances of the cabin [9, 12]. These studies have sought to identify contributions through individual panels.

Vibration levels for mechanical sources are conveniently measured at the connections between the source and the helicopter structure. The transfer function relates the measured vibration levels to vibration levels on the interior cabin surfaces which are then used to estimate the acoustic levels based on a radiation efficiency for the surface and an acoustic model for the cabin.

In the case of relatively simple structural elements such as gearbox struts, it is possible to analytically quantify their vibration transmission characteristics. A difficulty arises in analytically describing the gearbox and airframe attachments where the struts are connected. These involve considerably more complicated geometries. The typical approach for quantifying a vibration transfer function is to perform a measurement on the actual structure with mechanical shakers, and force and vibration sensors.

A similar experimental approach is also adopted for acoustic transmission paths. A speaker is used in place of the source on the actual helicopter in order to measure the transfer function in terms of a ratio of pressure levels. Where intermediate acoustic spaces are present such as the baggage compartment the procedure involves more than one acoustic transfer function.

For gearbox casing radiation acoustic energy reaches the cabin interior via transmission through overhead panels and potentially as well by transmission into the baggage compartment and then into the cabin through the rear passenger compartment bulkhead. For the former path a single acoustic transfer function (i.e., noise reduction ratio) is required. For the latter, two transfer functions are evaluated first from the cavity around the gearbox into the baggage compartment and subsequently with the speaker in the baggage compartment from the baggage compartment into the cabin.

In general, straightforward experimental techniques have been applied in generating descriptions of the helicopter cabin noise environment [1, 4, 5]. Their usage has been successful in providing a basis for the design of interior noise control treatments resulting in cabin noise levels near 80 dBA [8]. As lower levels are sought, consistent with the noise environment of commercial aircraft, greater detail and sophistication in modeling the noise environment and the effects of different treatments will be required.

The remainder of this section discusses the different approaches and techniques for source and path identification in greater detail. The first part deals with the practical engineering or experimental techniques. The second part describes more complicated procedures whose implementation has been greatly facilitated in recent years by the development of specialized instrumentation and computer systems capable of performing digital signal analysis quickly and relatively inexpensively.

Experimental Techniques

The goals of diagnostic tests in support of helicopter cabin quieting are:

1. identify and quantify sources of cabin noise.
2. identify and quantify the paths between those sources and the cabin.
3. describe the resulting in-cabin noise field.

In the development of treatments to reduce helicopter cabin noise it is necessary to create a description of the cabin noise environment showing the relation between all of the significant excitation sources and the resulting cabin noise level at the passenger locations.

In such a description an excitation source level is an acoustic, vibration, aerodynamic pressure, or other excitation acting on the helicopter in such a fashion as to cause noise in the cabin, and which is not expected to be altered by modifications produced in the noise reduction program. The relationship between a source excitation level and the noise level at a receiver point is a sound transmission path and it is described by a transfer function.

It should be noted that the definitions of "excitation source", "transfer path", and "receiver" are generated specifically for a problem, and that an excitation source for one problem may be a transmission path for another problem. Likewise the receiver for one specific problem may be a path link for another problem.

An example of this flexibility of definition is noise from the turbine air inlets. In a program to reduce turbine inlet noise entering the cabin, with treatments of the cabin surfaces but excluding any modification of the turbine or its operation, the inlet opening is a source as none of the treatments will affect its acoustic output. However, if the noise reduction program involves modifications to the turbine inlet ducting for the purpose of reducing the levels at the opening, then the inlet duct and opening become a part of the transmission path and the gas turbine is the excitation source.

General approach. - Important characteristics of source path modeling for linear systems are that path links can be combined, and multiple source path matrices can be combined to obtain an overall cabin response.

The amplitude spectral transfer function, $T_{k,n}(f)$, relating the excitation at source point n , $E_n(f)$, to the response at receiver point k , $R_{k,n}(f)$ is

$$T_{k,n}(f) = \frac{R_{k,n}(f)}{E_n(f)}. \quad (2)$$

When N sources have N paths of excitation to a single receiver, a series of transfer functions may be used to describe the response

$$R_k(f) = \sum_{n=1}^N E_n(f) \cdot T_{k,n}(f) \quad (3)$$

subject to the important criteria: 1) that the power flow along any of the transmission paths must be only positive in the direction from the source to the receiver, 2) that there must be no cross-excitation from one source to another, and 3) that the sources must all be incoherent. In realistic situations neither of the first two criteria is likely to be met, and the third criterion, while often met, is violated in some important cases. When it can be shown that the errors resulting from violation of these criteria are small, the superposition of source/path products is a useful modeling technique.

The requirements of positive power flow from source to receiver may be waived without introduction of significant errors if the power flow from the source to receiver is highly positive over the frequency range where the model shows that contribution to be significant to the cabin noise. The requirement against cross-excitation of sources may similarly be waived when it can be shown that the resulting errors are insignificant.

The requirement that all source/path combinations for a single receiver be incoherent is badly violated in a case where there are multiple coherent sources. Multiple coherent sources exist whenever multiple sources are defined to describe the transmission by various distinct paths from a single physical source. This is the case, as we see in a following section, when the gearbox attachment foundations are defined as individual sources, even though they are all excited by the same force interaction at the gear mesh.

Engineering methods for source identification. - The spectrum of helicopter cabin noise is typically dominated by distinct tones which are directly related to known mechanical occurrences, such as gear tooth clash, turbine blade passage, shaft rotation, rotor blade rate, hydraulic pump piston rate, etc. The most basic identification and quantification technique for the contributions from the sources is that of matching the tones of the measured cabin sound spectrum with those known physical excitations. In spite of the simplicity of approach, this technique is highly effective for most helicopters and is widely practiced. As a first level backup to this technique it is a frequent practice to measure an appropriate excitation (sound or vibration) at the source in order to determine that the calculated fundamental, harmonic, and side band tones for that source are actually excited, and also to determine if there are other identifiable discrete tones associated with the source and cabin response which were not otherwise predicted.

Limitations of the tone identification technique are that it is not useful for broad band random noise, and also that it cannot be used to discriminate between several sources exciting the same frequency at the receiver. In some cases crude experiments related to operating parameters of the different sources may be performed to better distinguish between sources when ambiguities exist. An example of such an experiment is comparison of measured levels in hover and forward cruise, using the same engine torque input for both cases, as a means of differentiating broad band noise due to machinery sources and that due to flow related

effects on the rotors and fuselage skins. In such an experiment measurement of machinery casing vibration would be done to determine that this source excitation had changed only a little, if at all. If the broad band cabin noise level changes significantly with speed, it can then be deduced that the dominant source is not the machinery. If it is proven that machinery and flow sources are the only possible sources, then relating the broad band noise to the flow sources follows. If such exclusion of alternate sources does not exist, it is necessary to either do further experiments to determine the exclusion of those other possible sources or else to determine a positive relation between the flow excitation and the cabin acoustic levels.

Other normally used crude methods of identifying acoustic sources and paths include flight or ground operation with a single element operating (electrically drive an oil cooling fan or a hydraulic pump while the helicopter is on the ground and all other machinery is stopped), or operation with a suspected dominant source isolated (e.g.: covering radiating cabin panels with heavy sound attenuating covers, sealing leaking door edge openings with mastic tape, etc.).

Using the simple techniques described here, it is generally possible to identify the most significant sources of helicopter cabin noise.

Contribution of source/path combinations to the cabin noise environment. - Quantification of the contributions to cabin noise of the various source path combinations is done by a stepwise process of determining the transfer functions for the particular paths and combining them with measured, or otherwise known excitation spectra. Source levels are generally determined from in-service measurement of the spectra of the appropriate excitation parameters. Transfer functions are generally measured during static ground tests in which paths are excited one at a time. The difficult challenge for this testing is the determination of methods to appropriately excite individual paths in a representative fashion of the in-flight excitation. For acoustic excitation the location and directivity of the loud speaker excitation source may be critical. For vibrational excitation the direction of force or moment excitation may be critical, as it is also obviously critical that appropriate locations be chosen for the point at which excitation is supplied and at which the related source level is measured.

Acoustic excitation. - For the case of acoustic excitation simulation, the example of turbine inlet noise provides a good demonstration of some of the considerations and limitations of this technique. The turbines are typically located aft of the cabin and gearbox. Combustion air is ducted from forward air scoops. Paths for inlet noise entering the cabin are: (1) acoustic transmission through the duct walls and then through the cabin overhead; (2) out of the throat and through the forward overhead panels; (3) out of the throat and through the forward cabin windows, and (4) through the various other cabin exterior surfaces.

The turbine inlet noise is characterized by high frequencies (2 to 10 kHz) which radiate in a highly directive fashion concentrated on the axis of the inlet duct. For the acoustic test, excitation is generated using several very small, high frequency loudspeakers placed well within the intake tubes, giving reasonable expectation that the available duct modes would be generally excited. Sound measurements are made for the purpose of establishing separate transfer functions for inlet noise in the cabin due to transmission through the overhead panels and through the windows. The transfer functions for the two paths are measured independently by alternately blocking transmission through the path not being measured, using a heavy covering of lead vinyl and fiberglass. The transfer function is given as the decibel noise reduction between turbine inlet opening and the passenger seats.

Having the transfer functions, these can be multiplied by the measured noise at the turbine inlet source SPL, to determine the resulting noise at passenger positions. Separate measurements are required to identify the acoustic levels of the turbine inlet during operation. The levels are increased by 3 dB accounting for two turbine configurations to yield the turbine intake noise at the passenger positions.

Looking back at this crude modeling technique it is appropriate to review the following critical approximations and simplifications which were made:

1. Frequency range of excitation limited to 2 to 12 kHz.
2. Random excitation from miniature loudspeakers presumed to represent the spinning turbine compressor excitation.
3. Effects of forward speed and boundary layer on inlet source directivity and transmission loss of panels have been ignored.

4. Incoherent addition, adding 3 dB, used for two turbine configurations and also to combine the contributions from transmission of sound arriving through different panel or window sections.

The frequency range selection is based on flight data for panel vibration and cabin noise as well as knowledge of the general source characteristics. The presumption of representative excitation of the inlet duct is based on the fact that the testing is done in a frequency range where the duct has many closely spaced modes and there is not expected to be any highly tuned response.

The effects of forward speed can be important due to the cabin boundary layer deflecting sound away from the cabin at locations forward of the inlet at near grazing angles. If this does occur it will reduce the sound transmitted through the overhead windows and panels.

The determination of which panels are significant transmitters of intake noise is based on the identification of high frequency intake tones in vibration spectra of the various panels.

The use of incoherent addition of tonal sources from two turbines, and when combining the sound from two transmitting panels, is not appropriate for any individual point in the cabin. The true coherent addition of paths results in strong standing wave patterns in the cabin sound field. However, because the tones for turbine noise (as well as those for the gearbox) occur at high frequency, the acoustic peaks and troughs are very closely spaced and, with the normal motions of a passenger's head, the ear is exposed to a range of levels which is best represented by the incoherent sum of the sources.

Vibration excitation. - For the case of simulating structureborne transmission in the helicopter by vibratory excitation, the case of gearbox noise transmitted to the cabin supplies a good example.

The gearbox is connected to the airframe at a number of major structural attachment points. Each of these attachments is a possible major path for structureborne noise to the cabin, therefore in any program to reduce cabin noise by modifying some or all of these mechanical paths it is necessary first to determine the relative acoustic energy transmitted by each. Using the transfer function technique we may define the attachment points as sources and determine the transfer from vibration at one of the points to

sound level in the cabin for a given configuration of cabin acoustic treatment. The transfer function may also be defined more specifically to relate vibration at individual gearbox attachment points to vibration of specific panels within the cabin. From this the individual panel radiation may be computed by a further transfer function, the panel radiation efficiency.

For this type of test it is critical to isolate as much as possible the excitation of the different significant structural paths during testing. For a rigidly mounted helicopter gearbox it is usually necessary to remove the gearbox to prevent such flanking path pollution of the transfer function. Several of the defined transmission paths may pass through a common point without the possibility of disengagement. This is the case when the different force directions and moment axes at a single attachment point are considered to be separate excitations.

At an individual attachment point it is important to properly orient the shaker so that it applies forces in only the desired direction. Motions in the other axis directions should be measured to evaluate the cross-coupling that occurs as a result of the complicated geometry of the structure. The question of correlated sources as it relates to different directions of excitation at the same attachment point is important in considering an incoherent summation of the contributions for the different directions. The simplest approach relevant for an engineering assessment of the cabin noise environment is to simply neglect the effects of coherent coupling, either in the form of coherent excitation source levels or as cross-coupling between transmission paths on the structure.

The following is a mention of some critical points to consider when designing experiments for determining transfer functions by structural excitation.

When designing experiments using vibration stimulation of structural transmission paths, the most critical points are generally the location and method of vibrator attachment. The considerations here are direction and mode (force or moment) of input, avoidance of local deformation effects, and maintaining dynamic similarity between the test structure and the in use vehicle. It should be noted that in many cases it is possible to make simplifications allowing for single, unidirectional excitation to describe a path with multidirectional driving. For complex structures which are large compared to bending waves at the frequency range of interest and have numerous asymmetries, uni-

directional point excitation is likely to result in the reverberant excitation and generalized modal response at points removed from the area directly adjacent to the excitation. For the generalized modal response the distribution of energy for the different directions at a given point will remain the same whether the excitation is the real or simulated one. In this situation it is then possible to characterize the source based on a single direction of vibration to be measured during flight and simulation.

Local contact deformation at the point of contact between the vibration exciter and the structure are likely to occur. For this reason it is usually not advisable to measure the source level with an accelerometer within the shaker attachment, as is found for a standard "impedance head". The location of the accelerometer should be far enough away from the point of contact to avoid membrane deformation effects.

Many of the helicopter components undergo considerable stress loads during flight. One place for concern about flight load effects is with strut-mounted gearboxes having self-aligning ball and socket type connections at each end of the strut. First, if there is any play in the bearing it is necessary that the testing be done with enough force applied across the joint to maintain bearing contact at the appropriate surface. Furthermore, if these mounts become rigid against moments under flight conditions it may be proper to stop the hinge action by stressing the joint or by use of chemical bonding of the joint during testing. Further study of these junctions is required before a judgement can be made on the necessity of bonding the joint during testing.

Signal Processing Techniques

The development of small, high speed computer systems and specialized instrumentation has resulted in the development and implementation of signal processing techniques for studying the dynamic behavior of mechanical systems. The procedures involve evaluations of higher order statistics of the measured response of the system in both time and frequency domains. Standard measurements simply involve a determination of the system's response level relative to an excitation level.

The following two sections provide an introductory description of the techniques and their uses in relation to the helicopter cabin noise problem. Discussion of techniques with potential for application to the helicopter noise problem appear in Appendix A.

The reader additionally is referred to the following texts for descriptions of the theoretical basis for and implementation of the signal processing techniques: [13, 14].

Source identification. - The coherence function provides a quantitative measure of the relationship between two or more signals. If one signal represents the output of the system and the others are input signals, then the coherence function is an indication of the causality between the output and the individual inputs. This description requires that the inputs be statistically independent.

The coherence function, $\gamma^2(f)$, is defined by the following for a system with an output, y , and n inputs x_i :

$$\gamma_{y,x_i}^2(f) = \frac{|G_{y,x_i}|^2}{G_{x_i,x_i} G_{y,y}} \quad || \text{ indicates magnitude of complex function} \quad (4)$$

where G_{y,x_i} is the cross-spectral density of the output y and an input x_i . G_{x_i,x_i} and $G_{y,y}$ are power spectral densities of the input and output signals, respectively [14].

The coherence function varies between 0 and 1. It equals zero when the output is unrelated to the input and 1 when the output is due only to the particular input with insignificant contributions from other sources. In between values give the fractional amounts of the output associated with each input. If all inputs are identified the coherence function values sum to one in the absence of extraneous noise in the measured signals.

Two significant problems with use of the coherence function in helicopter cabin diagnostics are related first to too great coherence, and second to too little coherence. Gear noise, which is the main source of cabin noise, is generated at the tooth-to-tooth points of contact between various pairs of gear wheels. The resulting cabin noise arrives through various paths including vibration carried across numerous mechanical connections between the gearbox and the cabin.

With inputs defined as the vibration levels at each of the attachment points of the gearbox and airframe they are likely to be highly mutually coherent. The coherence function is in this case incapable of distinguishing between the contributions to cabin noise due to transmission through individual attachment points.

It is capable of distinguishing between the attachment points treated collectively as a single source and other statistically independent sources.

The second major problem in the use of coherence techniques occurs when there is no dominance of the noise from any single source. Flow excitation provides a good example. Because of the spatially random nature of the flow disturbances causing the generation of noise, there is little mutual coherence of the vibration response of the aircraft window and skin at various individual locations on these radiating surfaces. Expected coherence between the cabin noise level and measured vibration response at a single location will be low, unless there are limited dominating local areas of vibration response with major contributions to the cabin noise. The situation is one where the distributed response over the surface involves relatively small patches of coherent response as a result of the spatially random nature of the flow excitation.

Transmission path identification. - The transmission of energy in a complicated system is characterized in general by the effects of propagation, attenuation, and reverberation. Propagation refers to the transmission of energy without reflection in an acoustic or mechanical system. Propagating energy is attenuated in amplitude and dissipated as heat. In air the dissipation is due to viscous and thermal losses which are generally significant only over long distances. In a structure the attenuation is the result of internal mechanical damping in the material and accounts also for the effect of added damping treatments.

Complicated acoustic and mechanical systems generally involve a great many internal reflections of the propagating energy leading to the creation of a reverberant field. The system response is characterized by its resonant modes. These are damped by propagation losses as well as dissipation at the boundaries of the system. For large and complicated systems it is convenient to evaluate the overall transmission in terms of individual structural subsystems and the connections between them. Statistical Energy Analysis is a procedure that has been developed in recent years to study the transmission in complicated structural and acoustical systems. Its application to vibration transmission in a helicopter airframe structure is an important basis for the overall modeling of the cabin noise environment in this study.

At the outset of this discussion it is important to distinguish between dispersive and non-dispersive wave propagation. A non-dispersive wave is one whose phase speed is constant with frequency while the phase speed for a dispersive wave varies with frequency. Sound in air is non-dispersive as are longitudinal and

shear waves in solids. Bending waves in beams and plates are dispersive. A system can be considered to be non-dispersive if the frequency bandwidth of interest is sufficiently narrow that the phase velocity is nearly constant across the band.

An important characteristic of non-dispersive waves is that the shape of the temporal waveform, moving at the phase velocity, does not change with time or space. In other words, there is no waveform distortion. Thus, the origin of the name non-dispersive wave signifies that an initial temporal pulse does not spread out or disperse with increasing time. This is because all the spectral components of the pulse propagate at the same speed. Conceptually, a disturbance in a non-dispersive system can be followed around in time to identify which paths it takes to go from the source of the disturbance to the response point of interest without the problem of having the disturbance change its shape except at boundaries.

INTERIOR NOISE PREDICTION MODEL

Sources of Cabin Noise

Acoustic/aerodynamic sources. - Acoustic sources of cabin noise include the acoustic radiation from the surface of the gearbox, acoustic radiation from the air inlets to the turbines, acoustic radiation into the turbine enclosure, excitation of the windows and fuselage skin by turbulent boundary layer pressure fluctuations, sound transmission and radiation from leaks around door seals, radiation by the tail and main rotors, and noise generation and transmission in the heating and airconditioning system. The acoustic radiation from the gearbox is the most significant source listed above. However, in a fully-treated cabin the other sources, in particular TBL excitation of the windows and doors leaks, can be major noise sources.

One of these sources, airborne gearbox noise, is caused by mechanical gear mesh forces which generate vibration that is transmitted through shafts and bearings to the gearbox case. The vibrations of the gearbox case radiate noise into the acoustic space enclosing the gearbox.

The acoustic power radiated by the gearbox at a particular frequency is related to its vibration by the radiation efficiency, the characteristic impedance of the acoustic space enclosing the gearbox, the surface area of the gearbox, and the mean-square velocity normal to the surface of the gearbox averaged over the gearbox surface (see Equation (1)).

The radiation efficiency for flat panels is a function of frequency relative to the critical frequency, f_c , at which the bending wavespeed in the panel equals the speed of sound in air. The critical frequency is dependent on the material properties of the panel and its thickness, h . For aluminum, steel or glass panels in air, the critical frequency is given by:

$$f_c = 12\,700/h \quad (5)$$

Below the critical frequency

$$\sigma_{\text{rad}} = \frac{\rho \lambda_c}{A_s \pi^2} \left(\frac{f}{f_c}\right)^{\frac{1}{2}} \beta \quad (6)$$

where p = perimeter of the structure

λ_c = acoustic wavelength at critical frequency = c_o/f_c

β = panel edge boundary condition factor

$\beta = 1$ simple edge support

$\beta = 2$ clamped edge support

Above the critical frequency the radiation efficiency is generally equal to one.

In a structure such as the gearbox casing many factors contribute to increasing the radiation efficiency above the value for a flat panel. These include supporting frames and ribs, curvature, and impedance discontinuities at changes in thickness or at bearing attachment points. The addition of a rigid or relatively heavy stiffener (rib) to a panel increases the radiation below the critical frequency due to the increase in radiating perimeter. For each rib of length L the radiating perimeter is increased by $2L$ in that the radiation occurs from the panel areas on both sides of the rib. Dynamically significant impedance discontinuities contribute in the same way as a rib in increasing the radiation efficiencies of the adjoining panels.

A second source of airborne noise is the turbine, which can be a source of both discrete frequency and broadband random noise. The discrete frequencies are at multiples of the rotation rates and blade passage frequencies while the broadband random noise results primarily from combustion.

The turbine noise can be divided into three components: airborne noise radiated from the turbine inlet, airborne noise radiated from the turbine casing, and structureborne noise from the turbine mounting brackets. The two airborne sources radiate noise into the acoustic spaces enclosing them. The formulation in terms of acoustic power radiation and transmission is similar to that for airborne gearbox noise.

Identification of a source level for the airborne noise radiated from the turbine casing requires measured vibration levels averaged over the casing and an estimate of the radiation efficiency. The source level for the turbine inlet noise requires either a measurement of sound power in a free field environment or equivalently a measurement of reverberant sound pressure level in the

turbine inlet space combined with a measurement of the acoustic absorption coefficient for the space. In the latter measurement it may be difficult to separate turbine inlet noise from airborne gearbox noise or airborne turbine casing noise.

The paths by which airborne turbine noise is transmitted to the cabin are not direct, and this suggests that the turbine noise is not a significant acoustic source. This suggestion is supported by the noise control program for the Agusta A-109. In this program structureborne noise from the turbine was found to be significant, but the airborne turbine inlet noise and turbine casing noise were found to be insignificant.

A third source of airborne noise to be considered is the turbulent boundary layer. At the higher flight speeds the pressure fluctuations in the turbulent boundary layer are a source of broadband random cabin noise. These pressure fluctuations act on the windows and outer skin of the aircraft. The resulting vibration causes direct sound radiation into the cabin from the windows and indirect radiation from trim panels that are coupled to the skin. In a well designed interior the trim panel radiation is not significant compared to the window radiation unless double windows are used.

At subsonic speeds the pressure fluctuations in a fully developed turbulent boundary layer over a smooth surface can be predicted empirically [15]. It is generally accepted that the rms fluctuating pressure, P_{rms} , is given by

$$P_{rms} = 0.006 q_0 \quad (7)$$

where q_0 is the free stream dynamic pressure,

$$q_0 = \rho U_c^2 / 2 \quad (8)$$

where ρ is the air density and U_c is free-stream velocity.

The spectrum of the TBL pressure fluctuations can be plotted in nondimensional form as shown in Figure 17. The spectrum peaks at a radian frequency of

$$\omega_{pk} = 0.25 \frac{U_c}{\delta^*} \quad (9)$$

where δ^* is the displacement thickness of the boundary layer. Below ω_{pk} the spectrum is not a strong function of frequency. However, above ω_{pk} it falls off approximately 6 dB per octave (ω^{-2} dependence).

The boundary layer displacement thickness depends on the geometry of the flowfield. Given an exact geometry it is possible to calculate the displacement thickness over the surface of the airframe. Because of the relationship of surface drag to this parameter the calculation is usually carried out as part of the airframe design. However, as an approximation for the purposes of cabin noise prediction, the displacement thickness can be determined from the equation

$$\delta^* = 0.0016 D \quad (10)$$

where D is the distance from the leading edge.

The effectiveness with which the TBL fluctuating pressure field excites the window or fuselage panels depends on the correlation lengths of the field. The spectrum of the modal force, $S_f(\omega)$ is related to the spectrum of the TBL pressure, $S_p(\omega)$ by the equation

$$S_f(\omega) = j^2 A^2 S_p(\omega) \quad (11)$$

where j is the joint acceptance and A is the window or panel area. The joint acceptance is determined by the relative size of the correlation lengths of the TBL pressure fluctuations and the panel area. It is given by the equation [16].

$$j^2 = \frac{0.28}{\pi} \frac{1}{A} \left(\frac{U}{\omega} \right)^2 \quad (12)$$

The panel response is found by computing the response of a typical panel mode and multiplying that response by the number of modes per unit frequency.

The response spectral density averaged over a band of frequency that includes several modes is given by

$$S_a(\omega) = \frac{\pi}{2} \frac{\omega}{m_s^2 A^2 \eta} j^2 S_p(\omega) \quad (13)$$

where ω is the band center frequency, m_s is the surface density of the panel, and η is the panel damping loss factor. The acoustic radiation into the cabin can be calculated from the vibration spectrum and the radiation efficiency.

ORIGINAL PAGE IS
OF POOR QUALITY

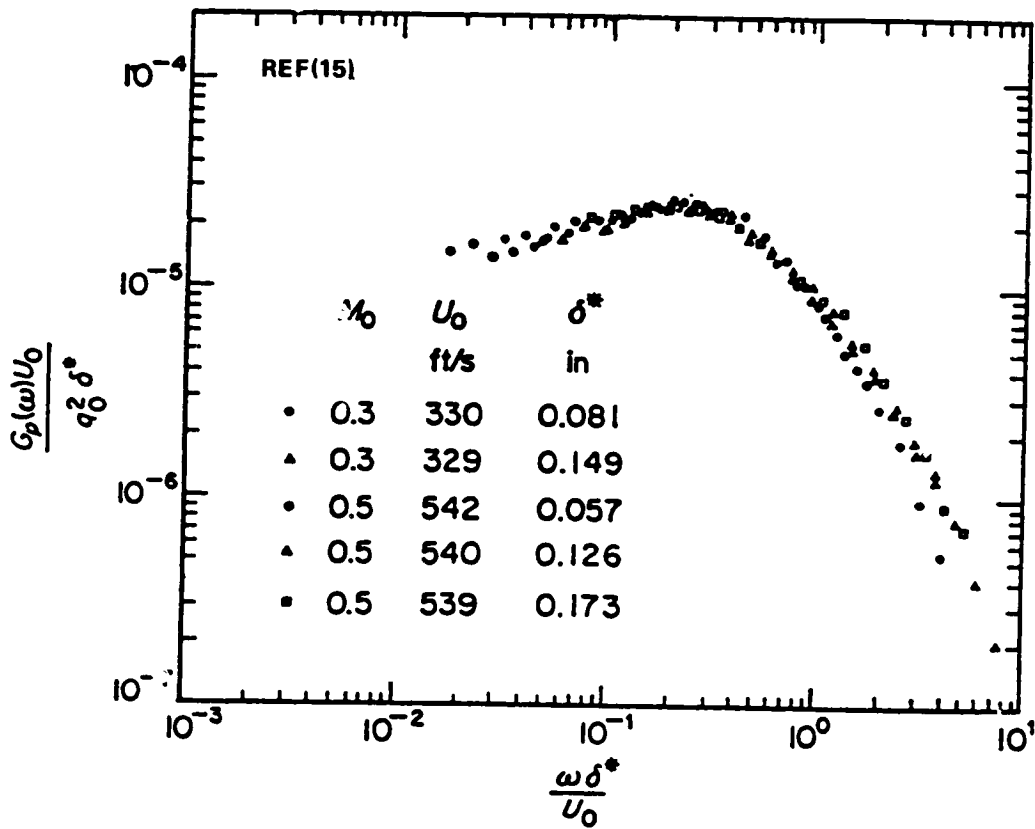


Figure 17. Frequency Spectrum of Wall-Pressure Fluctuations.

Vibration sources. - Vibration sources in modern helicopters are the most important contributors to the untreated cabin interior noise environment. The dominant vibration source is the gearbox which is the primary focus of the present study. A number of factors contribute to this assessment including the large amount of mechanical power available, the large reduction in rpm that the mechanical power feeds through from the high speed turbines to the considerably lower speed rotor, and the lightweight and compact nature of the helicopter design configuration.

An imperfect meshing of the gear teeth under large steady loads leads to a tonal excitation of the gear train and gearbox casing at fundamental and harmonic frequencies at the particular gear mesh and shaft rates. The vibration is transmitted to the casing through the bearings supporting the gear shafts. The present study is not concerned with the detailed mechanisms involved in the generation of dynamic gear mesh forces or with the transmission of vibration to the gear casing.

For the present study the source representation for the gearbox is defined in terms of the vibration levels at the attachment points with the airframe. For strut-mounted gearboxes the strut can be considered to be a part of the airframe. Also, attachments associated with torque restraints must be considered in defining the gearbox sources.

An appropriate representation for vibratory sources is one which is not dependent on the vibration characteristics of the structure to which the source is attached. Representing the source in this manner allows for modifications of the attached structures without the necessity of changing the source representation. An example of importance for the present study involves the design of gearbox isolation mounts. Independently representing the source allows for evaluating the effect of the mount without complications due to changes in the source levels for the gearbox.

The procedure is described for a point attachment with translational sources in three directions. The source level is represented either by blocked force levels or free vibration levels. The blocked force level is the force required at the attachment point to identically constrain the motion to zero. The free vibration level is that which would result if the attachment is disconnected and the force is zero.

Modeling the gearbox as a linear time invariant system the motions/forces at the attachment point can, in general, be related to the gear mesh forces/motions at the gear teeth by a mobility matrix:

$$\begin{pmatrix} v_1 \\ v_2 \\ v_3 \\ v_4 \\ \cdot \\ \cdot \\ \cdot \\ v_n \end{pmatrix} = \begin{pmatrix} Y_{11} & & & & & \\ & Y_{12} & & & & \\ & & Y_{13} & & & \\ & & & Y_{14} & \dots & \\ & & & & \dots & Y_n \end{pmatrix} \begin{pmatrix} f_1 \\ f_2 \\ f_3 \\ f_4 \\ \cdot \\ \cdot \\ \cdot \\ f_n \end{pmatrix} \quad (14)$$

where $v_1, v_2, v_3, f_1, f_2, f_3,$ are the translational velocities and forces, respectively, in three directions at the attachment point. $v_4 \dots v_n$ and $f_4 \dots f_n$ refer to velocities and forces at the points within the gearbox where the mesh forces are generated. The complex mobilities (ratio of velocity to applied force) $Y_{11}, Y_{12} \dots$ characterize the dynamic behavior of the gearbox structure (gears, shafts, bearings, and casing).

It is convenient when describing the system in terms of a mobility matrix to represent the sources in terms of free velocities where the attachment forces f_1, f_2, f_3 are zero. The internal gear mesh forces are in general not equal to zero. This defines a set of free velocities at the attachment point:

$$\begin{pmatrix} v_1 \text{ free} \\ v_2 \text{ free} \\ v_3 \text{ free} \end{pmatrix} = \begin{pmatrix} Y_{14} & \cdot & \cdot & \cdot & Y_{1n} \\ Y_{24} & \cdot & \cdot & \cdot & Y_{2n} \\ Y_{34} & \cdot & \cdot & \cdot & Y_{3n} \end{pmatrix} \begin{pmatrix} f_4 \\ \cdot \\ \cdot \\ \cdot \\ f_n \end{pmatrix} \quad (15)$$

With this representation and Equation (14) it is possible to characterize the attached system velocities at the attachment point in terms of the free velocities:

$$\begin{pmatrix} v_1 \\ v_2 \\ v_3 \end{pmatrix} = \begin{pmatrix} Y_{11} & & & \\ & Y_{22} & & \\ & & Y_{33} & \\ & & & \dots \end{pmatrix} \begin{pmatrix} f_1 \\ f_2 \\ f_3 \end{pmatrix} + \begin{pmatrix} v_1 \text{ free} \\ v_2 \text{ free} \\ v_3 \text{ free} \end{pmatrix} \quad (16)$$

which can be written as:

$$\bar{v} = [Y] \bar{f} + \bar{v}^{\text{free}}$$

The attached structure can be characterized by an impedance matrix

$$\bar{f} = \begin{Bmatrix} f_1 \\ f_2 \\ f_3 \end{Bmatrix} = - \begin{Bmatrix} Z_{11} & Z_{12} & Z_{13} \\ Z_{21} & Z_{22} & Z_{23} \\ Z_{31} & Z_{32} & Z_{33} \end{Bmatrix} \begin{Bmatrix} v_1 \\ v_2 \\ v_3 \end{Bmatrix} = -[Z] \bar{v} \quad (17)$$

where the impedances $Z_{11}, Z_{12} \dots$ describe the dynamic behavior of the attached structure in terms of forces/velocities at the attachment point. The minus sign accounts for the convention where velocities are positive into the particular structure. Velocities v_1, v_2, v_3 are defined as positive into the gearbox and therefore the velocities into the airframe are the negatives of these. Equations (16) with (17) yield:

$$\bar{v}^{\text{free}} = (1 + [Z][Y]) \bar{v} \quad (18)$$

The free velocities are independent of the impedance characteristics of the attached structure. The actual velocities depend on: 1) the attachment point structural impedances and 2) the dynamic behavior locking into the source at the attachment point as described by the mobility matrix $[Y]$. Modifications to the structure in the form of an isolation mount would result in changes in the impedance matrix $[Z]$.

The above description applies for only a single attachment point and translational forces and velocities. Similar representations may be generated for other attachment points, for moments and angular velocities and for other sources of vibratory energy such as the hydraulic system. The approach is general and requires that the source be spatially localized to a set of attachment points, that its dynamic input characteristics be measurable, and that the free velocity levels can be defined. It is often not convenient or possible to measure the free velocities as the device cannot be operated unattached. In that case it may be possible to calculate free velocity levels from measured attached levels based on Equation (18) and the dynamic characteristics of the source and attached structures. Once calculated, the free velocity levels can then be used to evaluate the effects of structural modifications.

The solution to the overall problem requires an additional piece of information relating the velocities of the attachment points to the cabin interior noise levels. It is often convenient to define a set of velocity transfer functions from the attachment points to locations on panels that radiate into the cabin. The panel vibration levels are combined with a radiation efficiency, including the effects of noise treatments, and a model of the cabin acoustic field to complete the overall model. Models for the velocity transfer functions of the airframe and cabin acoustic field are described in following sections.

The above analysis raises an important area of concern in modeling gearbox vibration transmission with respect to coherent sources and transmission paths. The internal gear mesh mechanisms within the gearbox are a source of coherent vibration at the different attachment points. Also, the transmission from a single attachment point to a vibrating point on a cabin panel surface or to a passenger position in the cabin acoustic field occurs by different but coherent transmission paths. It is easiest to ignore coherence effects in algebraically summing different source/path contributions as though they were statistically independent.

Coherence between source terms is described in relation to Equation (15). The free velocities will be incoherent in the unlikely event that the appropriate mobility terms in the matrix are zero so that the internal forces $f_1 \cdot \cdot \cdot f_n$ affect only one free velocity each. This is extremely unlikely considering the internal structure of the gearbox. The gearbox source terms can be expected to display a high degree of coherence.

The coupling at the attachment points due to non-zero, off-diagonal terms in the mobility and impedance matrices from Equations (14) and (17), respectively, will result in coherent attached velocities V_1, V_2, V_3 . Velocity transfer functions to points on radiating cabin panel surfaces will also involve different coherent paths. The overall effect of source and path coherence is mitigated by the fact that only average response levels within the cabin are of interest.

The above procedure for characterizing vibration sources has been described in general and can readily be applied for sources other than the gearbox, such as the hydraulic lines. These lines are mounted directly to the airframe at approximately 0.5m intervals between the pump, which is mounted on the gearbox, and the servos for the main and tail rotors and the landing gear.

Applying the above procedure for the hydraulics system requires that the attachment points and dynamically important motions at the attachments be identified. In addition, measurements are required of the input impedance and mobility functions of the airframe and looking into the hydraulics line at the attachment point. Actual source levels are determined from in-flight measurement of attachment point motions.

Statistical Energy Analysis (SEA) Model of Vibration and Acoustic Transmission in Helicopter Airframes

Statistical Energy Analysis (SEA) provides a means to study the dynamics of a complex mechanical system in terms of the behavior of a number of smaller subsystems which are coupled together. The system is modeled by a simple set of coupled linear equations that represent an overall power balance for each subsystem. Resonant vibratory or acoustic modes are responsible for the storage of energy within each subsystem.

A distinguishing feature of SEA is that the power flow between coupled subsystems is simply proportional to the subsystem energies. The power dissipated due to mechanical damping is also proportional to the subsystem energy. As will be seen further on, these features form the basis for the coupled linear algebraic equations of the SEA model. The basic theory behind SEA is discussed in detail by Lyon [17].

A major advantage of SEA results from grouping resonant modes together and treating their response statistically. This allows for a significant reduction in the number of degrees of freedom in the model. Although it is now computationally possible through finite element or modal analysis and the availability of large computers to deal with each mode individually, considerable effort and cost are required to implement and run the model for complex structures such as a helicopter.

The idea of dealing with modes statistically arose from statistical mechanics where systems were modeled as maximally disordered with each mode having the same energy. In SEA this statistical nature is used in grouping the modes. Modes within each group have the same energy, but modes within different groups are allowed to have different energies.

The concept of equipartition of modal energy also has its basis from the field of room acoustics. A large concert hall or other acoustic space can have thousands of modes within the frequency range of interest. To study such a complex system acousticians

use the concept of a diffuse field. In such a sound field acoustical energy at any point comes from all directions, with energy from different directions being uncorrelated. This wave description is equivalent to saying that there are a large number of modes, each with the same energy. Again, equipartition of energy is used to group modes together and to study complex dynamical systems without having to identify each individual mode of vibration.

As with any modeling procedure, the success in using SEA depends on the skill with which the model is set up. Often it is advantageous to compare SEA predictions with data from a laboratory study of a simplified structure which approximates in some general way the actual structure being considered. The goal of the laboratory study is not to obtain data that can be used directly to predict the structural response being considered. Nor is the goal to support the basic validity of SEA. The true purpose of the laboratory study is to support the validity of the particular model that has been set up using SEA so that the model can be applied to the complex structure being studied.

The success in using SEA depends in large part on grouping the modes into subsystems so that each mode within a subsystem has the same energy. The following principles are used:

1. all modes within a subsystem should have resonance frequencies in the same frequency band;
2. all modes within a subsystem should be identified with a particular structural subsection of the system, i.e., a plate, beam, or shell segment or an acoustic space;
3. all modes of a particular structural subsection should consist of the same type of vibratory motion, i.e., bending, compressional deformation, shear deformation, or torsion.

In highly complex structural subsections the modes may involve several types of vibratory motion. In this case all modes of the subsection having resonances within a frequency band can be considered to have the same energy and put in one group. For example, a straight section of a beam has three groups of modes: those involving longitudinal motion, those involving torsional motion, and those involving transverse motions. The transverse modes can be further divided into two groups corresponding to the two directions of the motion. If the beam has several bends along its length, SEA allows two approaches. In one approach each

straight section of the beam is considered to be a separate subsection, and the four groups of modes in each beam section are allowed to be coupled with each other and with modes of other beam sections. A second, far simpler approach, is to treat the entire beam as one subsection and group all modes into a single group. This is possible because the bends will result in normal modes for the beam that involve all types of motion - longitudinal, torsional, and transverse.

Because these modes consist of all types of motion they tend to be similarly excited by external sources, similarly damped, and similarly coupled to modes in other groups. Under these conditions the modes will tend to have equal energy.

An SEA model consists of a block diagram where the individual blocks represent groups of similar modes. A sample block diagram and the system it models are shown in Figure 18. The system consists of an acoustic space, a panel which is one of the bounding surfaces of the space, and a beam member which is attached to the panel. The configuration is representative of subsections from a helicopter airframe, but is by no means indicative of the full size model required for the complete airframe.

The groups of modes or blocks in the model include the acoustic resonances of the space, the bending modes of the panel, and torsional and bending modes of the beam. A more detailed description of the modeling of subsystems of this type is presented in subsequent sections of the report. Lines connecting the blocks represent power exchange between the different coupled groups of modes. Additional lines represent the power dissipated within each group of modes and the power input from external sources.

The input power in this case is due to other structures which are attached to the beam. The dissipated power is due to internal mechanical damping for the structural subsections and wall absorption for the acoustic space. The transmitted power is the result of mechanical connections between structural subsections and acoustic radiation into the acoustic space from the vibrating structural subsections.

The identification of power transmission paths is initially straightforward. Mode groups from adjacent structural subsections are almost always coupled, although cases can occur where this is not the case. For example, in the case of two beams joined at right angles, the longitudinal modes of one beam do not couple to the longitudinal modes of the second beam. However, this is the exception rather than the rule since the longitudinal modes will be coupled for any other angle of attachment.

Very subtle paths of vibration transmission can exist between modes of structural subsections that are only connected to one another through a third intervening subsection. In a given band of frequencies it is possible for the resonant modes of one structure to be coupled to the resonant modes of a second structure through non-resonant modes of a third intervening structure. The most common case in which this path or power transmission is important is that of two acoustic spaces separated by a plate or shell structure. The modes of one acoustic space are directly coupled to the resonant modes of the plate and indirectly coupled to the resonant modes of the other acoustic space through non-resonant mass-law controlled modes of the plate. This indirect path is often more important than the direct paths from the acoustic space to the plate and from the plate to the second acoustic space.

Introduction to SEA. - The equations of motion for steady-state conditions are derived by equating the time-average power input to a group of modes with the sum of the time-average power dissipated and the time-average power transmitted to other groups of modes. For example, power balance for the mode group identified as acoustic space modes in Figure 18 can be written as:

$$w_{diss}^{(4)} - w_{trans}^{(1,4)} - w_{trans}^{(2,4)} - w_{trans}^{(3,4)} = 0 \quad (19)$$

where $w_{trans}^{(i,j)}$ is the net time-average power transmitted from mode group i to mode group j with i and j taking on the value shown, and $w_{diss}^{(4)}$ is the time-average power dissipated in mode group 4.

ORIGINAL PAGE IS
OF POOR QUALITY

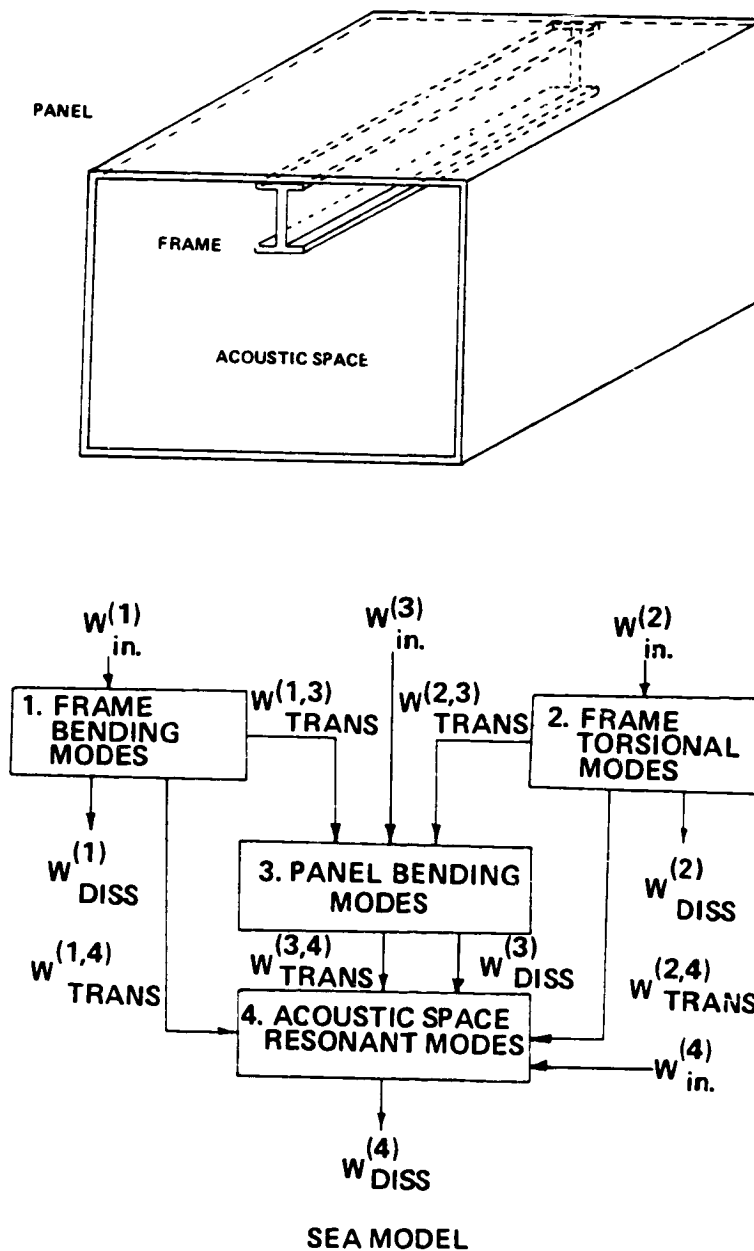


Figure 12. A Typical SEA Model.

Evaluation of the power balance equations depends on the basic SEA concept that the time-average power exchange between two groups of similar modes is proportional to the difference between the average energy per mode in each group. The time-average power transmitted from group i to group j can be written:

$$W_{\text{trans}}^{(i,j)} = \langle B \rangle^{(i,j)} N_i N_j \left[\frac{E_{i,\text{tot}}}{N_i} - \frac{E_{j,\text{tot}}}{N_j} \right] \quad (20)$$

where $\langle B \rangle^{(i,j)}$ is the average coupling coefficient between a mode in group i and a mode in group j , N_i is the number of modes in group i , and $E_{i,\text{tot}}$ is the total time-average energy of all modes in group i . The use of average coupling coefficients is a statistical concept that is an integral part of SEA.

The requirement that all modes in a group be similar includes the requirement that their resonance frequencies be within a given bandwidth, $\Delta\omega$. Given this requirement, the coupling term in Equation (20) is almost always replaced by a term containing a coupling loss factor and a band center frequency so that:

$$W_{\text{trans}}^{(i,j)} = \omega \eta_{ij} N_i \left[\frac{E_{i,\text{tot}}}{N_i} - \frac{E_{j,\text{tot}}}{N_j} \right] \quad (21)$$

where ω is the band center frequency and η_{ij} is the coupling loss factor. The time-average power, $W_{\text{trans}}^{(i,j)}$, is now the power within the band, $\Delta\omega$. Similarly, the mode counts, N_i and N_j , include only modes with resonance frequencies within the band $\Delta\omega$ and the total energies, $E_{i,\text{tot}}$ and $E_{j,\text{tot}}$, include only those modes within the band. All variables are allowed to be functions of frequency so that the dynamics of the system can be studied at different frequencies.

A further step is usually taken in evaluating the transmitted power. The mode counts, N_i and N_j , are evaluated in terms of a modal density, which is the average number of modes per unit frequency in an ensemble of systems in which the resonance frequencies are randomly distributed. The concept of an ensemble of systems with randomly distributed resonance frequencies is consistent with the use of an average mode to mode coupling factor, $\langle B \rangle$, in Equation (20). If the modal density is a slowly varying function of frequency, then the mode count N_i in the band $\Delta\omega$ can be written as:

$$N_i = n_i(\omega) \Delta\omega \quad (22)$$

where $n_i(\omega)$ is the modal density at the band center frequency ω . In cases where this is not true, Equation (22) is replaced by:

$$N_i = \int_{\Delta\omega} d\omega n_i(\omega) \quad (23)$$

In most cases, the added accuracy obtained by using Equation (23) instead of Equation (22) is not necessary. Thus, the power balance can be written:

$$W_{\text{trans}}^{(i,j)} = \omega \eta_{ij} n_i \left[\frac{E_{i,\text{tot}}}{n_i} - \frac{E_{j,\text{tot}}}{n_j} \right] \quad (24)$$

The reciprocal relationship that the power transmitted from subsystem i to j is minus the power from j to i can be combined with Equation (24) to obtain the result:

$$\eta_{ij} n_i = \eta_{ji} n_j \quad (25)$$

This relationship is very useful when calculating the coupling loss factor, since it is sometimes easier to calculate one of the coupling loss factors, η_{ij} or η_{ji} .

The time-average power dissipated within a group of modes can also be related to the total energy in the group and a loss factor. By definition of a damping loss factor, the time-average dissipated power in a band of frequencies is given by:

$$W_{\text{diss}}^{(i)} = \omega \eta_i E_{i,\text{tot}} \quad (26)$$

where η_i is the damping loss factor. Equation (26) is usually rewritten as

$$W_{\text{diss}}^{(i)} = \omega \eta_i n_i \left[\frac{E_{i,\text{tot}}}{n_i} \right] \quad (27)$$

so that it is in the same form as Equation (24).

If Equations (24) and (27) are used in the power balance equations, a set of linear algebraic equations can be obtained. For the system in Figure 18 these become:

Subsystem 1: Bending modes of the beam member:

$$n_1(\eta_1 + \eta_{13} + \eta_{14}) \frac{E_{1,tot}}{n_1} - n_1 \eta_{13} \frac{E_{3,tot}}{n_3} - n_1 \eta_{14} \frac{E_{4,tot}}{n_4} = W_{in}^{(1)} w \quad (28)$$

Subsystem 2: Torsional modes of the beam member:

$$n_2(\eta_2 + \eta_{23} + \eta_{24}) \frac{E_{2,tot}}{n_2} - n_2 \eta_{23} \frac{E_{3,tot}}{n_3} - n_2 \eta_{24} \frac{E_{4,tot}}{n_4} = 0 \quad (29)$$

Subsystem 3: Bending modes of the panel:

$$-n_3 \eta_{31} \frac{E_{1,tot}}{n_1} - n_3 \eta_{32} \frac{E_{2,tot}}{n_2} + n_3(\eta_3 + \eta_{31} + \eta_{32} + \eta_{34}) \frac{E_{3,tot}}{n_3} - n_3 \eta_{34} \frac{E_{4,tot}}{n_4} = 0 \quad (30)$$

Subsystem 4: Acoustic space modes:

$$-n_4 \eta_{41} \frac{E_{1,tot}}{n_1} - n_4 \eta_{42} \frac{E_{2,tot}}{n_2} - n_4 \eta_{43} \frac{E_{3,tot}}{n_3} + n_4(\eta_4 + \eta_{41} + \eta_{42} + \eta_{43}) \frac{E_{4,tot}}{n_4} = 0 \quad (31)$$

The sample system of Figure 18, which likely involves many hundreds of resonant structural and acoustical modes, requires only four independent subsystem energies in the SEA model of its dynamic behavior. The above equations are linear and algebraic and are readily solved by standard computational procedures once the SEA parameters have been determined for each subsystem in the frequency band of interest. The SEA parameters include the mode density and coupling and damping loss factors.

The application of SEA to more complicated systems can require a model with many groups of modes. The concept of time-average power balance and the relationship between power and energy variables continue to be valid. Solution of the power balance equations can be tedious. However, by use of numerical matrix inversion routines with a small digital computer, a solution can be easily obtained even for very large systems.

The simplicity of the SEA power balance equations is the major advantage of using an SEA model. Once the model has been set up and analytical expressions have been obtained for the required power inputs, loss factors, and modal densities, solutions can be quickly obtained for a variety of different design configurations.

In the following sections more advanced aspects of SEA modeling will be developed, with emphasis on solving practical problems involving typical mechanical structures and acoustic spaces.

The SEA matrix equation. - The SEA model allows the dynamics of a complex system to be described by a series of linear algebraic equations. The equations for the particular system in Figure 1 are straightforwardly extended for general systems. Each equation for the general system is obtained by balancing the time-average vibratory power input to a group of modes of vibration having resonance frequencies within a band $\Delta\omega$ with the sum of the time-average power transmitted to other groups of modes and the time-average power dissipated within the group. The time-average power variables are given by the following expressions:

Input Power Spectrum	$w_{in}^{(i)}$
Dissipated Power	$\omega\eta_i E_{i,tot}$
Transmitted Power to Mode Group j	$\omega\eta_{ij} n_i \left[\frac{E_{i,tot}}{n_i} - \frac{E_{j,tot}}{n_j} \right]$

where $w_{in}^{(i)}$ is the total time-average power input to all modes in the group from all sources external to the system, n_i is the modal density for the group, ω is the band center frequency, η_i is a dissipation loss factor for the modes, $E_{i,tot}$ is the total time-average energy of all modes in the group, and η_{ij} is a coupling loss factor describing the net time-average power transmitted from group i to group j.

Power balance for the i-th group of modes within a large system containing a total of m mode groups results in the equation

$$n_i \left(\eta_i + \sum_{\substack{j=1 \\ j \neq i}}^m \eta_{ij} \right) \left(\frac{E_{i,tot}}{n_i} \right) - n_i \sum_{\substack{j=1 \\ j \neq i}}^m \eta_{ij} \left(\frac{E_{j,tot}}{n_j} \right) = \frac{1}{\omega} S_{w_i}(\omega) \quad (32)$$

The matrix equation obtained from Eq. (32) is not symmetric. However, by observing that the net time-average power transmitted from group i to j must equal the negative of the time-average power transmitted from j to i , the following reciprocity relationship can be written:

$$n_i \eta_{ij} = n_j \eta_{ji} \quad (33)$$

This relationship can be used to obtain a symmetric matrix relating the energy per mode in each group to the input power. The linear set of equations can then be written as

$$\begin{bmatrix} n_1 \eta_{11} & -n_2 \eta_{21} & -n_3 \eta_{31} & \dots & \dots & -n_m \eta_{m1} \\ -n_2 \eta_{21} & n_2 \eta_{22} & -n_3 \eta_{32} & \dots & \dots & \dots \\ -n_3 \eta_{31} & -n_3 \eta_{32} & n_3 \eta_{33} & \dots & \dots & \dots \\ \dots & \dots & \dots & \dots & \dots & \dots \\ \dots & \dots & \dots & \dots & \dots & \dots \\ -n_m \eta_{m1} & \dots & \dots & \dots & \dots & n_m \eta_{mm} \end{bmatrix} \begin{pmatrix} \frac{E_{1,tot}}{n_1} \\ \bullet \\ \bullet \\ \bullet \\ \bullet \\ \frac{E_{m,tot}}{n_m} \end{pmatrix} = \begin{pmatrix} \frac{W_{in}^{(1)}}{\omega} \\ \bullet \\ \bullet \\ \bullet \\ \bullet \\ \frac{W_{in}^{(m)}}{\omega} \end{pmatrix} \quad (34)$$

where the total loss factor η_{ii} is defined as

$$\eta_{ii} = \eta_i + \sum_{\substack{j=1 \\ j \neq i}}^m \eta_{ij} \quad (35)$$

The coupling matrix $\underline{n_i \eta_{ij}}$ can be inverted using an appropriate numerical technique and then used to compute the modal energies, $E_{i, tot}/n_i$. These, in turn, can be used to calculate the desired response variables for different regions of the complex dynamic system being studied.

For large dynamic systems, where many mode groups or subsystems are needed, the matrix of loss factors will be sparsely populated with most η_{ij} equal to zero. This result depends on the degree of interconnectedness between the subsystems. The subsystems should be numbered so that non-zero terms in the matrix are as near as possible to the main diagonal. It is then possible to use specialized matrix inversion procedures to solve for the modal energies with a minimum of computational effort.

SEA parameters. - Previous sections have discussed the power balance equations of SEA in describing the fundamental approach. This section gives general procedures for evaluating the parameters in the SEA equations including the mode density and damping and coupling loss factors. Reference [17] by Lyon is also a valuable source of information for evaluating the SEA parameters, and contains an extensive listing of the open literature dealing with all aspects of SEA. A subsequent section describes the use of these expressions for the particular SEA model of the Sikorsky S-76.

Mode count for acoustical and structural subsystems. - The mode count describes the number of resonant modes of the subsystem that participate in the energy storage and transmission in a given frequency band. Three techniques exist for obtaining the mode count. One technique is to carry out a laboratory experiment in which a model structure is excited by a slowly-swept sine wave tone. Resonances are then counted in the form of response peaks in the frequency band of interest.

A second technique is to use a finite element analysis to obtain the resonance frequencies. This technique is feasible but not commonly used because of the cost and time to set up the finite element model for high frequencies where many modes of vibration must be considered.

The most common technique is to use analytical expressions that have been obtained for many structural elements and acoustic spaces. Expressions exist for beams, pipes, plates, cylindrical shells, spherical shells, and acoustic spaces. In many cases it is possible to model a complex structure in terms of these simple components and thereby use the analytical mode count.

The analytical expressions are given in terms of a mode density, $n(\omega)$, or average number of modes per unit frequency. Resonant modes of structures occur at discrete frequencies, and, therefore, a counting of the number of modes in a particular frequency band will exhibit step discontinuities as additional modes are included in the band. The analytical expressions for the mode density are smoothed estimates of the number of modes in the band.

The mode count N_i is evaluated from the mode density $n_i(\omega)$ according to the following:

$$N_i = \int_{\omega_0 - \Delta\omega/2}^{\omega_0 + \Delta\omega/2} \omega n_i(\omega) \quad (36)$$

In most cases the modal density is a fairly smooth function of frequency relative to the bandwidth of interest so that

$$N_i \cong n_i(\omega_0)\Delta\omega \quad (37)$$

The analytical expression for the mode density is derived for ideal structures having ideal boundary conditions and precisely accounts for the location and distribution of the resonant modes of such structures. Real structures are characterized by non-ideal boundary conditions and random non-uniformities in the structure itself. These act to shift the resonance frequencies in comparison with those of the ideal structure.

Although the mode density expression for the ideal structure is unlikely to give the correct number of modes for the actual structure, it does give a best estimate. That estimate is more accurate for broadband excitation at high frequencies where the number of modes is predicted to be large. At lower frequencies or for narrow band or pure tone excitation the uncertainties in the mode density and SEA estimates of the system response are greater.

Acoustical spaces can behave as one, two, or three-dimensional structures depending on the wavelength of sound at the frequency of interest relative to cross-sectional dimensions of the space. Cylindrically shaped volumes where the maximum cross-sectional dimension is less than the wavelength of sound are modeled as one-dimensional spaces. The mode density depends only on the length of the space, ℓ , and the speed of sound, c_0 .

$$n_{a,1}(\omega) = \ell / (\pi c_0) \quad (38)$$

Thin, flat volumes where the thickness is less than an acoustic wavelength are modeled as two-dimensional spaces. The mode density is given by,

$$n_{a,2}(\omega) = A\omega / (2\pi c_0^2) + P / (2\pi c_0) \quad (39)$$

where A is the area of the space and P the perimeter around the area. The mode density for a three-dimensional acoustic space is given by

$$n_{a,3}(\omega) = \omega^2 V / (2\pi^2 c_0^3) + \omega S / (8\pi c_0^2) + P / (16\pi c_0) \quad (40)$$

where V is the volume, S the surface area, and P the total edge length for the space.

Several types of deformation are of importance for structural subsystems including longitudinal, torsional, and flexural motions. The propagation wavespeeds for each are different. For longitudinal and torsional deformations the wavespeeds are constant with frequency, as is the case for the propagation of sound. Such systems are referred to as being non-dispersive. For one-dimensional systems the expression for sound propagation applies with the sound speed set equal to the appropriate value for longitudinal or torsional motion,

$$n_{s,1}(\omega) = \ell / (\pi c) \quad (41)$$

where for longitudinal motion in rods,

$$c = \sqrt{E/\rho} \quad (42)$$

E = Young's modulus

ρ = density

whereas for torsional motion of straight bars,

$$c = \sqrt{GJ / (\rho I_p)} \quad (43)$$

G = shear stiffness

J = torsional moment of rigidity

I_p = polar moment of inertia of the cross-section

The expression in Eq. (43) accounts for warping of the cross-section of the bar under torsion. For bars of circular cross-section no warping occurs and the moment of rigidity, J , equals the polar moment of inertia, I_p . The torsional wavespeed equals the shear wavespeed for the material.

The moment of rigidity, J , is discussed in references on the strength of materials [18]. A useful formula for approximating J is given by

$$J = \frac{4}{\frac{1}{I_x} + \frac{1}{I_y}} \quad (44)$$

where I_x and I_y are moments of inertia of the cross-section about the x and y axes. The polar moment of inertia of the cross-section, I_p , equals

$$I_p = I_x + I_y \quad (45)$$

For a square rectangular bar of side A the moment of rigidity is:

$$J = \frac{A^4}{6}, \quad I_x = I_y = \frac{A^4}{12} \quad (46)$$

For a narrow rectangular bar J becomes

$$J = \frac{ba^3}{3} \quad (47)$$

b = long dimension

a = short dimension

It is interesting to note for the narrow rectangular bar that as a result of warping, the torsional rigidity is significantly reduced. With no warping $J = I_p$, and the ratio of the torsional moment of rigidities accounting for warping relative to the no-warping condition becomes:

$$\frac{J_{\text{warping}}}{J_{\text{no-warping}}} = \frac{4a^2}{b^2} \ll 1 \text{ for } I_x \gg I_y \text{ or } b \gg a \quad (48)$$

For aircraft or helicopter structures vibration transmission involving torsional motion of frame members is often important. The frames may be made from angles, channels, or I-beams. The moments of rigidity for these structures can be evaluated using the expression for the narrow rectangular bar. The frame is divided into rectangular sections, and the moment of rigidity is approximated as the sum of the moments of rigidity for the individual rectangular sections. Alternatively the moment of rigidity can be evaluated from Eq. (44) directly where I_x and I_y apply for the full cross-section.

For bending or flexural wave propagation in beams and plates the wavespeed is a function of frequency:

$$c_b = \sqrt{k_r c_l^2 \omega} \quad (49)$$

k_r = radius of gyration
of cross-section

c_l = longitudinal wave
speed in material

For a narrow beam:

$$c_b = \sqrt{E/\rho} \quad (50)$$

For a plate:

$$c_{\ell}^1 = \sqrt{E/[\rho(1-\sigma^2)]}$$

$$\sigma = \text{Poisson's ratio} \quad (51)$$

E = Young's modulus

$$\kappa_r^2 = h^2/12$$

$$\rho = \text{density} \quad (52)$$

h = height of cross-section

For dispersive systems where the wavespeed is a function of frequency the mode density is evaluated from the following expressions:

For a one-dimensional structure of length ℓ :

$$n_{s,1}(\omega) = \frac{\ell}{\pi c} \left(1 - \frac{\omega}{c} \frac{dc}{d\omega}\right) \quad (53)$$

and for a two-dimensional structure of area A:

$$n_{s,2}(\omega) = \frac{A\omega}{2\pi c^2} \left(1 - \frac{\omega}{c} \frac{dc}{d\omega}\right) \quad (54)$$

For beams or plates these yield, along with Eqs. (50) - (54) the following equations:

For a beam

$$n_{\text{beam}}(\omega) = \frac{\ell}{2\pi c_b} \quad (55)$$

and for a plate

$$n_{\text{plate}}(\omega) = \frac{A}{4\pi \kappa_r c_{\ell}^1} \quad (56)$$

Damping loss factor. - The damping loss factor scales the power dissipated within a subsystem relative to the stored energy.

$$W_{\text{diss}}^{(i)} = \omega \eta_i E_{i,\text{tot}} \quad (57)$$

where η_i is the damping loss factor and $E_{i,\text{tot}}$ is the stored energy. Sources of damping include the dissipation mechanisms within the bulk materials of the subsystem, dissipation occurring at the structural connections and that due to add-on damping treatments. An additional source for some problems is the acoustic energy radiated by vibrating structures which is otherwise not accounted for in the SEA model.

Material damping involves a variety of mechanisms at the molecular level. For metals the mechanisms include thermal conduction, grain boundary motion, molecular site transition, and dislocation oscillation [17]. Aluminum alloys used in aircraft structures have damping values in the range from 0.002 to .2 where the larger values occur for cast iron and special alloys of manganese and copper. Softer polymeric materials have values in the same range. Still softer elastomeric materials have higher loss factors ranging from .1 to .5.

Elastomeric materials are used as components in add-on damping treatments. Such treatments can effectively increase the damping of the panel to which they are added. They are typically used either in the form of free extensional or constrained layer treatments. Their effectiveness depends on the material properties of the base panel and damping treatment as well as geometric factors including the thicknesses of the different layers. Useful analytic estimates of composite damping loss factors with the add-on treatments may be found in Reference [19].

As a result of thermodynamic relaxation processes within elastomeric materials, their damping and elastic properties are functions of both temperature and frequency. Manufacturers of add-on treatments typically design materials for use in particular frequency and temperature ranges. Design charts are provided for determining composite loss factors for the treatments when added to different thickness panels.

For untreated panels typical of built up aircraft structures the damping values are generally larger than the values for the metal itself as a result of damping due to riveted connections, attached fixtures, etc. Damping values for built up structures are known to have a broad range of values near .01.

Two theories are proposed to explain the greater damping for riveted structures. One theory is based on a surface slip model and involves plastic deformation of the contact asperities of the joined surfaces. A gas pumping mechanism is proposed as the source of the dissipation for the other theory [20]. Viscous losses are generated as gas in the gap between the contacting surfaces is pumped back and forth by the vibration of the surfaces. The air pumping mechanism has been shown to provide damping estimates consistent with measured values for riveted aerospace structures.

The distribution of damping levels throughout the structure is important in establishing the vibration response levels. Add-on damping treatments are often a first approach in designing for reduced vibration transmission and noise. The lack of precision that exists in estimating damping loss factors is a significant problem for all vibration analysis techniques including SEA.

Damping in acoustic subsystems occurs as a result of wall or air absorption. Air absorption involves the conversion of acoustic energy into heat as sound propagates through air. For smaller acoustic spaces in the audio frequency range air absorption is not typically significant in comparison with wall absorption.

Wall absorption refers to the decrease in energy of the sound wave on reflection off the walls of the acoustic space. For SEA models that include the resonant modes of the wall structure or of an adjacent acoustic space on the other side of the wall structure, the energy transmitted to these modes is not included as dissipation in the source space but is accounted for by a coupling loss factor. Wall absorption accounts only for the energy dissipated at the wall surface as a result of viscous losses and the flow resistance of the wall. Absorbing wall treatments in the form of carpets or fiberglass blankets contribute to the wall absorption.

When the resonant modes of the walls and adjacent acoustic spaces are not included in the SEA model, the energy transmitted into the wall structure and through it to the adjacent acoustic space is then accounted for as dissipation in the source space.

The damping loss factor for an acoustic space is related to the average wall absorption coefficient, $\bar{\alpha}$, is as follows:

$$\eta = \frac{c_o S}{8\pi V f} \bar{\alpha} \quad (58)$$

where

c_0 = speed of sound

S = total wall surface area in the space

V = volume of the space

f = frequency Hz

The weighted absorption coefficient is determined from an area weighted average of the absorption coefficients for individual surfaces in the space:

$$\bar{\alpha} = \frac{1}{S} \sum_i S_i \alpha_i \quad (59)$$

where

S_i = area of individual surface

α_i = absorption coefficient for individual surface

In most practical situations, particularly those involving absorbing wall treatments, the energy dissipated at the wall is significantly greater than the energy transmitted through the wall to an adjoining acoustic space or into the resonant modes of the wall structure. Reverberation time measurements then provide an accurate estimate of the energy dissipated at the walls. The measured damping loss factor according to Eq. (58) can, therefore, be used directly to represent the energy dissipation in the SEA equation for the acoustic space.

Often in carrying out an SEA prediction one is interested in evaluating the effect of an added absorbing treatment in an acoustic space. Data on existing treatments is generally in the form of an absorption coefficient for the material. The new damping loss factor for the space with the absorbing wall treatment is evaluated from Eqs. (58) and (59). The treated area, S_t , is characterized by the absorption coefficient for the added absorbing material, α_t . The untreated area, S_{ut} , is characterized by the average absorption for the untreated space, α_{ut} :

$$\bar{\alpha}_t = \frac{S_{ut} \alpha_{ut} + S_t \alpha_t}{S_{ut} + S_t} \quad (60)$$

The damping loss factor with the treatment is then evaluated from Eq. (58).

Coupling loss factor. - The coupling loss factor (CLF) is unique to SEA. It characterizes the dynamic behavior at the junctions between connected structural and acoustical subsystems of the overall model. Specifically the coupling loss factor determines the power flow across the junction relative to the stored energy of the source subsystem. The calculation of coupling loss factors can be the most complicated analytical step in SEA, and, therefore, requires greater experience and understanding of the dynamic behavior of mechanical and acoustical systems.

The coupling loss factor is important in determining the distribution of vibratory energy levels amongst the different subsystems. For a system with uniformly distributed damping levels the vibratory energy levels will be greater near the source for the case where the subsystems are weakly coupled, that is when the coupling loss factors are small. For large CLF's vibratory energy is distributed more uniformly throughout the structure.

The most common procedure for analytically evaluating the CLF is to replace the connected structures with semi infinite structures while maintaining the same junction geometry. The power transmitted across the junction is evaluated for travelling wave incidence in the source subsystem. The ratio of the transmitted power to the incident power in the travelling waves defines a transmission coefficient, τ .

$$\tau = \frac{\Pi_{trans}}{\Pi_{inc}} \quad (61)$$

For one-dimensional systems such as frames which deform in bending or torsion the transmission coefficient is related to input impedances for the connected subsystems according to:

$$\tau_{1,2} = \frac{4\text{Re}(Z_1) \text{Re}(Z_2)}{|\sum_i Z_i|^2} \quad (62)$$

where

Z_1, Z_2 = input impedance of source,
receiving subsystem

$\sum_i Z_i$ = sum of input impedances at the
junction for all attached
subsystems including source and
receiving subsystems

The impedances are either for force or moment inputs depending on the geometry and the type of motion allowed at the junction. The above expression applies when the transmission is due only to a single type of junction motion, either angular rotation or linear translation.

Accounting for the difference between the transmission coefficient (where the transmitted power is proportional to an incident power) and the coupling loss factor (where it is proportional to the stored energy) results in the following expression:

$$\eta_{1,2} = \frac{c_g}{2\omega\ell} \tau_{1,2} \quad (63)$$

where c_g = group velocity for the particular type of motion

$c_g = 2c_b$ for bending waves

$c_g = c_t$ or c_ℓ for torsional or longitudinal motion

ℓ = length of one-dimensional subsystem

With Eqs. (41) or (55) and (62), Eq. (63) becomes

$$\eta_{1,2} = \frac{2}{\pi \omega n_1} \frac{\text{Re}(Z_1) \text{Re}(Z_2)}{|\sum_i Z_i|^2} \quad (64)$$

n_1 = mode density of source subsystem

Eq. (64) is in a convenient form for evaluating the coupling loss factor. Expressions for the mode density of the source subsystem are readily available for a variety of subsystem types. The input impedances are also readily available for many common subsystems. For example reference [21] presents expressions for rods (longitudinal motion) and beams and plates for both force and moment inputs.

For subsystems connected along a line such as occurs between plate subsystems the transmission coefficient is a function of the angle of the incident energy with respect to the junction. The relationship between the coupling loss factor and transmission coefficient, therefore, involves an average over the incidence angle [17]:

$$\eta_{1,2} = \frac{c \ell'}{2\omega A_s} \langle \tau(\theta) \cos \theta \rangle \quad (65)$$

where

$\langle \rangle$ denotes the average over angle

ℓ' is the length of the line junction between the subsystems

θ is the angle of incidence

A_s is the area of the source subsystem

Acoustic spaces are coupled to each other and to bounding panel surfaces over an area. The relationship between the transmission coefficient between two acoustic spaces and the coupling loss factor is

$$\eta = \bar{\tau} \frac{c_o A_w}{4\omega V_s} \quad (66)$$

where

A_w = the area of the wall connecting the spaces

V_s = volume of the source space

$\bar{\tau}$ = average transmission coefficient which is related to the standard transmission loss (TL) of the panel by

$$TL = -10 \text{ Log}_{10} (\bar{\tau}) \quad (67)$$

Measured data for the transmission loss of panels is directly applicable for determining the coupling loss factor according to Eqs. (66) and (67).

The coupling between panel structures and adjacent acoustic spaces is characterized by the radiation efficiency, σ_{rad} , as opposed to a transmission coefficient. This occurs in general for the coupling between subsystems which differ by one in the number of dimensions that describe the subsystem. A panel is a two-dimensional subsystem while an acoustic space involves three dimensions. The coupling loss factor and radiation efficiency are related by

$$\eta_{1,2} = \frac{\rho c A_p}{w M_p} \sigma_{rad} \quad (68)$$

where

ρc = characteristic impedance of the acoustic medium

A_p = area of radiating panel

M_p = total mass of radiating panel

An analytical expression for the radiation efficiency of panels is given in the section on acoustic/aerodynamic sources. The reciprocal relationship for coupling loss factors is conveniently used to determine the coupling loss factor between an acoustic space and a panel:

$$\eta_{2,1} = \frac{n_1 \eta_{1,2}}{n_2} \quad (69)$$

Power input evaluation. - The SEA equations describe the power exchange between subsystems of the SEA model. The inputs to the model are the power inputs to the subsystems through contacts with external sources. A direct measurement of the power inputs under actual operating conditions is usually very difficult although new techniques such as acoustic intensity measurements offer some promise. The usual approach is to measure the vibration or pressure levels at the contact points under actual operating conditions and then to relate these measured levels to the power inputs through calculated or measured input impedances.

The time-average power input to a group of modes can be evaluated in two ways. First, it can be done on a mode-by-mode basis. Second, it can be done using input impedances. The impedance approach can be carried out analytically or using measured impedance data. The following material will show that the modal and impedance approaches lead to the same result.

Following the mode-by-mode approach, the equation of motion for a single mode is

$$\ddot{u}_i + \eta_i \omega_i \dot{u}_i + \omega_i^2 u_i = \frac{1}{M} f_i(t) \quad (70)$$

where $u_i(t)$ is the modal response, M is the system mass, η_i is a viscous damping loss factor, ω_i is the resonance frequency, and $f_i(t)$ is the modal force given by

$$f_i(t) = \int d\mathbf{x} \vec{s}(\mathbf{x}, t) \cdot \vec{\psi}_i(\mathbf{x}) \quad (71)$$

where $\vec{s}(\mathbf{x}, t)$ is the vector stress acting on the system from external sources, and $\vec{\psi}_i(\mathbf{x})$ is the mode shape, and the integral is over the spatial extent of the system. In the case where the modal force is broadband random stationary time history with a flat spectral density, the power input to mode i is given by

$$w_{in}^{(i)} = \frac{\pi}{2} \frac{S_{f_i}}{M} \quad (72)$$

where S_{f_i} is the spectral density. The time-average power input to a group of modes is found by summing over the group

$$W_{in} = \sum_i \frac{\pi}{2} \frac{1}{M} S_{f_i} \quad (73)$$

Equation 73 can be rewritten as

$$W_{in} = \frac{\pi}{2} \frac{N}{M} \overline{S_{f_i}} \quad (74)$$

where N is the number of modes in the group and $\overline{S_{f_i}}$ is an average over the group.

If an ensemble of systems is defined in which the resonance frequencies are distributed randomly, the number of modes, N , in a frequency band, $\Delta\omega$, can be written in terms of the modal density, $n(\omega)$, as

$$N = n(\omega) \Delta\omega \quad (75)$$

The power input in that frequency band is then given by

$$W_{in}(\omega) = \frac{\pi}{2} \frac{n(\omega)}{M} \overline{S_{f_i}}(\omega) \Delta\omega \quad (76)$$

where ω is the band center frequency.

For the case where the excitation is a point force, the spectrum of the modal force becomes

$$S_{f_i} = \psi_i^2(x_0) S_f \quad (77)$$

where x_0 is the location at which the force is applied and S_f is the spectrum of the applied force. The average over the group becomes

$$\overline{S_{f_i}} = \overline{\psi_i^2(x_0)} S_f \quad (78)$$

where $\bar{\psi}_1^2$ is the value of the mode shape squared at location \underline{x}_0 averaged over all modes in the group.

In systems where the mass density is uniform, the value of $\bar{\psi}_1^2$ tends towards one as the number of modes in the group increases. However, at points near boundaries to the system, the value of $\bar{\psi}_1^2$ may be significantly above or below one.

If the concept of an ensemble of systems is expanded to include systems in which the point of application of the force is a random variable over the spatial extent of the system, it can be formally shown that the average of $\psi_1^2(\underline{x}_0)$ over the ensemble is one. In cases where the mode shapes are not known, this result is useful and is commonly a part of a SEA model. The power input for this case can be written from Eq. (76) as

$$W_{in} = \frac{\pi}{2} \frac{n(\omega)}{M} S_f \Delta\omega \quad (79)$$

The formulation above can be expanded to include cases where the excitation includes moments and multiple excitation points. It can also include a distributed excitation along a line or over a surface. For example, the formulation can be expanded to include a distributed excitation due to a turbulent boundary layer or acoustic pressure field.

For the case in which a two dimensional structure is excited by a distributed pressure field, the spectrum of the modal force becomes

$$S_{f_i} = \int d\underline{x}_1 \int d\underline{x}_2 S_{p(\underline{x}_1) p(\underline{x}_2)} \psi_i(\underline{x}_1) \psi_i(\underline{x}_2) \quad (80)$$

where $S_{p(\underline{x}_1) p(\underline{x}_2)}$ is the cross-spectrum of the pressures at \underline{x}_1 and \underline{x}_2 and the integrals are over the spatial extent of the structure. If, in addition, the excitation is homogeneous in space, the cross-spectrum depends only on the difference $\underline{x}_1 - \underline{x}_2$ and Equation (80) can be written

$$S_{f_i} = \int d\underline{k} S_p(\omega, \underline{k}) |\psi_i(\underline{k})|^2 \quad (81)$$

where $S_p(\omega, \underline{k})$ is the Fourier transform of the cross-spectrum, k is the wave number spectrum of the pressure field, and $|\psi_i(\underline{k})|^2$ is the magnitude-squared of the Fourier transform of the mode shape $\psi_i(\underline{x})$.

The formulation represented by Equation (81) is particularly useful in calculating the power input from an acoustic pressure field or turbulent boundary layer pressure fluctuations. It can be used directly in Eq. (73) to obtain the power input or an average can be taken over the modes, and the average spectrum of the modal force can be used in Equation (76) to obtain a statistical estimate of the power input.

The impedance (or mobility) approach can be most easily demonstrated when the excitation is a point force. When a single-frequency, pure-tone force with complex amplitude, F , is applied at a point \underline{x}_0 , the response velocity, V , is by definition

$$V = \frac{F}{Z(\omega, \underline{x}_0)} \quad (82)$$

where $Z(\omega, \underline{x}_0)$ is the driving point impedance. The time-average power input is equal to

$$W_{in} = \frac{1}{2} \text{Re } FV^* \quad (83)$$

where Re signifies "the real part of". Combining Eqs. (82) and (83) yields

$$W_{in} = \frac{1}{2} |V|^2 \text{Re } Z(\omega, \underline{x}_0) \quad (84)$$

or

$$W_{in} = \frac{1}{2} |F|^2 \text{Re} \frac{1}{Z(\omega, \underline{x}_0)} \quad (85)$$

When the excitation is a random process, the force and velocity variables in Eqs. (84) and (85) can be replaced by spectra so that the power input in a band of frequencies $\Delta\omega$ is given by

$$W_{in} = \int_{\Delta\omega} d\omega S_v(\omega) \operatorname{Re} Z(\omega, x_0) \quad (86)$$

or

$$W_{in} = \int_{\Delta\omega} d\omega S_f(\omega) \operatorname{Re} \frac{1}{Z(\omega, x_0)} \quad (87)$$

where the integral is over the band $\Delta\omega$.

The variables in Eq. (86) can often be measured. The easiest measurement involves the velocity. Measurement of forces requires that a force gauge or load cell be inserted between the source and subsystem during operation. This may not be feasible as, for example, in the case of the gearbox connection to the airframe of a helicopter.

The input impedance of a structure can be determined from measurements on the structure through use of an impedance head. This is a device which attaches to the structure and measures simultaneously both the applied force and acceleration (velocity) at the contact point. A shaker is used in conjunction with the impedance head to generate the applied force. It is usually not necessary for the level of the excitation to equal that of the actual source, since the assumption of dynamic linearity is almost always valid. However, in some cases it is necessary to apply the same static load to the structure so that the measured impedance is equal to that seen under operating conditions.

The voltage excitation to the shaker can be in the form of a sinusoid at discrete frequencies or a broadband random noise signal. In the former case the sine wave is swept over the desired frequency band. The relative amplitudes and phase of the forces and acceleration signals are monitored to give the desired impedance. For the broadband excitation the outputs are processed digitally by sampling the random signals and then evaluating the impedance in terms of Fourier transforms of the sampled signals.

The power flow is dependent on only the real component of the impedance or mobility (inverse of impedance). In cases where the reactive or imaginary component of impedance is large compared to the real component, the accuracy of the measured value of the real component is reduced.

In the absence of accurate impedance measurements, analytical expressions for the input impedance can be used with measured velocities (or forces) to determine the input power.

The input impedance can be calculated using a modal formulation or by solving the differential equations of motion. However, when the subsystem being excited is coupled to a number of other subsystems, an exact calculation of the impedance becomes formidable. However, as is the case of using the modal approach to calculate power input, a statistical approach can be used. It is known from the theory of room acoustics that the real part of the admittance (reciprocal of impedance) for a point volume velocity source in a large room is equal to the admittance of an infinite acoustic space. The relationship between the real part of the admittance of a finite system and that for an infinite system exists for any dynamic system under the following conditions:

- a) when many modes contribute to the response at a single frequency, or
- b) an average is taken over a band of frequencies containing many resonances, or
- c) an average is taken over all possible locations of the excitation.

With this result the power input from Eq. (86) can be written

$$W_{in} = S_f(\omega) \operatorname{Re} \frac{1}{Z_{inf}(\omega)} \Delta\omega \quad (88)$$

where Z_{inf} is the impedance of the infinite system, provided that $S_f(\omega)$ and $Z_{inf}(\omega)$ are constant over the band $\Delta\omega$.

Although it is not immediately obvious, Eq. (88) is identical to Eq. (79). For example, if the system being excited is a flat plate, the impedance is given by [22]

$$Z_{inf. \text{ plate}} = 8m_s \kappa c_\ell \quad (89)$$

where m_s is the surface density (mass per unit area), κ is the bending radius of gyration, and c_ℓ is the longitudinal wavespeed. The modal density for a flat plate is given by

$$n(\omega) = \frac{A}{4\pi\kappa c_\ell} \quad (90)$$

where A is the area of the plate. It is left as an exercise for the reader to show that Eqs. (79) and (88) are equal with these expressions.

An extension of the impedance approach to cases in which the excitation includes moments and/or excitation by coherent sources at multiple points becomes a good deal more complicated. However, use of the statistical concepts introduced earlier makes these extensions possible and many special cases have been worked out.

Up to this point, the excitation has been a stationary random process with a flat or white spectrum. In cases where the spectrum is broadband and varies slowly over frequency, a white spectrum gives a good approximation to the time-average power input to a single mode as long as the spectrum is flat over the resonant response bandwidth.

If the excitation is at a single frequency, the time-average power input can be derived from Equation (32) as

$$W_{in}^{(i)} = \frac{1}{2} |F_i|^2 \frac{1}{M} \frac{\omega_i^2 \eta_i \omega_i}{(\omega_i^2 - \omega^2)^2 + \omega_i^2 \eta_i^2 \omega_i^2} \quad (91)$$

where F_i is the complex amplitude of the modal force and ω is the radian frequency of the excitation. The power input to a group of modes is found by summing over the modes.

$$W_{in} = \sum_i W_{in}^{(i)} \quad (92)$$

Equation (92) can be evaluated exactly in cases where the resonance frequencies and damping loss factors are known. However, if the modes are coupled to modes of other systems, which is usually the case, the resonance frequencies are shifted and the damping loss factors must be changed to account for the apparent damping due to energy transmitted to other modes. Evaluation of the resonance frequencies and damping loss factors in the coupled system requires solution of the entire system equations of motion which negates the simplicity of the SEA model. In addition, the accuracy of the computed resonance frequencies and loss factors is often poor because the system cannot be described with sufficient detail.

A statistical approach simplifies the problem. If an ensemble of systems are defined in which the resonance frequencies are randomly distributed with a uniform probability distribution, the power input to a single mode i averaged over the ensemble is given by

$$\bar{w}_{in}^{(i)} = \frac{\pi}{2} \frac{1}{M} \frac{1}{2} |F_i|^2 \quad (93)$$

where $\bar{w}_{in}^{(i)}$ is an average over the ensemble. This equation is similar to Equation (72) with the spectrum of the random modal force replaced by the amplitude squared of the pure tone modal force. This result allows an SEA model to be used for pure tone excitation.

An alternative to the calculation of input power involves measurements of the energies of the directly excited subsystem under actual operating conditions. In that an evaluation of the input power involves a measurement of applied force or resulting point velocity, it is often as convenient to simply measure the response energy levels in the directly excited subsystem.

For gearbox airborne noise it may be convenient to measure the pressure levels in the space surrounding the gearbox as opposed to measuring vibration levels on the gearbox casing from which the radiated acoustic power is inferred based on an estimate of the radiation efficiency. Where structural attachments unambiguously involve a single subsystem, the measured response of that subsystem may more appropriately characterize the source than measuring the attachment point velocity or force and estimating the power based on the modal or impedance approaches.

For either acoustical or structural subsections the measured space-time average response levels are used to determine the subsystem energy. For acoustical subsystems the total energy is given by:

$$E_{tot}^{ac} = V * D \quad (94)$$

where V is the volume of the space and D is the energy density

$$D = \langle p^2 \rangle_x / (\rho c^2) \quad (95)$$

and $\langle p^2 \rangle_x$ is the space average mean square pressure in the space.

For structural subsystems

$$E_{\text{tot}}^{\text{str}} = M \langle v^2 \rangle_x \quad (96)$$

where M is the total mass of the subsystem and $\langle v^2 \rangle_x$ is the space average mean square velocity response level.

The power balance equations for the directly excited subsystems are simply removed from the overall SEA matrix equation since the subsystem energies for these have been determined from measured response levels. The terms proportional to the measured subsystem energies in the remaining power balance equations are moved to the right hand side of the equations and become source terms in solving for the system response levels.

System response evaluation. - The solution of the SEA matrix equations yields the modal energies for the subsystems of the model. The total energy in each subsystem is simply obtained from the modal energy and mode density according to:

$$E_{i,\text{tot}} = \left(\frac{E_{i,\text{tot}}}{n_i} \right) n_i(\omega) \quad (97)$$

where the quantity in parenthesis is the modal energy.

The total energies can be expressed in terms of physical quantities according to the following for structural and acoustical subsystems:

Acoustical subsystems:

$$\langle p_i^2 \rangle_x = \left(\frac{E_{i,\text{tot}}}{n_i} \right) \frac{\omega^3 \rho}{2\pi^2 c_o} \quad (98)$$

where $\langle p_i^2 \rangle_x$ is the space average mean square pressure in the space. This result occurs when the volume term in the expression for the mode density of an acoustic space, Eq. (40), is considerably larger than the other terms.

Structural subsystems:

$$\langle V_i^2 \rangle_x = \left(\frac{E_{i,tot}}{n_i} \right) \frac{n_i}{M_i} \quad (99)$$

where

n_i = mode density for structural subsystem

M_i = total mass of subsystem

$\langle V_i^2 \rangle_x$ = space average mean square velocity

The above equation applies where the motions involve translational velocities, as is the case for bending deformation in beams and plates.

For beams deforming in torsion the motion is in terms of angular velocities

$$\langle \dot{\theta}_i^2 \rangle_x:$$

$$\langle \dot{\theta}_i^2 \rangle_x = \left(\frac{E_{i,tot}}{n_i} \right) \frac{n_i}{\rho_i L_i I_{p,i}} \quad (100)$$

where $I_{p,i}$ is the total polar moment of inertia of the cross section, ρ_i is the density, and L_i is the length of the beam.

Space average acceleration and displacement levels are determined according to:

$$\langle a_i^2 \rangle_x = \omega_o^2 \langle V_i^2 \rangle_x \quad (101)$$

and

$$\langle d_i^2 \rangle_x = \langle V_i^2 \rangle_x / \omega_o^2 \quad (102)$$

ω_0 = center frequency of band

$\langle a_i^2 \rangle_x$ - space average mean square acceleration level

$\langle d_i^2 \rangle_x$ - space average mean square displacement level

Similar expressions occur for angular accelerations and displacements.

(- 2

SEA Model of the Sikorsky S-76

The previous sections described the general features and required steps for implementing a SEA model of noise and vibration transmission. The fundamental approach of SEA was presented in terms of the power balance equations between individual subsystems of the overall model. General procedures for computing the parameters in the system equations were also described.

Though the basic approach of SEA is conceptually straightforward and easily understood its implementation requires a well developed understanding of the dynamic behavior of mechanical and acoustical systems, in general, and also of the particular structure under investigation. Sectioning the structure into multiply-connected structural subsections requires an understanding of the types of deformation occurring and the nature of the junctions that couple subsections together.

The following sections illustrate the implementation of the SEA approach for a specific helicopter that is representative of the general class of civilian/commercial helicopters. The helicopter chosen, the Sikorsky S-76, is a twin turbine powered helicopter with a certified maximum speed of 80 m/s, a cruise speed of 75 m/s, and a range of over 740 km. It has a maximum certified gross weight of 45 kN. In a standard configuration the S-76 can accommodate up to 13 passengers and from 4 to 8 passengers in wide body executive comfort.

The development of an SEA model for a particular application involves a series of steps that are identified in Figure 19. The various steps have been discussed at length in the general section describing SEA and are presented here in block diagram form to help focus the discussion of the SEA model for the S-76.

The first part of this section involves a description of the S-76 helicopter and the considerations leading to the selection of the SEA subsystems of the model. A second part deals with the evaluation of the SEA parameters of the model including the mode density and damping and coupling loss factors. Reference is made to standard expressions from the general section on SEA that are applicable for the S-76 SEA model. Where non-standard expressions are required they are described within this section. An example is the dynamic behavior of the composite honeycomb panels that are used extensively on the S-76.

An important part of this section deals with an evaluation of coupling loss factors. A variety of coupling configurations are involved including: frame to frame, frame to panel, panel to acoustic space, and acoustic space to acoustic space. Of particular importance for the S-76 model is the coupling between frame members at junctions with cross frames. A derivation of the coupling loss factor expressions for frame junctions is given in Appendix B.

In addition, this section deals with the evaluation of input power, formation of the system matrix equations, and solution for the subsystem energies and response levels. The input power evaluation relies on the prior discussion of source levels for helicopters. The estimation of source levels is dependent primarily on inflight measurements. The procedures for formation of the system matrix equations and solution for the subsystem energies and response levels are discussed in the general SEA section.

Description of the S-76 airframe . - As previously described, the primary source of helicopter cabin noise in an untreated configuration is the gearbox. It is a source of both acoustic and vibratory energy that is transmitted into the cabin acoustically through intervening panels and spaces and vibrationally through the airframe structure to panel surfaces that radiate directly into the cabin. The gearbox on the S-76 is pad mounted directly to the airframe at four attachment points. On other helicopters the gearbox may be similarly mounted or it may be supported by struts and torque restraint mechanisms.

Internal details of the S-76 airframe structure are displayed in Figure 2. The overhead framing in the cabin consists of two main fore/aft members that reach from the gearbox forward to the pilot's windows. The gearbox is mounted directly onto the fore/aft frames. Immediately underneath the gearbox the frames are an integral I beam construction with added plating for additional support. Forward of the gearbox the framing is a riveted, lighter weight construction where the weight decreases moving forward.

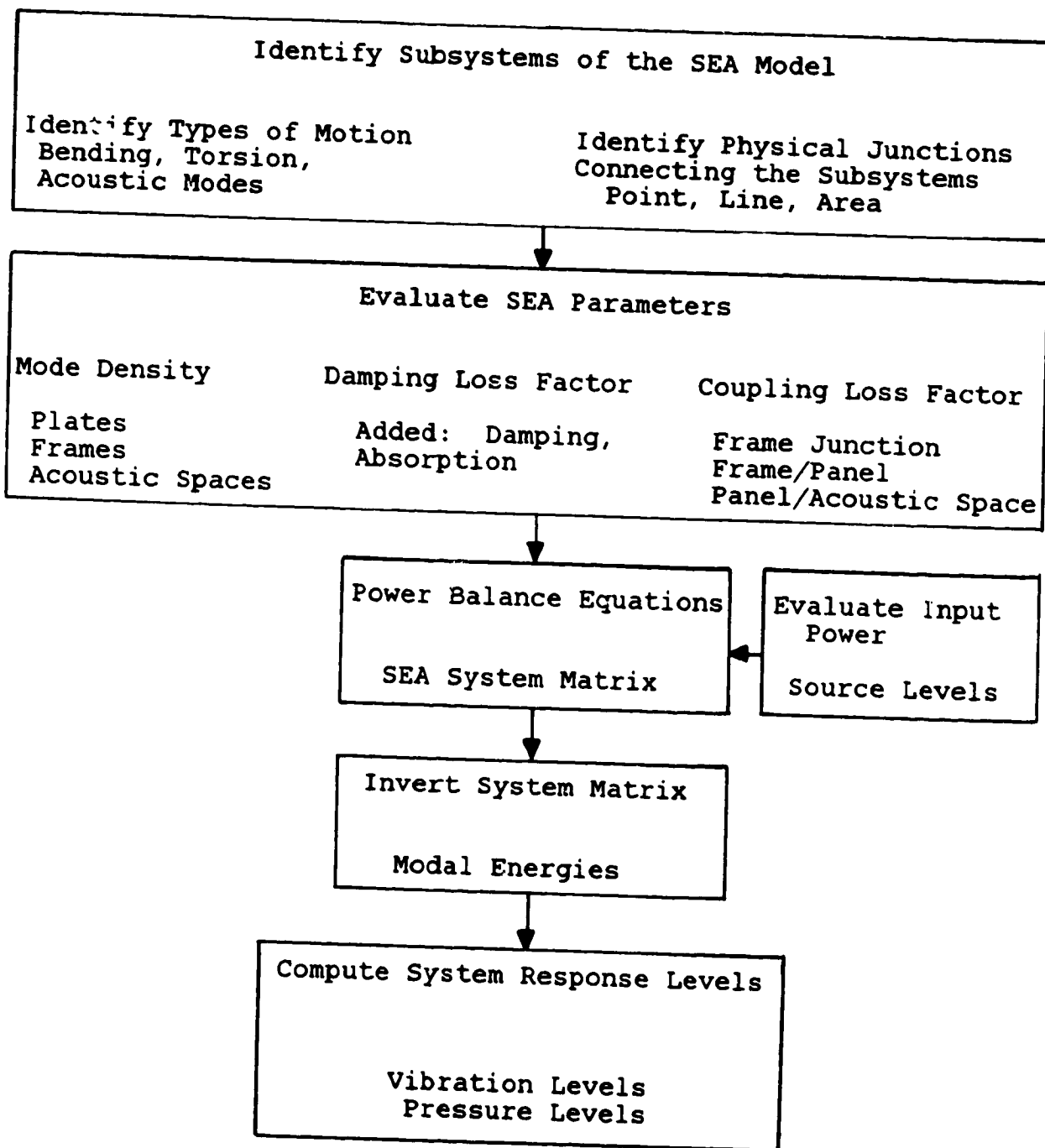


Figure 19. Block Diagram for SEA System Response Evaluation.

Cross frames in the cabin overhead are of a riveted construction and extend down around the sides of the cabin to support the floor structure. The skin panels for both the overhead and sides of the cabin are a light weight honeycomb construction and are riveted to the frames. In the bare condition with no interior treatment the framing and honeycomb skin panels are completely exposed.

Between the pilot and copilot's seats there is a frame structure that connects between the overhead frames and the floor (called the "broom closet"). Control cables and levers for the main and tail rotor controls pass through this structure to the exterior overhead surface of the cabin. The entire nose section of the helicopter extending forward from the top framing section over the pilot/copilot's seats is a fiberglass construction. The tail section is a typical rib/stringer type construction.

The space around the gearbox is enclosed by a fiberglass cowling which also covers the control linkages mounted to the exterior skin surfaces forward of the gearbox. A bulkhead separates the gearbox from a plenum chamber for the turbine inlet air supply. The plenum chamber is also separated from the turbines themselves by a bulkhead. Immediately aft of the rear passenger bulkhead is a luggage compartment that lies below the gearbox and turbine inlet spaces. Behind it and beneath the turbines is a space occupied by the environmental control units. Dimensions of the cabin are shown in Figure 20.

Selection of SEA subsystems for the S-76 model. - Subsystems in a SEA model consist of groups of resonant modes in component sections of the total structure which exhibit similar dynamic behavior. The dynamic behavior is characterized by the type of deformation within the structure as well as the nature of the coupling to adjacent structures. Possible types of deformation include bending or flexural, torsional, longitudinal, and shear motions. Each differs in the way in which energy is stored within the structure.

In structures with extremely complicated geometries these motions are often internally well coupled by changes in cross-section, bends, attached brackets, etc. In such cases the modes with different types of motion have comparable modal energies and can be treated collectively as a single subsystem within the SEA model.

The first step in selecting the SEA subsystems is to physically section the total structure into individual components called structural subsections. This is most easily accomplished by considering the physical discontinuities that occur within the

ORIGINAL FILED
AUG 19 1964

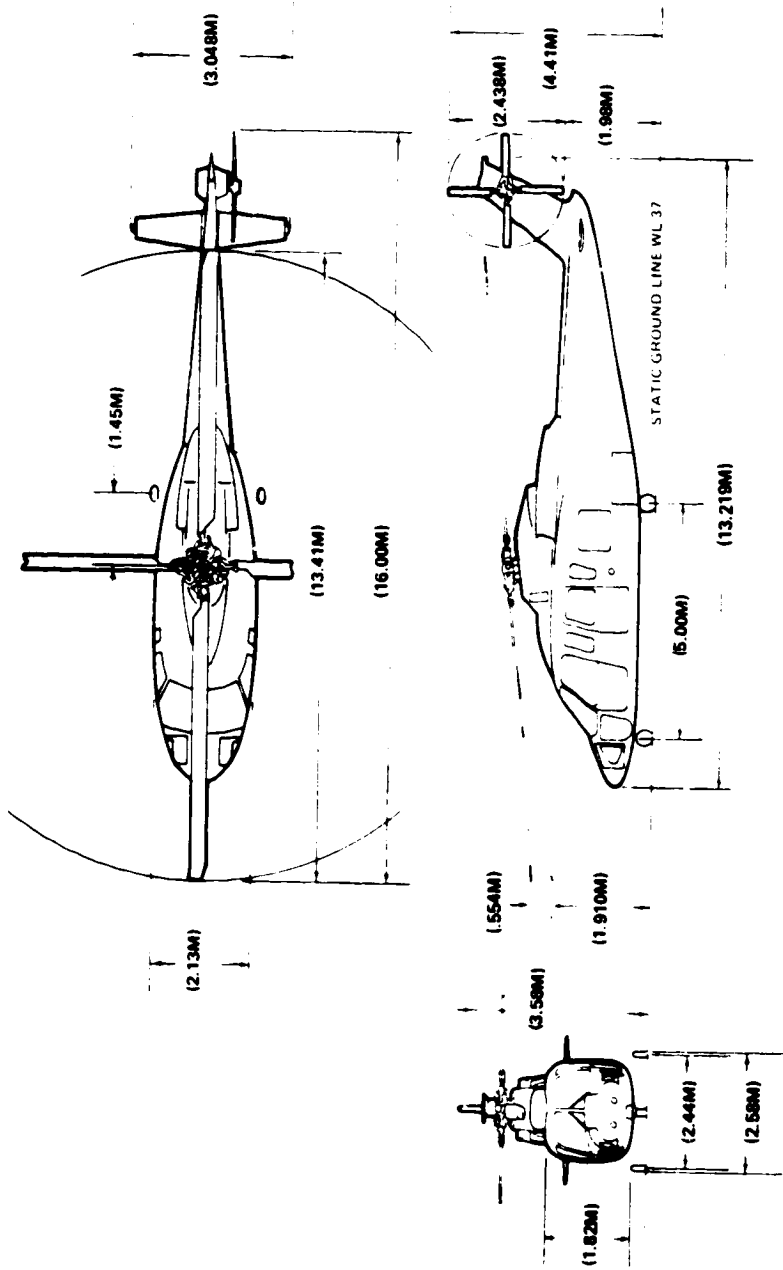


Figure 20. S-76 Cabin Dimensions.

ORIGINAL PAGE IS
OF POOR QUALITY

structure. Skin panels are sectioned by the framing to which they are attached. Framing is sectioned by junctions with cross frames. This is also where changes in frame cross-sectional geometry occur on the S-76. Acoustic spaces are sectioned by bulkheads, cowlings, and other panel surfaces which physically define these spaces.

In many situations on the actual structure there are potentially significant structural non-uniformities in the form of cutouts, attachment brackets for cabling, hydraulic lines, etc., stiffening angles and plates, as well as local changes in cross-sectional geometry. For acoustic spaces the partitions may be only partial with significant open areas between the spaces. Decisions must be made concerning the degree of detail that is accounted for in selecting the subsections. Accounting for additional detail results in a larger number of subsystems. The costs to implement and run the model increase, and there is also the potential for greater computational error. The trade off must also take into account the anticipated accuracy of the modeling procedure itself in deciding the degree of detail included in the model.

The structural subsectioning of the S-76 airframe for the initial SEA model is given in Table 1. It includes the panel sections between frames, frame sections between junctions, bulkheads, window and door panels, and assorted other structural elements. In addition to the cabin itself other acoustic spaces include the different overhead compartments around the gearbox, turbines, the inlet air plenum, and the luggage and ECU compartments. These are listed in Table 2.

Within each structural subsection, subsystems have been included which account for mode groups containing different types of motion. This occurs primarily for the framing at lower frequencies where the final subsystem selection accounts for torsional motions and bending motions about two axes perpendicular to the axis of the frame. The SEA model as formulated for the S-76 does not account for longitudinal motions in the frame due to the nature of the gearbox motions, which predominantly excite the attachment frames in bending and torsion.

A total of 82 structural subsections are used in describing the S-76 airframe. Of these 45 are frame structures and 37 are panel structures. For each frame three types of motion are considered, yielding a total of 135 frame subsystems in the SEA model. In addition there are 8 acoustic spaces listed in Table 2 that are included as subsystems in the SEA model. This brings the total number of SEA subsystems for the S-76 to 180.

The cabin is the primary space for establishing the interior noise environment. The other spaces act as sources (e.g., gearbox and turbine spaces) or as connecting spaces (e.g., luggage compartment). Others, such as the nose compartment and environmental control unit space, are less important as connecting spaces since they physically are not on a direct path from the source to the cabin. They are of importance in that they potentially affect the distribution of acoustic levels throughout the helicopter.

From Figure 2 it is seen that there is a great deal of symmetry in the airframe about a fore/aft center line. This symmetry is also reflected in the structural subsections in the SEA model. Panel or frame sections on the left and right sides of the cabin have identical surrounding structural subsections. If the power inputs for the different sources are also symmetric, then the modal energies of the symmetric subsystems will be the same. This fact allows for potentially significant simplifications in formulating and solving the power balance equations.

For symmetric subsystems the modal energies, coupling and damping loss factors, and mode densities are identical term by term in the power balance equations. One of the identical equations for each symmetric subsystem pair is simply removed to reduce the number of degrees of freedom (i.e., independent modal energies) in the SEA system matrix. The effect on equations for middle subsystems with no symmetric counterparts is to combine off-diagonal coupling terms for the symmetric pairs.

For Table 1 the number of structural subsections for the symmetric structure with symmetric excitation is 48 which is significantly smaller than the original total of 82. The total number of subsystems accounting for bending and torsional motions in the frames is 106 as compared to 180 originally.

As a final note, it should be emphasized that these reductions depend not only on the symmetric nature of the structure, but also of the excitation as well. If we are considering the response due to excitation at only one of the gearbox attachment points, then the problem is not symmetric. Also if the actual gearbox excitations are not left/right symmetric, the problem again is not symmetric and must be solved in its full form.

In a compact structure such as a helicopter airframe there is a high degree of interconnectedness between the possible paths from sources to receivers. It is difficult to describe the overall transmission in terms of paths that are independent of each other.

The extent to which this is possible depends on the existence of a sequence of strongly coupled subsystems with relatively larger modal energies than surrounding subsystems. In this case the power flow will be along the path of the strongly coupled subsystems with lateral flow out into the surrounding subsystems.

Prior measurements of a preliminary nature on the S-76 have suggested that the flow of vibratory energy from the gearbox along the main fore/aft frame members constitutes an important path in important frequency bands below 1 kHz. The gearbox is directly and strongly coupled to this path and as well it is anticipated that the coupling between sections along the framing is strong. Important lateral flows of energy from the path would be into the adjacent skin panel sections and also the cross frames at frame junctions.

Other potentially important paths from the gearbox that are accounted for in the SEA model are into the drip pan immediately beneath the gearbox and the rear passenger bulkhead. Both are excited by vibration transmission through the frame to which the gearbox is directly mounted.

Acoustic spaces in the helicopter airframe are an integral part of the overall SEA model. Energy stored in the resonant acoustic modes of the space are coupled to the resonant modes of adjacent structural subsystems. In addition the spaces are coupled to each other directly through non-resonant mass-law controlled response of the intervening panel structures. The presence of holes or other openings in the panels also contributes to the direct coupling between acoustic spaces.

The number of acoustic spaces in the helicopter airframe is small compared to the number of structural subsystems. In some cases the transmission is from the source space through a panel structure directly into the cabin such as occurs for the gearbox acoustic space through the overhead panels into the cabin. For other paths the transmission may involve a single intermediate acoustic space. Airborne transmission from the spaces around both the gearbox and turbine can involve the luggage compartment as an intermediate step in the path to the cabin.

Vibration and acoustic transmission in the helicopter airframe are inherently coupled. The degree of the coupling depends on the parameters of the particular model so that it may be appropriate to describe independent airborne and structureborne transmission problems. For helicopter airframes both probably must be con-

sidered together within the context of the full SEA model. The contributions from acoustic and vibration sources can be assessed by independently evaluating the cabin noise levels for each. The transmission for each source may importantly depend on both vibratory and acoustic paths.

Table 1 - Structural Subsections for S-76 SEA Model

<u>Subsection #</u>	<u>Description</u>	<u>Identification Code</u>
1.	<u>Cabin Overhead Frame Subsections</u>	
	<u>1.1 Main Longitudinal Frame Members</u>	
	1,2 Between cross-frames* 1 and 2, left-right sides	LF LF12L, LF12R
	3,4 Between cross-frames* 2 and 3, left-right sides	LF23L, LF23R
	5,6 Between cross-frames* 3 and 4, left-right sides	LF34L, LF34R
	7,8 Between cross-frames* 4 and 5, left-right sides	LF45L, LF45R
	9,10 Seam to top of front window	LF5WL, LF5WR
	<u>1.2 Perimeter Frame Members</u>	
	11,12 Between cross-frames 1 and 2, left-right sides	PF PF12L, PF12R
	13 14 Between cross-frames 2 and 3, left-right sides	PF23L, PF23R
	15,16 Between cross-frames 3 and 4, left-right sides	PF34L, PF34R
	17,18 Between cross-frames 4 and 5, left-right sides	PF45L, PF45R
	19,20 From 5 to centerline along top of front window	PF5WL, PF5WR
	<u>1.3 Cross-Frame Members</u>	
	21,22 Location 2A - left-right sides	CF CF2AL, CF2AR
	23,24 Location 2B - left-right sides	CF2BL, CF2BR
	25 Location 2 - mid section	CF2M
	26,27,28 Location 3 - left-mid-right sides	CF3L, CF3M, CF3R
	29,30,31 Location 4 - left-mid-right sides	CF4L, CF4M, CF4R
	<u>1.4 Miscellaneous Overhead Frames</u>	
32	Tail Rotor Yoke Frame cross frame between locations 2 and 3 mid section only	YF2/3M

Table 1 - Structural Subsections for S-76 SEA Model (cont'd)

<u>Subsection #</u>	<u>Description</u>	<u>Identification Code</u>
<u>2. Cabin Overhead Panel Subsections (OHP)</u>		
33,34	Between cross-frames 1 and 2, left and right sides	OHP12L, OHP12R
35	Drip pan-underneath gearbox (DP)	OHP12DP
36,37,38	Between cross-frames 2 and 3, left-mid-right sides	OHP23L, OHP23M, OHP23R
39,40,41	Between cross-frames 3 and 4, left-mid-right sides	OHP34L, OHP34M, OHP34R
42,43	Between cross-frame 4 and station 5 honeycomb section, left-right sides	OHP45L, OHP45R
44,45	Fiberglass panel between station 5 and top of front windows	OHP5WL, OHP5WR
<u>3. Cabin Wall Subsections</u>		
<u>3.1 General Sidewall Subsections</u>		
46	Rear passenger bulkhead	RPB
47,48	Rear passenger side panel (SP)	SP12L, SP12R
49,50	Rear passenger window	SP12WL, SP12WR
51,52	Rear passenger door - upper frame members	DF23L, DF23R
53,54	- window	DW23L, DW23R
55,56	- lower panel section	DLP23L, DLP23R
57,58	Mid passenger side panel	SP34L, SP34R
59,60	Mid passenger window	SP34WL, SP34WR
61,62	Pilot/copilot door - upper frames	DF45L, DF45R
63,64	- window	DW45L, DW45R
65,66	- lower panel section	DLP45L, DLP45R
67,68	Pilot/copilot windows	FWL, FWR
69	Nose cone	NC

Table 1 - Structural Subsections for S-76 SEA Model (cont'd)

<u>Subsection #</u>	<u>Description</u>	<u>Identification Code</u>
<u>3.2 Sidewall Frame Subsections</u>		
70,71	At frame 2 location	SWF2L, SWF2R
72,73	At frame 3 location	SWF3L, SWF3R
74,75	At frame 4 location	SWF4L, SWF4R
76,77	At frame 5 location (front frame for pilot/ copilot door)	SWF5L, SWF5R
78	Between pilot/copilot windows	FWF
<u>4. Miscellaneous Subsections</u>		
79	Instrument panel window	IPW
80	Main and Tail Rotor Control lever column (broom closet) connects between floor and overhead frames/panel	BC
81	Gas tank	GT
82	Floor	FL

*Cross frame location 1 occurs at the rear passenger bulkhead.
 Cross frame location 2 occurs between the rear passenger window and door.
 Cross frame location 3 occurs between the rear passenger door and mid passenger window.
 Cross frame location 4 occurs between the mid passenger window and pilot's door.
 Cross frame location 5 is over the pilot/copilot seats and is actually a seam between the honeycomb panels and fiberglass nose section.

Table 2

Acoustical Subsections for the S-76 SEA Model

<u>Description</u>	<u>Identification Code</u>
Space around gearbox and under forward cowling	GBA
Turbine inlet air plenum	TIA
Space around turbines, left and right sides	TAL, TAR
Luggage compartment	LCA
Environmental control unit space	ECUA
Cabin	CA
Nose compartment	NCA

Evaluation of SEA parameters for the S-76 model. - The meaning and significance of the SEA parameters has been discussed. Analytic expressions were also given for evaluating the SEA parameters for common types of subsystems and junctions. These expressions form the basis for evaluating the parameters of the specific SEA model of the Sikorsky S-76 as presented in Tables 1 and 2. Additional expressions to account for distinctive features of the model are presented in the following sections.

Mode density for the S-76. - The S-76 model is comprised of frame, panel, and acoustic subsystems. The frames allow for torsion and bending deformations. The general expressions given for evaluating the mode density of a beam or frame subsystem deforming in bending and torsion are directly applicable for the frame subsystems of the S-76 model. The applicable equations are shown in Table 3.

Table 3

Summary of Parameter Requirements for Frame and Acoustical Subsystems

<u>Frame Subsystems</u>	<u>Applicable Equations and S-76 Subsections</u>
Torsional resonances	Eq. (41) with wavespeed from Eq. (43)
Bending resonances	Eq. (53) with wavespeed from Eqs. (49) and (50) which yields Eq. (55)
S-76 frame substructure #'s from Table 1	1-32, 51, 52, 61, 62, 70-78
<u>Input Parameters Required</u>	<u>Symbol</u>
- length of frame subsystem	l
Torsional Motion	
- torsional moment of rigidity	J
- polar moment of inertia of cross-section	I_p
Bending Motion (about each of two axes perpendicular to the frame axis)	
- radius of gyration of cross-section	K_1, K_2
<u>Material Properties</u>	
- Young's modulus	E
- Shear modulus	G
- density	ρ
<u>Acoustical Subsystems</u>	
Acoustic resonances	Eq. (40)
S-76 acoustical subsystems from Table 2	Total # = 8

Table 3 (continued)

Input Parameters Required

- Volume of space V
- Surface area S
- Edge length P

Physical Properties

- Speed of sound - (Possible temperature and ambient pressure effects) c_0

For plate subsystems additional expressions are required characterizing the dynamic behavior of composite honeycomb panels. Conventional single layer panel subsystems include the rear passenger bulkhead, windows, the drip pan underneath the gearbox, and panel surfaces on the doors and nose cone. For the conventional single layer panels the required parameters and applicable analytic expressions are given in Table 4.

Table 4

Summary of Parameter Requirements for Single Layer Panel Subsystems

<u>Panel Subsystems</u>	<u>Applicable Equations and S-76 Subsections</u>
Bending resonances	Eqs. (49), (50), and (54) which yield Eq. (56)
S-76 Single Layer Panel Subsystems from Table 1	35, 44, 45, 46, 49, 50, 53-56, 59, 60, 63-66, 69, 79-82

<u>Input Parameters Required</u>	<u>Symbol</u>
- Area of panel	A
- Thickness of panel	h (used to compute κ , radius of gyration)
 <u>Material Properties</u>	
- Young's modulus	E
- Poisson's ratio	σ
- density	ρ

The dynamic behavior of composite honeycomb panels is illustrated in Figure 21 [23]. The wavespeed for bending deformation involves three distinct regions. For typical helicopter honeycomb panels the honeycomb core material is sufficiently rigid as to effectively prohibit any thickness deformation of the composite until very high frequencies, well above the range of interest.

At low frequencies in Region 1 the wavespeed increases proportional to the square root of frequency consistent with the result for a panel deforming in bending. The bending rigidity of the composite cross-section is dependent upon extensional deformation in the face sheets which are spaced apart by the thickness of the honeycomb core.

$$D_1 = \frac{Et_{fs}(H + t_{fs})^2}{2(1-\sigma^2)} \quad (103)$$

t_{fs} = thickness of face sheet

H = thickness of honeycomb core

E = Young's modulus of face sheet material

σ = Poisson's ratio of face sheet material

The expression for the wavespeed is:

$$c_1 = \left[\frac{D_1}{(2\rho_{fs} + \rho_c H)} \right]^{\frac{1}{2}} \sqrt{\omega} \quad (104)$$

ρ_{fs} = surface density of one face sheet

ρ_c = density of honeycomb core (in expanded form)

The bending rigidity of the honeycomb core itself does not contribute significantly to the overall composite panel rigidity.

At higher frequency shear effects within the honeycomb core become important, and the wavespeed in Region 2 becomes more nearly independent of frequency consistent with shear wave propagation.

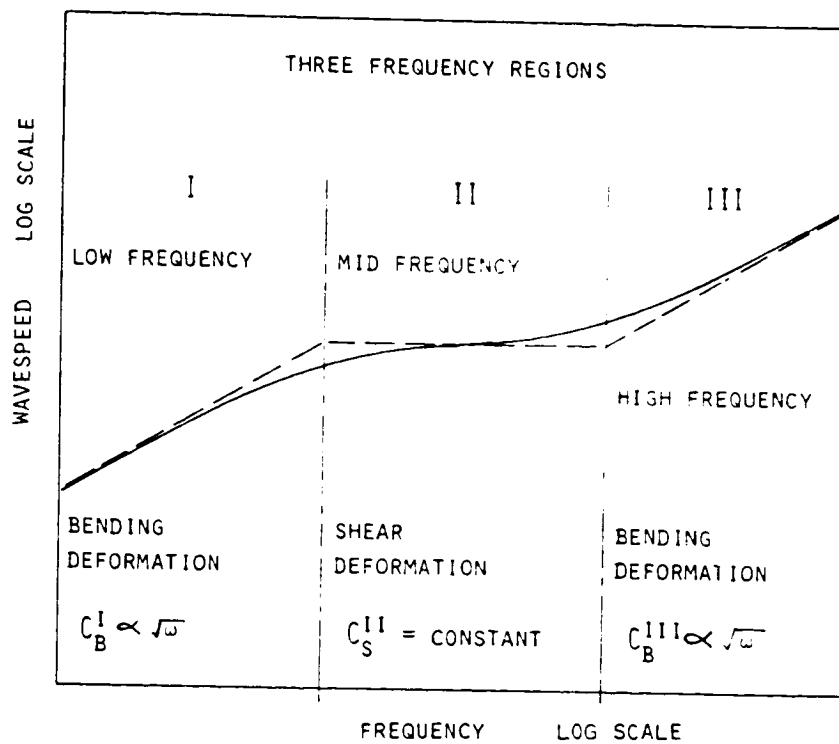


Figure 21. Dynamic Behavior of Composite Honeycomb Panel.

The value of the wavespeed for shear wave propagation is:

$$c_2 = \left[\frac{GH}{(2\rho_{fs} + \rho_c H)} \right]^{\frac{1}{2}} \quad (105)$$

G = shear stiffness of
honeycomb core (in
expanded form)

At still higher frequencies the behavior again represents bending deformation but with a smaller effective bending rigidity. The bending rigidity in Region 3 is determined by an individual face sheet deforming in bending:

$$D_3 = \frac{Et_{fs}^3}{12(1-\sigma^2)} \quad (106)$$

The wavespeed is given by:

$$c_3 = \left[\frac{D_3}{(\rho_{fs} + \frac{1}{6} \rho_c H)} \right]^{\frac{1}{2}} \sqrt{\omega} \quad (107)$$

The mode density for a honeycomb panel is evaluated depending on frequency from Eqs. (104), (105), or (107) and Eq. (54).

In Region 1: Low frequency bending of the entire composite

$$n_1(\omega) = \frac{A}{4\pi \left[\frac{D_1}{(2\rho_{fs} + \rho_c H)} \right]^{\frac{1}{2}}} \quad (108)$$

In Region 2: Shear deformation of the honeycomb core

$$n_2(\omega) = \frac{A\omega}{2\pi c_2^2} \quad (109)$$

In Region 3: High frequency bending of the face sheets

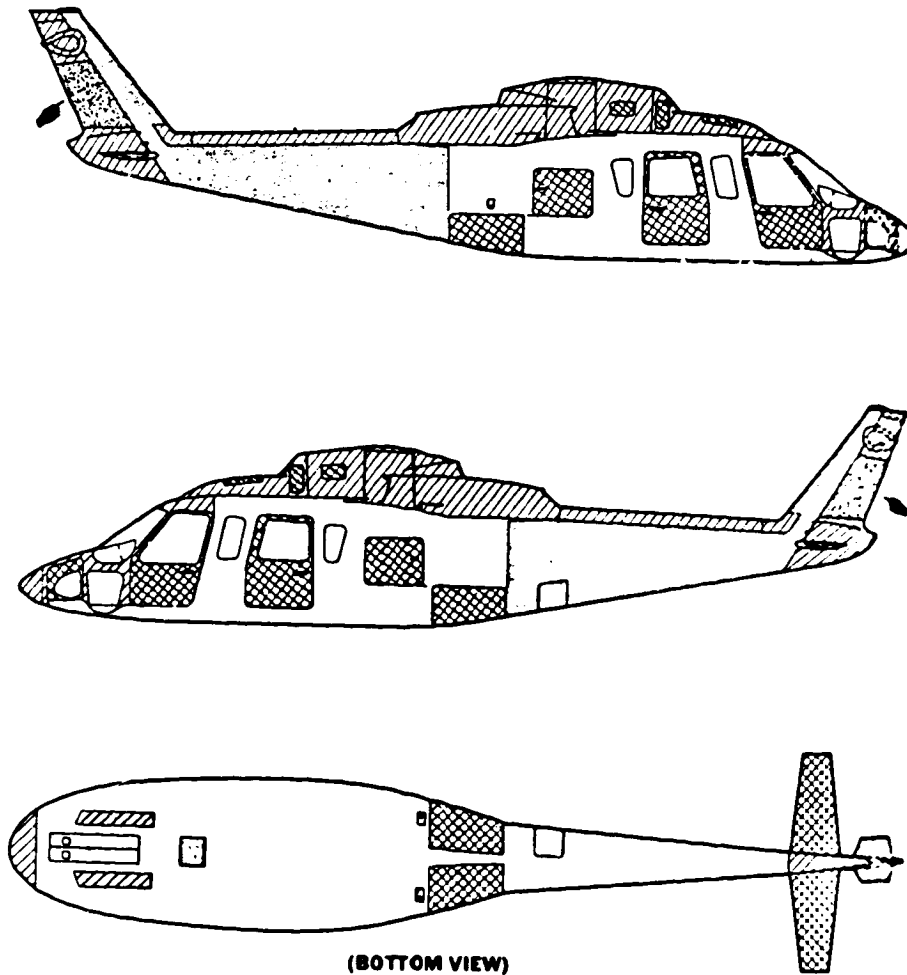
$$n_3(\omega) = \frac{A}{4\pi \left[\frac{D_3}{(\rho_{fs} + \frac{1}{6} \rho_c H)} \right]^{\frac{1}{2}}} \quad (110)$$

The honeycomb panels on the S-76 are of varied construction involving aluminum face sheets and either aluminum or kevlar cores as shown in Figure 22. Total panel thicknesses vary from 12.5mm to 25mm with the face sheets being from 0.75mm to 1.25mm thick. A typical surface density for 25mm thick composite panels with an aluminum core is approximately 6.1 Kg/m².

The shear wavespeed in Region 2 for the 25mm thick aluminum core construction is approximately 1300 m/s which significantly exceeds the speed of sound in air (344 m/s). The transition between Regions 1 and 2 occurs at approximately 3900 Hz. Coincidence occurs in Region 1 near 300 Hz. These numerical results for the S-76 aluminum core panels mean that in computing mode densities the expression for Region 1, Eq. (108), is of primary importance and that the panel vibration is above coincidence over almost the entire frequency range of interest. As will be seen in a subsequent section, the radiation efficiency can be taken to be equal to 1 in this case regardless of the type of deformation occurring within the panel.

Damping loss factor for the S-76. - Most of the frame structures and some of the panels on the S-76 are of a conventional riveted aircraft construction. For such structures dampings have a broad range of values near .01. In the absence of specific information for the S-76 this value will be used in the initial model predictions. Where such panels are treated with damping materials manufacturers' estimates of the resulting composite loss factor values will be used.

SIKORSKY 76
 MAINTENANCE MANUAL, SA 4047-76-2








LEGEND	
	KEVLAR SHEET
	KEVLAR HONEYCOMB
	SHEET ALUMINUM
	ALUMINUM HONEYCOMB
	FIBERGLASS HONEYCOMB

Figure 22 S-76 Plate and Skin Materials

Other panels are either of a honeycomb or fiberglass construction. Damping values for the fiberglass material itself depend on the formulation, the type of resin used, the density and orientation of the fibers, etc. Reported values are in the range from .003 to .02. Additional information will need to be obtained, if available, from the manufacturers of the fiberglass sections. A question for the built up structure is whether there are significant contributions from interface damping due to gas pumping or other sources. The greater the inherent damping of the material itself the less will be the influence of the other sources of damping.

For composite honeycomb panels the damping levels will exceed the levels for the individual component materials alone. The composite levels will depend on the nature and quality of the bonding including the type of adhesive used. In the absence of manufacturers data, experiments, as described in a subsequent section, will be needed to estimate damping levels for the honeycomb panels. Particular front window designs involve a multi-layer construction with an adhesive middle layer. Here damping levels must also be estimated based on experimental measurements on the actual material.

A difficulty in performing such measurements is isolating the desired damping mechanisms from energy which is transmitted to other attached structures. If the interface damping is important, it is not feasible to simply remove the panel of interest from the remaining structure since this also removes the desired contributions due to interface damping. For structures where interface damping is not expected to make a significant contribution as for composite panel constructions, the panel may be tested separate from the attached structure.

Damping for the acoustic spaces in the S-76 model includes only the energy dissipated within the space and not the energy transmitted to adjacent spaces or which is coupled into resonant vibration of the bounding panel surfaces of the space. Air absorption for the small spaces on the helicopter in the frequency range of interest is negligible. Where added treatments provide significant absorption in comparison with the totally bare configuration the damping can be estimated based on the supplied absorption characteristics of the treatment while completely neglecting other contributions.

Estimating damping levels of acoustic spaces based on experimental measurements of reverberation time is feasible to the extent that the dissipated energy within the space is large compared to the transmitted energy. This depends in part on the transmission loss levels for the bounding panels. Where holes or gaps contribute significantly to the transmission, covering them can reduce their contribution and improve the validity of the damping estimate for the space.

Damping level estimates are a source of uncertainty for all vibration prediction methods involving the resonant response of structures. This is true of finite element methods, the methods of classical mechanics, and of SEA as well. Damping does not readily allow for convenient analytical prediction procedures for real structures. Unfortunately it is important for the prediction of vibration response and transmission.

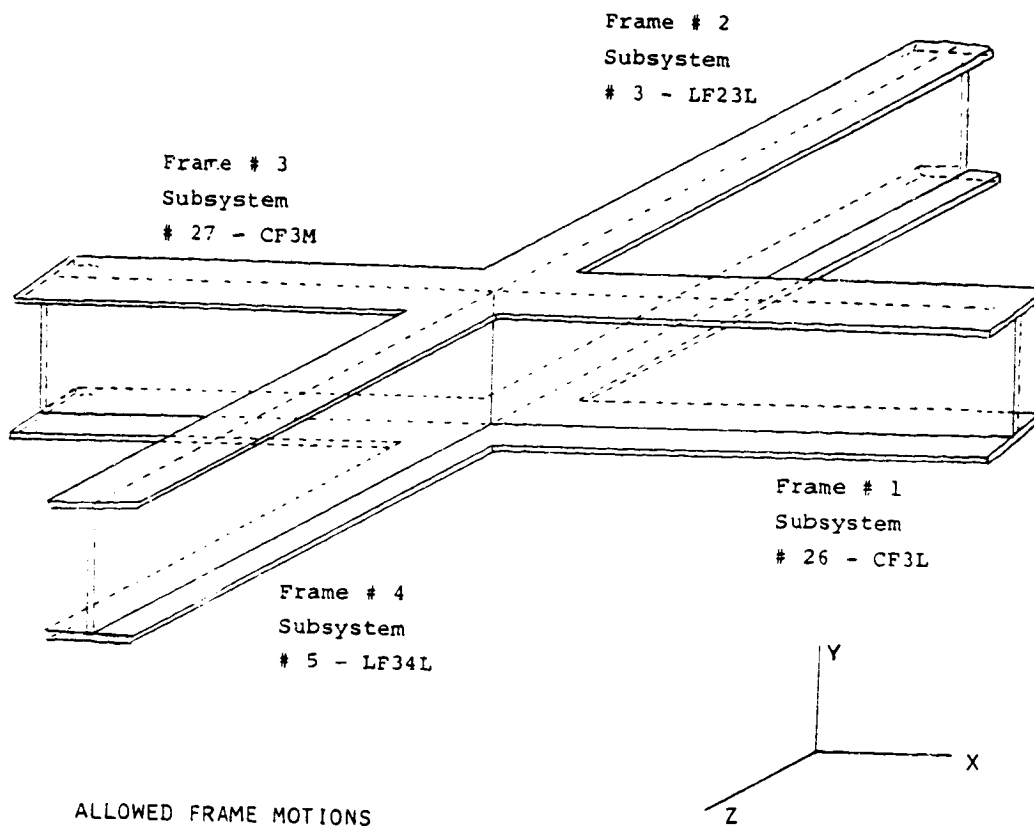
Coupling loss factors for the S-76. - The required coupling loss factors for the S-76 SEA model in Tables 1 and 2 are identified by the junctions between the subsystems. The junction types for the S-76 model include point, line, and area connections. The frame subsystems are considered to be connected to each other at a point. Junctions between frames and panels occur along the length of the frame, and panels are "connected" to the acoustic spaces over their areas.

To illustrate the identification of coupling loss factors consider the frame junction shown in Figure 23. The junction is located at cross frame location 3 between the rear passenger door and mid passenger window, in this case on the left side of the cabin. Four frame substructures are connected at the junction. Their numbers are as follows:

Substructure #
(from Table 1)

- | | | |
|----|-----------|---|
| 1) | 3 - LF23L | Main longitudinal frame section between cross frame locations 2 and 3 |
| 2) | 5 - LF34L | Main longitudinal frame section between cross frame locations 3 and 4 |
| 3) | 26 - CF3L | Cross frame at location 3 - left frame section |
| 4) | 27 - CF3M | Cross frame at location 3 - mid frame section |

ORIGINAL DRAWING
OF POOR QUALITY



ALLOWED FRAME MOTIONS
FRAME # 1
BENDING ABOUT Z AXIS
BENDING ABOUT Y AXIS
TORSION ABOUT X AXIS

Figure 23. Typical Crossed Frame Junction

The allowed motions for frame subsystems include bending about two axes and torsional motion. In total 12 different SEA subsystems are connected at this one frame junction. With complete generality where all of the subsystems are connected with each other there are 66 different coupling loss factors characterizing the junction.

In actuality the total number is not this large. As a result of the geometry of the junction certain motions are simply not coupled to each other. For example, bending motion in the plane of the framing is not coupled to either torsional or out-of-plane bending motions for any of the four frames. Symmetries occur when opposing frame substructures have identical cross-sectional geometries which further reduce the total number of coupling loss factors. For a symmetric frame junction the total number of independent coupling loss factors that must be evaluated is 22. If, further, all of the frames are identical the number of numerically different and independent coupling loss factors is reduced to 11.

Frame junctions are the most complicated as a result of the large number of subsystems involved. Other junction types are considerably less complicated. Consider the line junction between a frame and the panels on either side to which it is attached. The total number of subsystems is five; three for the frame and one for each panel. For the completely general case the total number of coupling loss factors is 10. For identical panels on both sides of the frame the total number of coupling loss factors to be evaluated is three. Area junctions between a panel and adjacent acoustic spaces are the least complicated and involve only two coupling loss factors between the three SEA subsystems.

Frame junction coupling loss factor evaluation for the S-76. - The analytical procedure for evaluating the coupling loss factors at a frame junction is described in Appendix B. The approach involves a computation of energy transmission coefficients where the frames are extended to infinity away from the junction. Reverberation in the frame sections is accounted for in the expression relating the transmission coefficient to the coupling loss factor.

Frame-panel coupling loss factor evaluation for the S-76. - Frame subsystems are connected to panels along the length of the frame. The subsystems differ by one in the number of dimensions that characterize them. The frames are one dimensional along their length while the panels are two dimensional over an area. This situation is more appropriately described by a radiation efficiency for the one dimensional subsystem, i.e., the frame, which relates the vibratory motion of the frame to the power it radiates into the plate.

Analogous to the case of radiation by a panel into an acoustic space the radiation depends on the wavespeed in the frame relative to the panel wavespeed. When the frame wavespeed exceeds the value for the panel a matching or coincidence condition occurs where power is radiated more efficiently into the panel. The behavior is more complicated than for panel and acoustic spaces because even above coincidence a near field disturbance remains in the panel due to the nature of bending deformation.

Below coincidence for an infinitely long connection no power is radiated into the panel, and the radiation efficiency is zero. For finite length connections power radiates into the panel as a result of the discontinuities at the ends of the frame. Unfortunately expressions have not been derived to predict the radiation efficiency for the different frame motions below coincidence.

The approach followed here is to evaluate the radiated power for uniform motion of the frame along its length. This corresponds to normal radiation at right angles to the line junction. For torsional motion of the frame, θ_f , the total radiated power is given by the following:

$$\Pi_{\text{rad}} = L \left\{ \frac{1}{2} [\text{Re}(Z_f)a^2 + \text{Re}(Z_m)] + \text{Re}[Z_{m,\eta}] \right\} |\dot{\theta}_f|^2 \quad (111)$$

- where
- Z_f = transverse force impedance of panel
 - Z_m = moment impedance of panel
 - $Z_{m,\eta}$ = cross coupling impedance between moments transverse displacements forces angular rotations
 - a = distance between axis of torsional motion and line connection to panel (half width of frame where it connects to panel)
 - L = total length of line junction

Expressions for the impedances are contained in Table 7 of Appendix B. In the equations of Table 7, B is the bending rigidity of the panel per unit length along the line connection. For composite honeycomb panels at low frequency the expression for D_1 in Eq. (103) is substituted for the bending rigidity B.

The radiated power is related to the coupling loss factor and frame motion according to the definition of the coupling loss factor.

$$\Pi_{\text{rad}} = \omega \eta_{f,p}^t E_{\text{tot},f}^t \quad (112)$$

$E_{\text{tot},f}^t$ = total energy of frame in torsion

$\eta_{f,p}^t$ = frame to panel coupling loss factor for torsional motion in the frame

where

$$E_{\text{tot},f}^t = L \rho_f I_{p,f} |\dot{\theta}_f|^2 \quad (113)$$

$I_{p,f}$ = polar moment of inertia of frame cross section

ρ_f = density of frame

These three equations, when combined, give the coupling loss factor between torsional motion in the frame and bending motion in the panel as follows:

$$\eta_{f,p}^t = \frac{1}{\omega \rho_f I_{p,f}} \left(\frac{1}{2} [\text{Re}(Z_f) a^2 + \text{Re}(Z_m)] + \text{Re}(Z_{m,\dot{\eta}}) a \right) \quad (114)$$

For bending motion of the frame, η_f , the following expression for the radiated power results:

$$\Pi_{\text{rad}} = \frac{L}{2} \text{Re}(Z_f) |\dot{\eta}_f|^2 \quad (115)$$

The radiated power, coupling loss factor, and amplitude of the transverse bending motion are related by:

$$\Pi_{\text{rad}} = \omega \eta_{f,p}^b E_{\text{tot},f}^b \quad (116)$$

$E_{\text{tot},f}^b$ = total frame energy in bending

$\eta_{f,p}^b$ = coupling loss factor between a frame and panel for out-of-plane bending of the frame

and

$$E_{\text{tot},f}^b = M_f |\dot{\eta}_f|^2 \quad (117)$$

M_f = total mass of frame

The coupling loss factor is given by

$$\eta_{f,p}^b = \frac{L}{2\omega M_f} \text{Re}(Z_f) \quad (118)$$

The above expressions for the coupling loss factors between a frame and attached panel are highly approximate. The validity of the approximations made in deriving these expressions will be assessed in Phase II by designing specific experiments to determine the coupling loss factors for comparison with the predictions.

Panel-acoustic space coupling loss factor evaluation for the S-76.
The coupling between a vibrating panel and an adjacent acoustic space has been described in general. It is based on evaluating a radiation efficiency for the panel which depends on frequency relative to the coincidence frequency. For single layer panels the determination of the coincidence frequency and radiation efficiency is straightforward (see the section on acoustic/aerodynamic sources for expressions for the coincidence frequency and radiation efficiency). As discussed earlier in this section, composite honeycomb panels display different behavior in three regions. This potentially affects the dependence of the radiation efficiency on frequency.

At low frequencies the behavior involves bending deformation where the bending wavespeed is given by Eq. (104). The coincidence frequency for this type of deformation is determined by setting c_1 equal to c_0 in Eq. (104) and solving for ω_c (i.e. $2\pi f_c$). Radiation efficiencies below coincidence for deformation in Region 1 are then determined from the above value for f_c and Eq. (6) which is repeated here for convenience

$$\sigma_{\text{rad}} = \frac{P\lambda_c}{A\pi^2} \left(\frac{f}{f_c}\right)^{\frac{1}{2}} \beta \quad (6)$$

P = perimeter of panel

λ_c = wavelength at coincidence frequency
($=c_0/f_c$)

β = boundary condition factor

$\beta = 1$ simple edge support

$\beta = 1$ clamped edge support

In the mid frequency region shear deformation in the core is important, and the wavespeed is independent of frequency. If the shear wavespeed, as given in Eq. (105), is greater than c_0 , then conditions are above coincidence and the radiation efficiency is set equal to one. When the shear wavespeed is less than c_0 , the following approach is adopted for computing the radiation efficiency.

The radiation efficiency is given as a function of $(f/f_c)^{\frac{1}{2}}$. This can be recast in an equivalent form for bending deformation as:

$$\left(\frac{f}{f_c}\right)^{\frac{1}{2}} = \frac{\lambda_p}{\lambda_0} \quad (119)$$

λ_0 = acoustic wavelength at frequency, f

λ_p = panel wavelength at frequency, f

The term λ_c can be expressed in terms of the panel and acoustic wavelengths at frequency, f :

$$\lambda_c = \frac{\lambda_p^2}{\lambda_o} \quad (120)$$

The expression for the radiation efficiency now becomes:

$$\sigma_{rad} = \frac{P}{A\pi^2} \frac{\lambda_p^3}{\lambda_o^2} \beta \quad (121)$$

The appropriate value for λ_o is determined from the shear wave-speed of Eq. (105). It should be noted that the radiation efficiency in Region 2 varies inversely with frequency.

At high frequencies when the wavespeed in the panel, c_3 , is less than c_o , the critical frequency is determined by setting $c_3 = c_o$. The original expression for σ_{rad} is then used to evaluate the coupling loss factor.

Direct coupling between acoustic spaces for the S-76. - Direct coupling between adjacent acoustic spaces arises from two sources. One involves the acoustic transmission through openings in the intervening panel between the spaces, and the other is due to non-resonant response of the panel. Resonant panel motion is accounted for in the SEA model by coupling loss factors between the panel and the adjacent spaces. Non-resonant or mass controlled panel motion that is strongly coupled spatially to the acoustic resonances can constitute an important source of direct coupling at frequencies below coincidence.

The acoustic transmission through an opening depends on the acoustic impedance of the opening looking into the spaces. The transmission coefficient is given by the following:

$$\tau_h = \frac{\text{Re}(Z_h)\rho c}{|Z_h|^2} \frac{A_h}{A_p} \quad (122)$$

where

ρc = acoustic impedance

A_h = area of opening

A_p = area of panel between the spaces

Z_h = acoustic impedance of opening
looking into one of the spaces

For circular holes [24]:

$$Z_h = \rho c \left[\frac{(ka)^2}{2} - \frac{i8ka}{3\pi} \right] \quad (123)$$

$$k = \text{acoustic wavenumber} = \frac{c_0}{2\pi f}$$

a = radius of hole

For rectangular holes [24]:

$$Z_h = \rho c \left[\frac{k^2(a^2 + b^2)}{16} - \frac{i8k}{9\pi} \left(\frac{a^2 + ab + b^2}{a+b} \right) \right] \quad (124)$$

a, b = dimensions of hole

The above expressions apply in the limit when the acoustic wavelength is large compared to the dimension of the opening (i.e.: as $ka \rightarrow 0$). For circular holes Eq. (122) becomes

$$\tau_h = \frac{.7}{1 + \frac{(ka)^2}{2.88}} \frac{A_h}{A_p} \quad (125)$$

at low frequencies which reaches a constant value of $.7A_h/A_p$.

In the other limit when the opening is large compared to the acoustic wavelength (i.e.: as $ka \rightarrow \infty$) the transmission coefficient simplifies to the value $\tau_{\infty} = A_h/A_p$. For multiple openings the transmission coefficient values for each opening computed separately are simply added together. The calculations are based on the same panel area between the spaces.

Acoustic transmission between the spaces through non-resonant mass law controlled motion of the panel is evaluated from the following expression:

$$\tau_{ml} = 3.16 / [1 + (\frac{\omega \rho_p}{2\rho c})^2] \quad (126)$$

$\omega = 2\pi f$, frequency

ρ_p = surface density of the panel

The result applies for diffuse acoustic fields in the spaces.

The total direct transmission between the spaces is the sum of individual contributions due to openings and non-resonant transmission:

$$\tau_d = \sum_i \tau_{h,i} + \tau_{ml} \quad (127)$$

where the sum is over all of the holes connecting between the spaces. The coupling loss factor is evaluated from τ_d and Eq. (66):

$$\eta_{12} = \frac{c_o A_p}{4\omega V_1} \tau_d \quad (128)$$

V_1 = volume of source space

Input power evaluation for the S-76 model. - Important sources for the S-76 include the mechanical connections between the airframe and the hydraulics system and the gearbox as vibratory sources where they attach to the airframe and also as an acoustic source due to radiation from the gearbox casing and turbulent boundary layer pressure fluctuations over the exterior skin. The gearbox is the dominant source for both the untreated and treated cabin interior.

The procedures for quantifying the input power for each of the above sources are described in previous sections dealing with acoustic/aerodynamic and vibratory sources or in the general SEA section dealing with the input power. For the TBL pressure fluctuations the results in Equations 9-13 and 79 and Figure 17 are applicable for evaluating the source levels or input power.

For vibratory sources involving point attachments to the airframe Equation 8b is used to evaluate the input power in terms of a measured attachment point velocity. Experimental measurements or statistical estimates are used for the attachment point impedances. The measurements are described in a subsequent section and the statistical impedance description is discussed in relation to Equations 79 and 88.

Acoustic sources are characterized in Equation 4 by measurements of vibration levels, for example on the casing surfaces of the gearbox, and inferred values for a radiation efficiency. An alternate approach is to measure the acoustic pressure levels in adjacent spaces into which the source radiates. This approach is described in relation to Equations 94-96.

The SEA matrix equation for the S-76 model. - The form of the SEA matrix equations in terms of the subsystem modal energies, the SEA parameters, and the input power is described in a prior section. Cambridge Collaborative has developed a proprietary computer code, called SEAM, that assembles the matrix equations in terms of the SEA parameters and performs the matrix inversion to solve for the subsystem modal energies. The program also evaluates the response levels according to the procedures described in the general section entitled system response evaluation.

The program evaluates mode densities and coupling loss factors for a variety of relatively standard subsystem and junction types. Its usage in Phase II to generate predictions for comparison with measured data from the flight measurements will involve adaptations to account for cases particular to the S-76 that have been described in this section.

MEASUREMENT PROGRAM FOR MODEL VERIFICATION

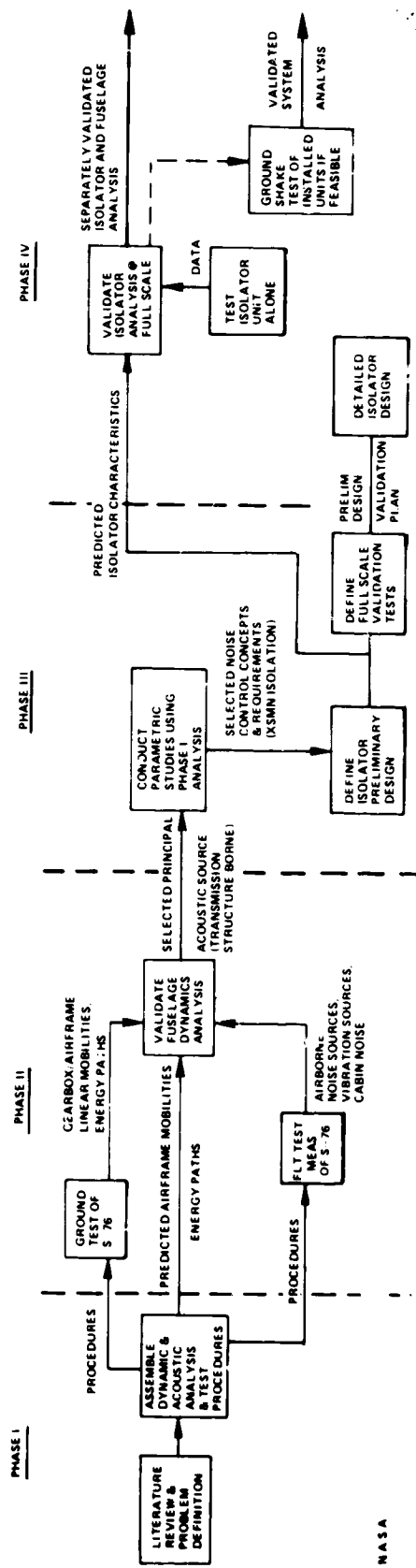
Objectives

The Phase II measurement program includes a series of ground/laboratory experiments and in-flight measurements with the general objective of validating the cabin interior noise model developed in Phase I. Specific objectives are as follows:

- to provide acoustic and vibration source levels for input into the analytic model
- to provide intermediate levels along transmission paths for comparison with the model predictions
- to provide cabin interior noise levels and vibration levels on panel surfaces that radiate directly into the cabin
- to provide data necessary to define or validate values of important parameters in the model (e.g. structural damping, acoustic absorption, vibration coupling loss factor)
- to provide data relevant to assessing validity of general predictions of the model (e.g. source coherence at gearbox attachment points, the relative importance in the airframe model of vibration transmission in the framing and skin panels)

The detailed comparisons and other experimentation are intended to identify weaknesses in the model, uncertainties in parameter values, etc. as the basis for refining the model.

The measurements fall into two categories: 1) ground or laboratory tests with the in-flight sources simulated either by mechanical shakers or acoustic speakers, and 2) flight test measurements with the actual in-flight sources (gearbox, hydraulics, aerodynamic noise sources, etc.) in operation. The ground and laboratory testing will involve the fully assembled aircraft, the fully assembled airframe minus the gearbox, and separate individual sections of aircraft including the gearbox and other airframe subsections. The Phase II effort and an overview of its place in the total program is shown in the Flow of Activities (Figure 24).



NASA

Figure 24. Flow of Activities

The intended end result of the Phase II measurements and comparisons is a cabin noise model that:

- has been thoroughly validated in terms of the fuselage dynamics and acoustic characteristics, and
- is readily applicable for evaluating the effectiveness of a variety of noise control treatments (Phase III).

Ground Test Measurement Program

The ground testing is designed to provide information for validating individual sections of the model. The primary focus is for vibration transmission in the airframe (see Figure 2), from the gearbox attachment locations through the frames and skin panels to the panel surfaces that radiate into the cabin. Acoustic transmission between the different compartmented spaces (i.e. around the gearbox, the turbine inlet, luggage compartment, etc.) and the cabin will also be investigated. A mechanical shaker or acoustic speaker is used as the source. Intermediate levels are measured along the path from the source to the cabin where the measured levels may be either the acoustic levels in the cabin or vibration levels on panels that radiate into the cabin.

Such experiments are necessary to validate an analytical model for a system as complicated as a helicopter airframe. The modeling approach, Statistical Energy Analysis (SEA), describes the system in terms of the energies of individual sections or subsystems. For structural subsystems such as framing members the energies are related to average vibration levels on the frames, while for acoustic subsystems the energies are related to the average pressure levels within the spaces. These extensive measurements involve a direct determination of the distribution of subsystem energy levels throughout the helicopter for individual source locations. Between three and five measurement locations are required for each subsystem. The SEA model accounts for individual sources for each subsystem and is directly applicable for modeling the distribution of subsystem energies in response to an individual source.

Other source locations in addition to the gearbox attachment points include locations where the hydraulics lines are attached to the airframe.

Vibration level distribution measurements. - The vibration energy level distribution measurements will be performed on a fully assembled airframe with the gearbox removed and also, on an airframe without the skin panels attached. The latter configuration is intended to substantiate the preliminary prediction of the SEA airframe model that the framing constitutes the important vibration transmission path from the gearbox to the cabin. The reader is referred to Table 1 for a compilation of the structural subsections for the Sikorsky S-76.

Vibration source coherence measurements. - Another experiment will investigate the effects of source coherence at the different gearbox attachment points. For these measurements multiple shakers with coherent electrical excitation are mounted at the attachment locations. The response is measured at several locations on the airframe for three excitation configurations: 1) both shakers active, 2) one shaker active, and 3) the other shaker active. A comparison of the response levels for both shakers active with the incoherent sum of response levels when the shakers are individually active provides a measure of the effects of source coherence between the different gearbox attachment locations.

Acoustic level distribution measurements. - The acoustic energy level distribution measurements involve placing a speaker in the particular source space and measuring average pressure levels in the source space, adjacent spaces, and the cabin. (Refer to Table 2 for the acoustical subsections for the Sikorsky S-76.) The primary source spaces for the S-76 are around the gearbox, the turbine inlet, and around the turbines. It is important in performing these measurements that the spaces and the intervening bulkheads and panels are in a representative configuration with respect to absorbing materials, holes, and the presence of wires and cables that pass through the holes, etc.

SEA parameter estimation measurements. - The SEA model contains three sets of parameters which must be evaluated. The following sections describe measurements which are intended to provide information verifying individual parameter values in the overall system model. The three types of measurements involved are:

- Attachment point impedances
- Damping loss factors
- Coupling loss factors

Attachment point impedances. - Attachment point impedances are required to appropriately determine vibration source levels independently of the structural attachment to the airframe. Source levels in the form of free velocities are determined from measured in-flight vibration levels and the impedances looking into the source and airframe at the attachment location. Although the primary interest is with the gearbox attachment points, measurements also will be performed for the attachments between the hydraulic lines and the airframe. Of particular interest will be the hydraulics attachment points at the cabin rear bulkhead. The impedances will be determined using conventional impedance heads and mechanical shakers.

The shaker is connected to the structure through an impedance head. The impedance head provides electrical outputs proportional to the force applied to the structure and the acceleration response at the attachment location. The electrical excitation can either be a swept sinusoid or a continuous broadband random noise signal.

The impedance is a complex quantity with real and imaginary components. The phase angle between the force and acceleration is, therefore, important in evaluating the impedance. Also, impedance relates force to velocity, and this requires integrating the acceleration signal to obtain the velocity.

For a swept sine wave excitation, processing of the output signals is most commonly done on an analog basis, including the integration to obtain velocity. If a broad frequency range is of interest this process can be relatively slow. With the advent of two channel signal processing analyzers, the broadband random excitation is to be preferred. All of the frequency information is generated at the same time. Such instruments are quite flexible in presenting the results in the form of plots of the real and imaginary components or of magnitude and phase. They are capable of performing the required integration of the acceleration signal as well.

Damping loss factors. - Damping loss factors are extremely important in estimating the flow of resonant vibratory energy in a structure. For aerospace structures with riveted joints, honeycomb panels, and a large amount of attached structure the damping levels significantly exceed levels for the base materials. Damping levels for built up aerospace structures are typically estimated based on general rules of thumb which have been developed from past experience.

For structures where the connections between attached components significantly contribute to the damping (so called interface damping), it is not feasible to use measured damping levels for the unattached components. Measurements on the attached structure in addition to actual damping losses include losses associated with transmission across the interfaces into adjoining components. The total measured loss factor includes damping and coupling loss factors.

Values of total loss factor for different structural subsystems determined from decay time measurements on the built up structure will be compared with model predictions in assessing the overall validity of the damping and coupling loss factor estimates.

For some structural components it is feasible to measure damping loss factors separate from the rest of the structure. This is the case where the damping levels of the component are expected to be greater than interface damping as a result of applied damping treatments. In addition to skin and framing panels with applied damping treatments, measurements will be performed on multi-layer window configurations with lossy constrained adhesive layers.

The measurement of damping loss factors involves a straightforward experiment in which the steady noise excitation to the structure is abruptly turned off and the decay of reverberant energy is measured. The energy decay occurs according to the following relationship:

$$E(t) = E_0 e^{-\eta \omega_0 t} \quad \omega_0 \text{ - center frequency of excitation noise bandwidth} \quad (129)$$

The measured reverberation time, T_r , is the time required for the energy level to decrease by 60 dB from the initial level. The reverberation time is related to the damping (η) by the relation:

$$\eta = \frac{13.8}{\omega_0 T_r} \quad (130)$$

The energy level of a structure is proportional to the mean square vibration level over the surface. It is sufficient to measure and average the decay at a limited number of representative locations using an accelerometer. Three to five locations are quite adequate for most situations.

Coupling loss factors. - The determination of appropriate coupling loss factor values involves laboratory measurements on component sections of the overall structure by focusing on individual structural connections or junctions. The experiments result in empirical estimations of the coupling loss factor between the attached subsystems. One of the structural subsystems is excited with a shaker, and the average vibratory energy levels are measured in the source and receiving structures. Vibration transmission through a right angle junction of the airframe framing is an important case for consideration in performing such measurements.

While the emphasis for the present study is on the coupling between structural subsystems, coupling loss factors between acoustic spaces and between structures and acoustic spaces are also readily evaluated experimentally. The experiments for the different types of subsystems are, in general, the same. The source subsystem is excited with a shaker or speaker and the space average response levels are measured in both the source and receiving systems. An independent measurement of the dissipation of the receiving subsystem is also required for the evaluation of the coupling loss factor.

The basis for the experimental determination is described with reference to the energy balance equations for two subsystems where only one is excited. The power balance for the unexcited subsystem yields the following result [17]:

$$\frac{E_{r,tot}}{N_r} = \frac{E_{s,tot}}{N_s} \frac{\eta_{r,s}}{\eta_r + \eta_{r,s}} \quad (131)$$

$E_{r,tot}$	Total energy of receiving(r) or source(s) subsystem
$E_{s,tot}$	
	N_r, N_s - # of modes in excitation bandwidth
	$\eta_{r,s}$ - coupling loss factor
	η_r - damping loss factor in receiving subsystem

Measured quantities include the total energies $E_{r,tot}$, $E_{s,tot}$, and the damping loss factor η_r . The mode count is determined from appropriate analytical expressions for the particular subsystems.

The total energies are determined from the space average response levels. For an acoustic subsystem the total energy is the energy density, D , times the volume of the space, V :

$$E_{\text{tot}}^{\text{ac}} = V \times D \quad (132)$$

where:

$$D = \frac{\langle p^2 \rangle_x}{\rho c^2} \quad \langle p^2 \rangle_x \text{ space average mean square pressure} \quad (133)$$

For a structural subsystem the total energy is related to the measured vibration response according to:

$$E_{\text{tot}}^{\text{vib}} = \sum_i \rho_i \langle V^2 \rangle_i A_i \quad (134)$$

ρ_i - surface density of structure at i^{th} vibration measurement location

A_i - surface area associated with i^{th} measurement location

$\langle V^2 \rangle_i$ - measured square vibration level at i^{th} location

For a uniform structure with evenly spaced measurement locations this simplifies to:

$$E_{\text{tot}}^{\text{vib}} = M_s \langle V^2 \rangle_x \quad (135)$$

where:

M_s - total mass of subsystem

$\langle V^2 \rangle_x$ - space average mean square velocity

The accuracy of using the above equations to experimentally determine the coupling loss factor is dependent on the damping level in the receiving subsystem relative to the coupling loss factor. If the damping, η_r , is small compared to $\eta_{r,s}$, it is not feasible to solve Equation (131) for the coupling loss factor $\eta_{r,s}$. This is a condition where the modal energies of the subsystems are equal. It is often necessary in performing a laboratory measurement according to Equation (131) to artificially increase the damping in the receiving subsystem to improve the measurement accuracy. For acoustic systems this involves the use of absorbing materials such as fiberglass or open cell foam. Damping treatments for structures typically involve added lossy viscoelastic materials in the form of free extensional or constrained layers.

An alternative approach for an experimental evaluation of the coupling loss factor between acoustic spaces is to measure the transmission loss of the intervening panel surfaces. The coupling loss factor is then determined from the measured transmission loss according to Eqs. (66) and (67). Three techniques are applicable for measuring the transmission loss: 1) the room acoustics method, 2) the near field pressure method, and 3) the acoustic intensity method.

For all three techniques a speaker is placed in the source space to generate the noise field. The acoustic intensity incident on the intervening panel between the source and receiving space is evaluated for all three techniques according to the following:

$$I_{inc} = \frac{\langle p_s^2 \rangle}{4\rho c} \quad (136)$$

$\langle p_s^2 \rangle$ = space average mean square pressure in source space

The techniques differ in the manner in which the transmitted acoustic intensity is evaluated.

For the room acoustics method a prior calibration of the receiving space is performed which relates the measured space average mean square pressure levels to the power transmitted into the space under steady state conditions. The prior calibration involves a reverberation decay time measurement to quantify the energy absorption in the space.

The difference in measured space average pressure levels in the source and receiving spaces with speaker excitation is related to the transmission loss by

$$TL = NR + 10 \log_{10} \frac{A_p}{R} \quad (137)$$

TL = transmission loss

NR = noise reduction

NR = $\langle p_s^2 \rangle - \langle p_r^2 \rangle$ = difference in space average pressure levels in source (s) and receiving (r) spaces

A_p = area of intervening panel

R = room constant for receiving space [19]

A key factor in applying this method for helicopter spaces is that it evaluates the total power transmitted into the receiving space, not just the power transmitted through the intervening panel of interest. For the transmission loss values to accurately reflect the behavior of the panel, flanking transmission must be held to a minimum.

The other techniques involve direct estimations of the transmitted power through the panel of interest and are not sensitive to flanking transmission errors. In the near field pressure method a microphone is swept at close distance over the receiving side of the panel. The transmitted intensity is related to the average near field pressure according to the following approximate expression:

$$I_{trans} = \frac{\langle p_{nf}^2 \rangle}{K_g \rho c} \quad (138)$$

where $\langle p_{nf}^2 \rangle$ is the average near field pressure over the surface of the panel and K_g is an empirical factor that depends on the radiation characteristics of the surface including the effects of curvature. Typical values for K_g are in the range from 2 to 4.

For aircraft structures additional empirical information may be required to specify the value of K_g .

The advent of small, high speed computers capable of efficiently performing digital signal processing operations has resulted in the implementation of methods for measuring acoustic intensity. A two microphone probe is used to measure the intensity of the radiating noise field in the vicinity of a vibrating surface. A more detailed discussion of the theoretical basis of the intensity probe is given in Appendix C. The application of the intensity method for measuring the transmission loss of aircraft panels is discussed in References [25, 26].

The intensity probe is used to measure the net radiated intensity from the intervening panel by scanning over the surface at a sufficient number of locations. The transmission loss is then determined by the ratio of transmitted to incident intensities.

$$\tau = \frac{I_{trans}}{I_{inc}} \quad (139)$$

$$TL = -10 \text{ Log}_{10} (\tau) \quad (140)$$

where I_{inc} is evaluated from Eq. (136) and I_{trans} is the net power transmitted through the panel as measured with the intensity probe.

The intensity techniques can also be used to evaluate coupling loss factors between panels and the adjacent acoustic spaces. These evaluations are based on an experimental determination of the radiation efficiency for the panel. With the panel excited by a noise field on the opposite side from the space of interest, the power radiated by the panel is related to the radiation efficiency, σ_{rad} , by the following:

$$W_{rad} = \rho c A_p \sigma_{rad} \langle V_p^2 \rangle \quad (141)$$

where $\langle V_p^2 \rangle$ is the space average mean squared velocity level on the panel. The radiated power is determined by the acoustic intensity method accounting for the total radiating area of the panel. The experimentally evaluated radiation efficiency is then related to the coupling loss factor according to Eq. (68) as follows:

$$\eta_{1,2} = \frac{\Pi_{\text{rad}}}{\omega M_p \langle V^2 \rangle} \quad (142)$$

Preliminary Airframe Vibration Transmission Measurements

Preliminary vibration transmission measurements were carried out on an S-76 airframe with the following objectives in mind:

- A) Familiarization with S-76 airframe to assist in design and implementation of full Phase II ground test measurement program.
 - Identify measurement requirements
 - source excitation
 - sensor location
 - data acquisition and reduction
- B) Provide limited quantitative descriptions of vibration transmission to assist in development of S-76 airframe model.
 - Help identify important structural elements and paths.

The measurements were performed on a partially assembled S-76 airframe on the Sikorsky S-76 assembly line. All of the major structural components of the airframe were in place. The pilot/copilot doors and windows had not yet been mounted. The gearbox was also not installed, and this conveniently allowed access for mounting a mechanical shaker to the gearbox attachment locations on the airframe. Control and electrical cables were not installed. This allowed convenient access for mounting an accelerometer on the various frame and panel members of the airframe.

For the measurements a mechanical shaker was mounted separately at two gearbox attachment locations. The shaker was excited with a broadband random noise signal in the frequency band from approximately 200 - 7000 Hz. One lightweight accelerometer was permanently mounted at the source location while a second accelero-

meter was moved to different locations on the frames and panels of the airframe. A total of 40 different locations were used for the measurements. The locations covered the structure around the cabin including overhead panels and frames, side panels, windows, doors, etc. and extended from near the source in the rear of the cabin forward to the nose structure. As a result of the symmetry of the airframe structure, the measurement locations were limited to the middle and left side of the cabin. The shaker positions included the rear most attachment point on the same side as the measurement locations and the forward point on the other side of the cabin. Lightweight .5 gm accelerometers were used so as not to influence the vibration levels being measured.

The data were acquired and processed with a two-channel FFT analyzer which computed the transfer function between the vibration levels at the source and measurement locations. Coherence function measurements also were recorded to indicate frequencies where potential contamination by extraneous noise sources occurred.

A sample plot of these measurements is shown in Figure 25 with the shaker located at the rear attachment point on the left side (RAL) of the gearbox and the measurement location at a random point on the overhead panel on the left side of the cabin near the rear bulkhead. The overhead panel is of a composite honeycomb construction. Refer to Table 1 for frame and panel designations.

The narrowband plot of the transfer function is characterized by peaks and dips that are indicative of the resonant structure of the panel response plus the fact that the result involves no spatial averaging over the area of the panel. The coherence levels are in general high, indicative of a large signal to noise ratio. The dips in the coherence function correspond to the dips in the transfer function. Dips occur where the accelerometer is located at a node of individual panel resonances. The measured panel signal at the dip is dominated by extraneous noise that is uncorrelated with the source signal.

As shown in Figure 26 the overall coherence levels decrease for panels further from the source as a result of the decreasing vibration transmission. The transfer function magnitude is evaluated from the cross spectrum of the source and measured panel levels, and therefore, discriminates against noise in the panel levels. Even though the coherence, in general, is decreasing due to noise the accuracy of the transfer function estimate is maintained.

The variation in overhead panel levels is shown in Figure 27 for the shaker at the front attachment point on the right side (FAR). The overhead panel levels were measured on the left side of the cabin. A comparison of levels on different panels is influenced by differences in the mechanical characteristics of the panel. The thicknesses of the composite honeycomb panels vary from 12 to 25mm throughout the cabin.

In an SEA model of vibration transmission, the modal energy is the important quantity in determining the flow of vibratory power. Differences in modal energies between attached structures result in a net flow of power. An equilibrium results when the modal energies are identical and therefore no net power flow exists. The modal energy is scaled by the space average vibration level where the constant of proportionality is dependent on panel parameters including thickness. The result of this is that a comparison of vibration levels is not sufficient for characterizing the vibration transmission when the parameters differ from panel to panel.

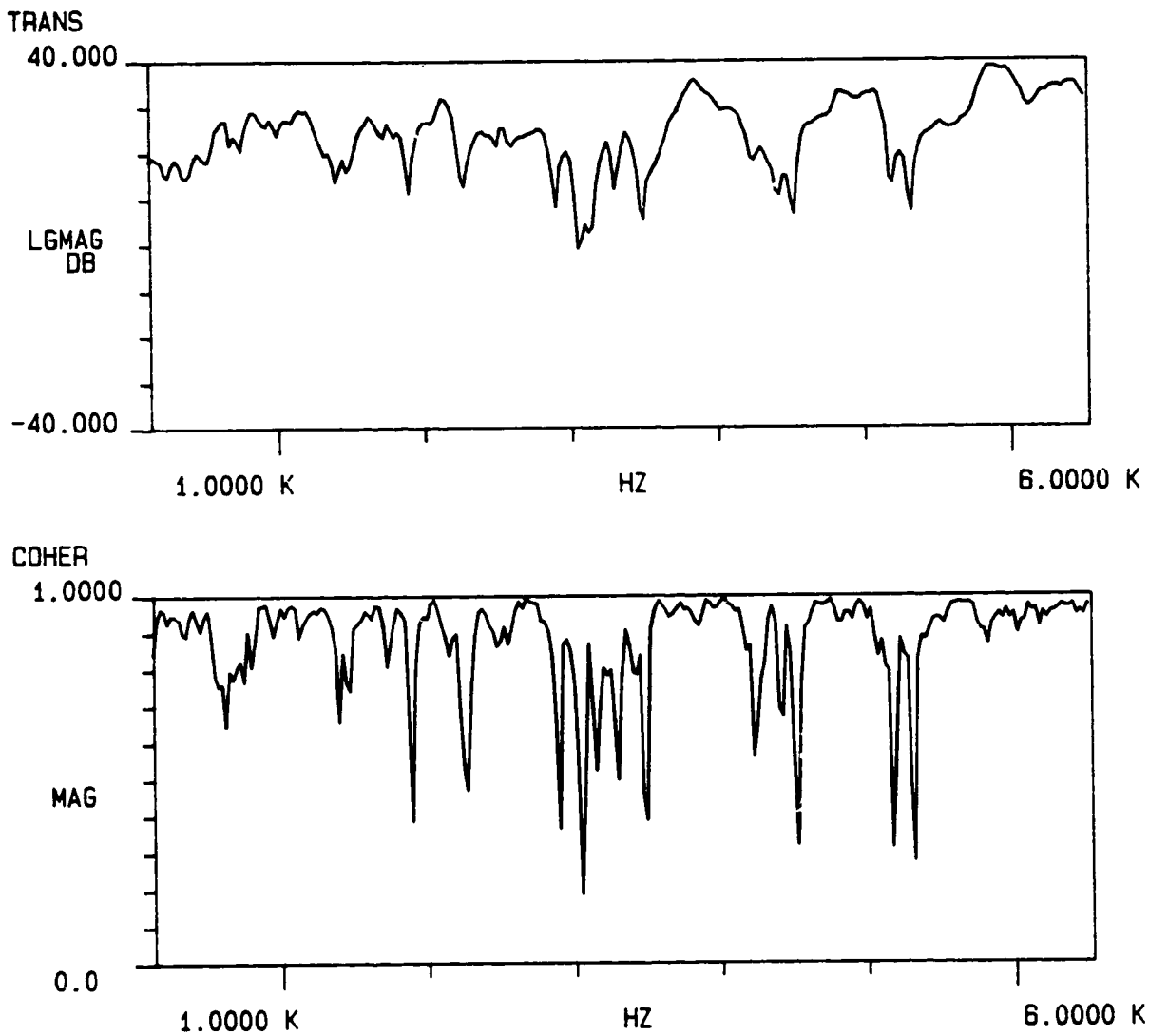


Figure 25. Typical Transfer and Coherence Function Measurement.

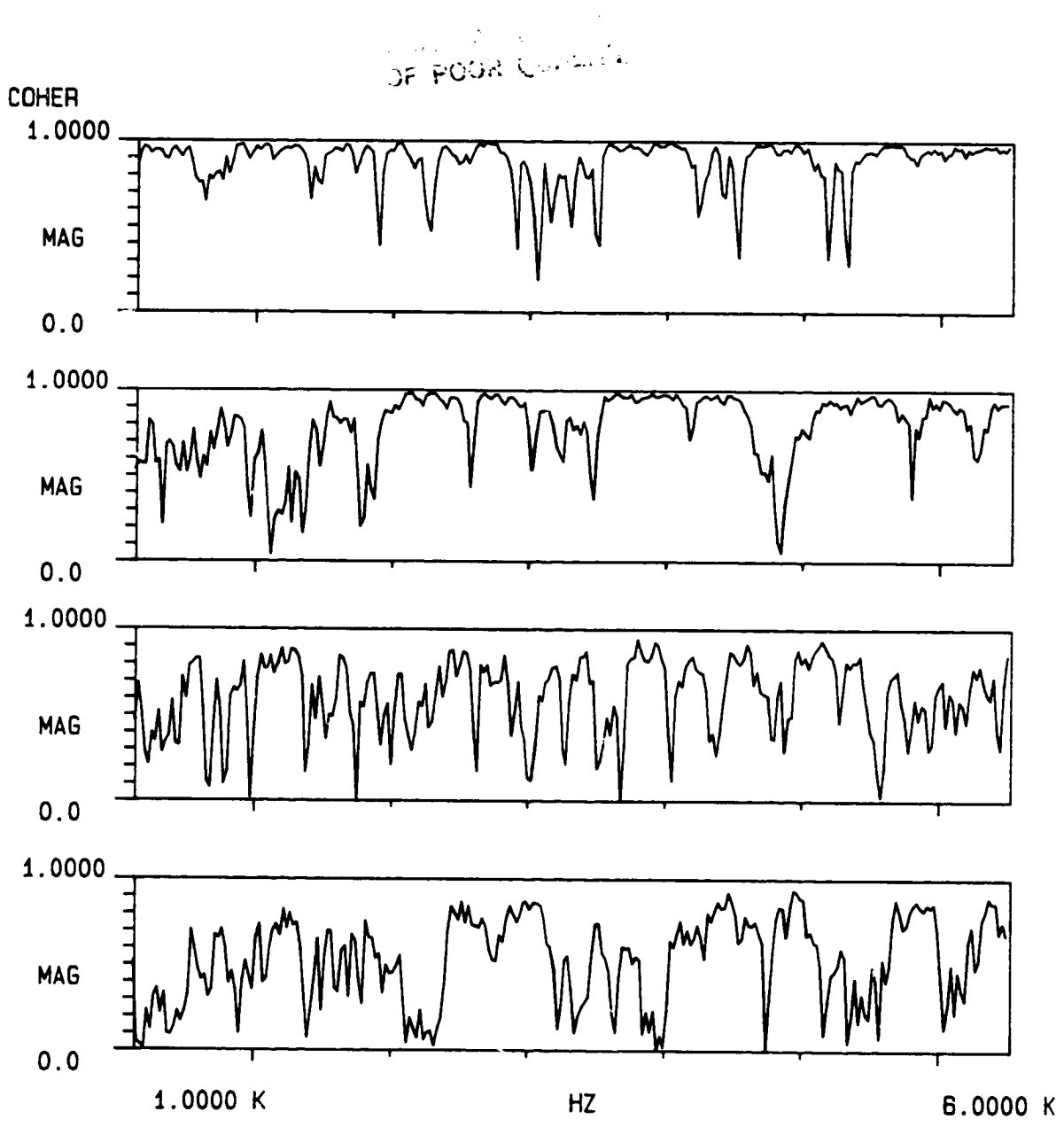


Figure 26. Variation of Coherence Function Levels for Overhead Panels vs. RAL Excitation.

ORIGINAL PAGE IS
OF POOR QUALITY

ACOUSTIC DATA - OCTAVE SPECTRUM

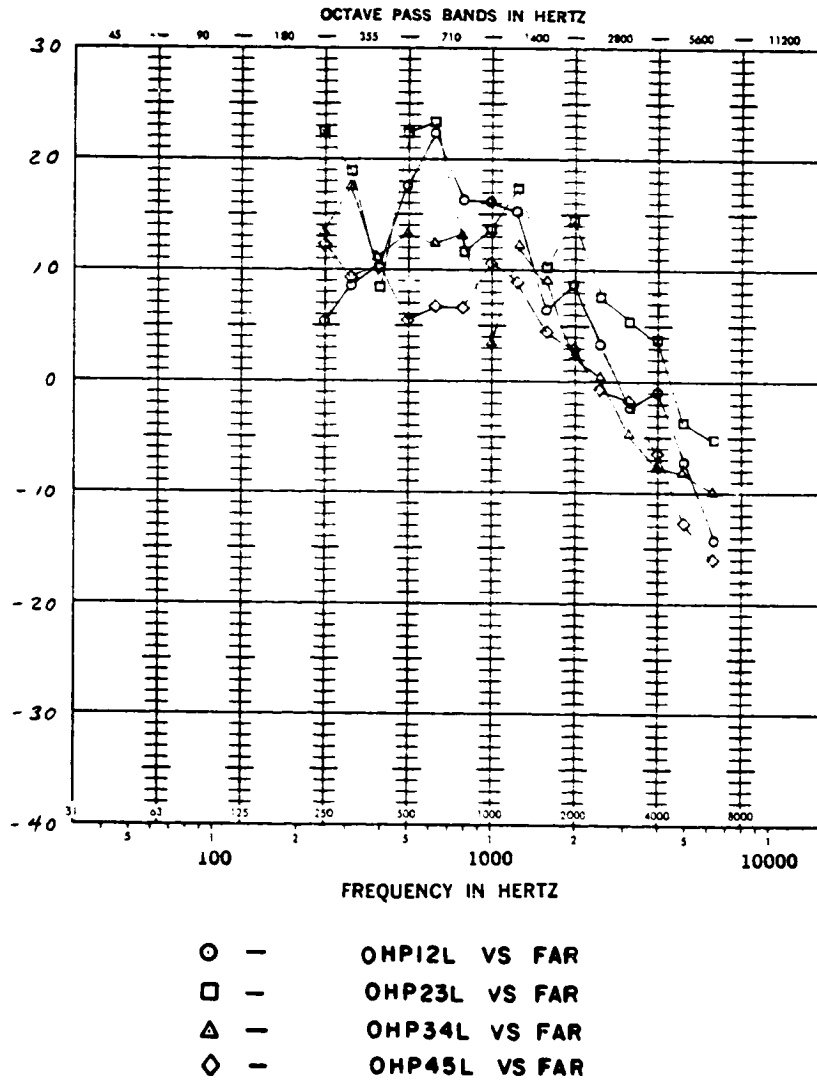


Figure 27. Variation of Transfer Function Levels for Overhead Panels vs. FAR Excitation.

From Figure 27 the variation in level from the rear of the cabin forward to locations at the copilot's position is relatively minor, on the order of 5 - 7 dB. The absolute magnitudes of the transfer functions can be significantly greater than 1. This depends on the fact that the gearbox is attached to relatively heavy and stiff framing. If the framing is well coupled to the panels so that the modal energies are comparable, then the vibration levels will be greater on the lighter weight panels.

Differences in levels for individual panels for the excitations at two different gearbox attachment points (RAL vs. FAR) are shown in Figure 28. These differences are more pronounced for panels further aft closer to the source attachment points. For the forward panels the levels are more comparable. The differences are more accentuated at higher frequency. The source on the left side (where the panels are located) is closer and more directly coupled into the panels in comparison with the attachment location on the right side.

Transfer functions for important panel surfaces in the rear of the cabin are shown in Figures 29 and 30. The drip pan is the overhead panel immediately beneath the gearbox that is supported from the framing to which the gearbox is directly mounted. The rear passenger bulkhead is also directly coupled to the same framing. Both panels are more equally excited by the two attachment point locations at lower frequency. At higher frequencies the rear attachment point is more effective than the forward location in exciting both the bulkhead and drip pan.

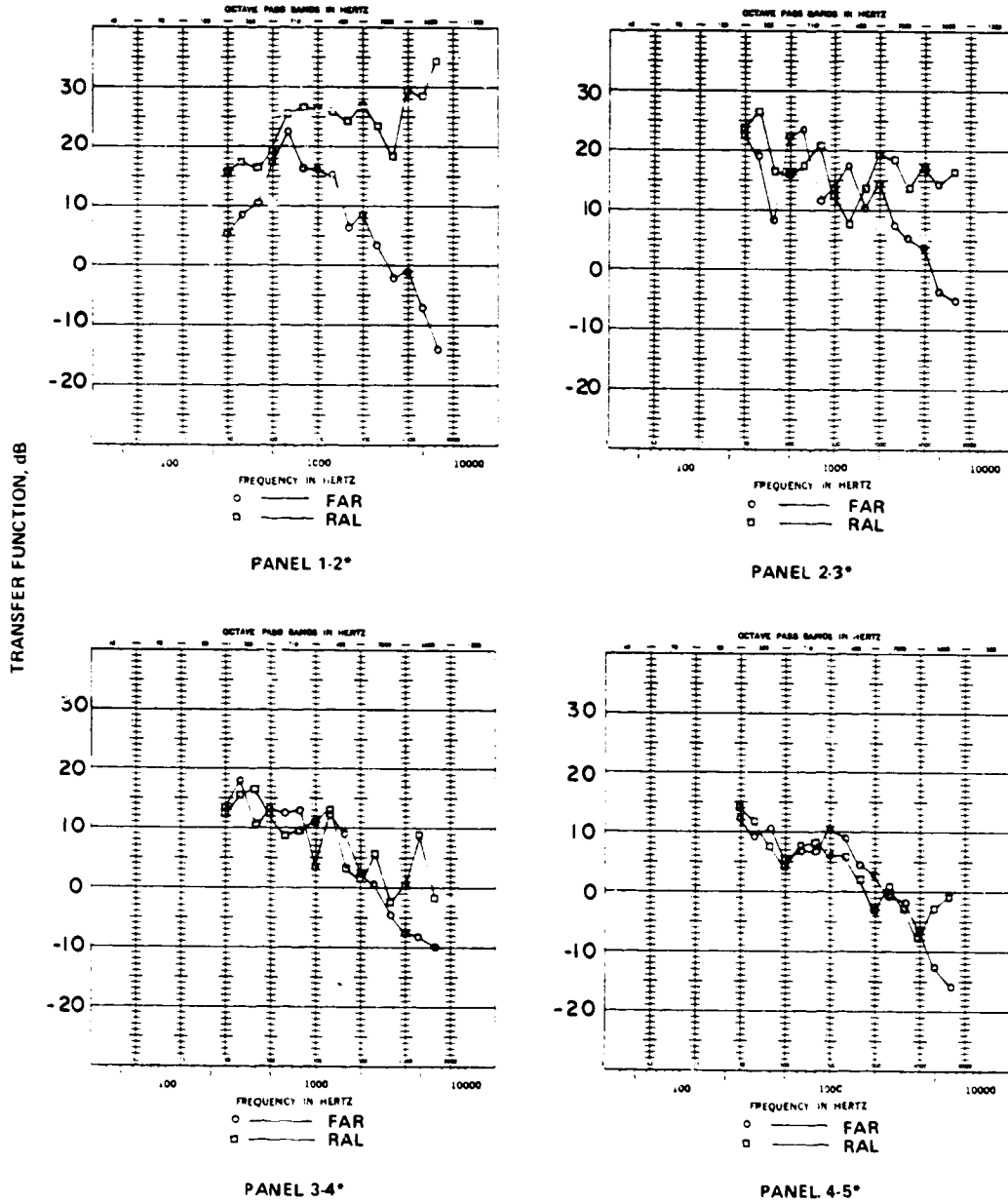
The variations in vibration levels on the webs of the main fore/aft frame members are shown in Figures 31 and 32. The rear attachment location (RAL), Figure 31, is at the aft-most point of the fore/aft frame. The levels are greatest on the first frame section, particularly at higher frequencies. The decrease in level forward of the gearbox is not significant. In fact there is an increase in level for the furthestmost forward frame section. The decreasing weight of the frame members moving forward contributes to this result.

The variation in vibration level for the right side source location (FAR), Figure 32, also does not show significant changes in level. The source is directly coupled into the cross frame between fore/aft frame sections one and two. Levels in frame section one are smaller than for section two because frame section one, which directly supports the gearbox, is of a heavier construction.

ORIGINAL PANELS
OF POGR QUALITY

SHAKER MOUNTED FOR VERTICAL EXCITATION AT :

FAR : FRONT GEARBOX ATTACHMENT LOCATION ON RIGHT SIDE
RAL : REAR GEARBOX ATTACHMENT LOCATION ON LEFT SIDE



* PANEL SECTIONS ON LEFT SIDE BETWEEN CROSS FRAMES.
SEE FIGURE 4 FOR CROSS FRAME LOCATIONS.

Figure 28. Effect of Excitation Point on Panel Transfer Function.

OF

ACOUSTIC DATA - OCTAVE SPECTRUM

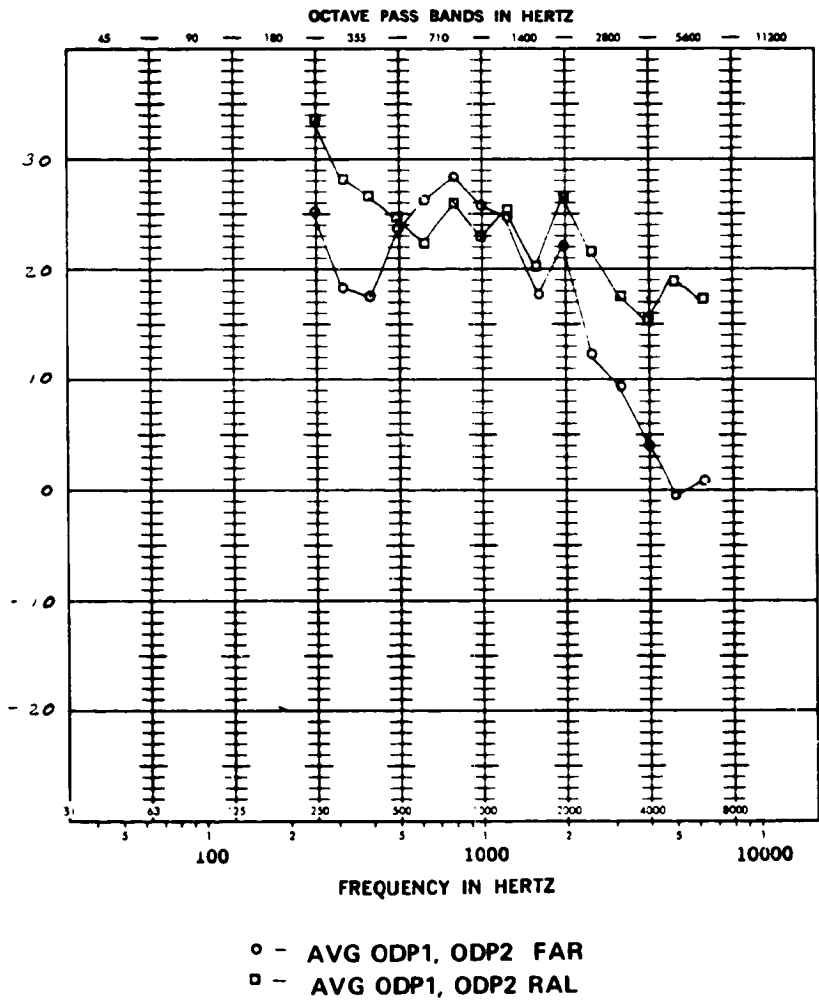


Figure 29. Effect of Excitation Point on Drip Pan Transfer Function.

ORIGINALLY
POOR QUALITY

ACOUSTIC DATA - OCTAVE SPECTRUM

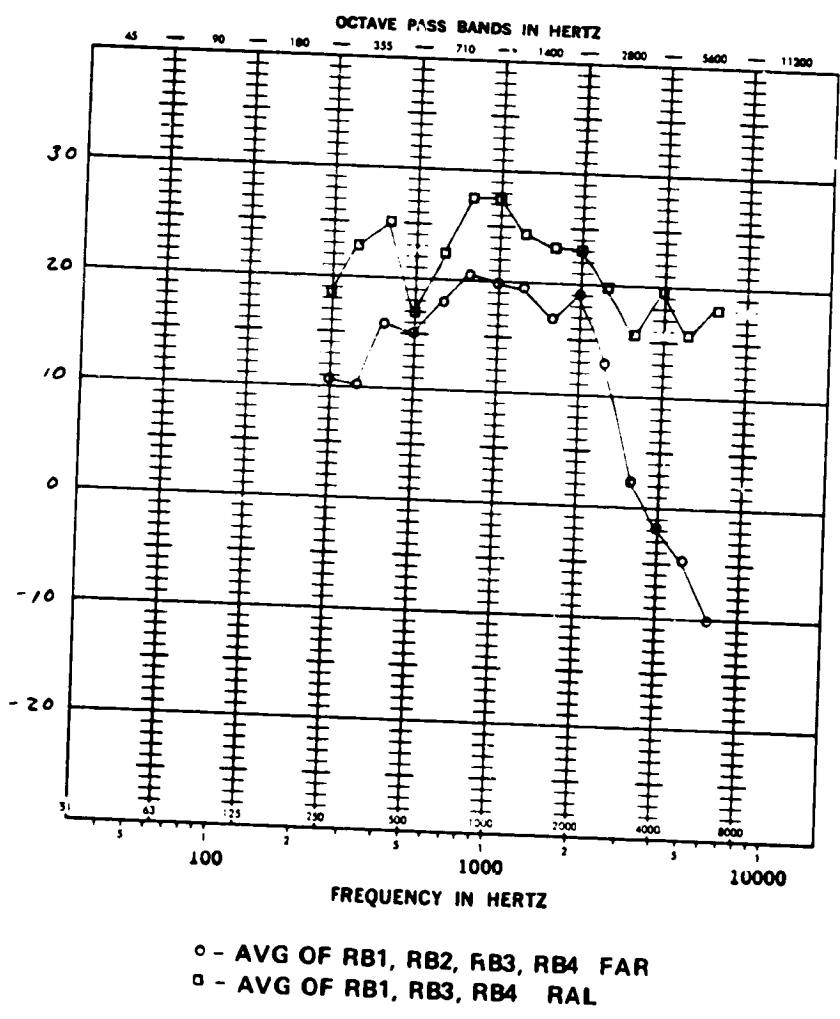


Figure 30. Effect of Excitation Point on Rear Bulkhead Transfer Function.

ORIGINAL COPY
OF POOR QUALITY

ACOUSTIC DATA - OCTAVE SPECTRUM

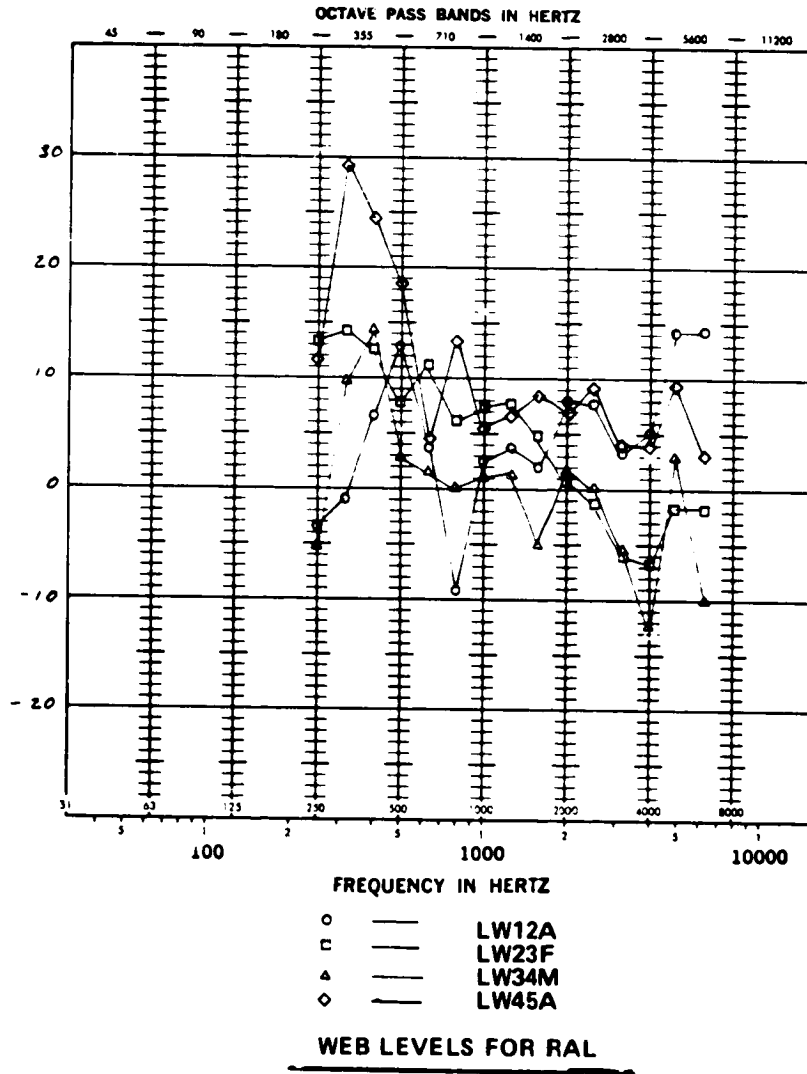


Figure 31. Web Transfer Functions for RAL Excitation

ORIGINAL PAGE IS
OF POOR QUALITY

ACOUSTIC DATA - OCTAVE SPECTRUM

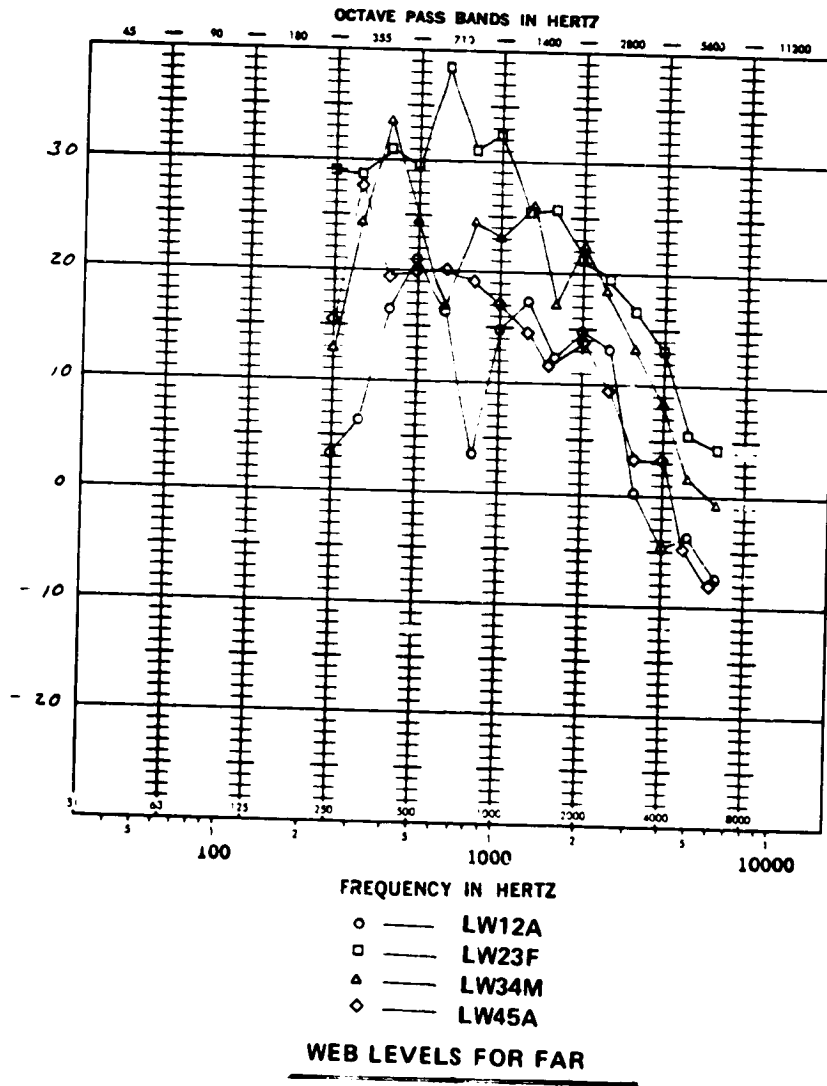


Figure 32. Web Transfer Functions for FAR Excitation.

Figure 33 shows the relative vibration levels at the top and bottom of frame section one at the source location. Both accelerometers measured the vertical displacement of the frame. At low and mid frequencies the levels are equal, i.e. the value of the transfer function is approximately 0 dB. The resonance at higher frequency near 5.1 kHz involves a deformation of the frame cross section in the vertical direction. This presents a limitation in modeling the frame as deforming in bending as this does not allow for deformation of the cross section.

Vertical displacements were also measured at different locations forward on the longitudinal frames, as shown in Figures 34 and 35. The levels do not decrease significantly moving forward in the cabin. The decrease in frame weight influences this result. With the source at the front attachment point on the right side (Figure 35) the levels at position LF2 are less than further forward. This position is at the junction of the fore/aft frame and the cross frame at the front of the gearbox which may explain the reduced levels.

Measured acoustic levels under flight conditions have suggested that the fore/aft frames are an important path for gearbox-generated tones forward to the front windshields (see Figure 14). Though the windshields were not yet installed, measurements were made on the central frame or window post that extends down between the pilot's and copilot's windshields. The frame is of a fiberglass construction.

The results for the two source locations are shown in Figure 36. The differences between the curves are minor. Also notable are the absolute transfer function levels. The levels above 1 kHz are in the range from -15 to -30 dB. The coherence was generally poor though there were regions of high coherence which may correspond to bands of efficient transmission forward along the main fore/aft frame.

Flight Test Measurement Program

Measurements of the distribution of acoustic and vibration levels in flight have obvious differences from the ground tests in relation to the source characteristics. For example, for the gearbox, the ground tests are not fully capable of simulating the source vibration characteristics at the attached points with respect to the coherence between the different motions and attachment points, and the detailed spectral characteristics of the source.

ORIGINAL PHOTO
OF POOR COPY

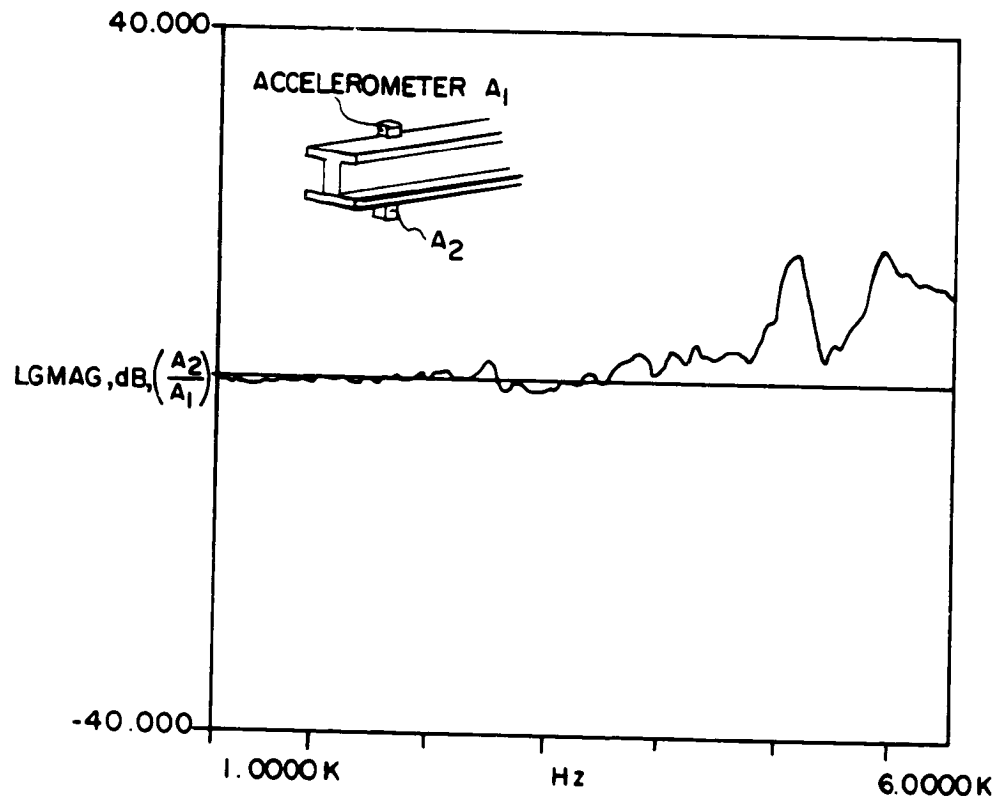


Figure 33. Transfer Function at Frame Section 1 for RAL Excitation.

ACOUSTIC DATA - OCTAVE SPECTRUM

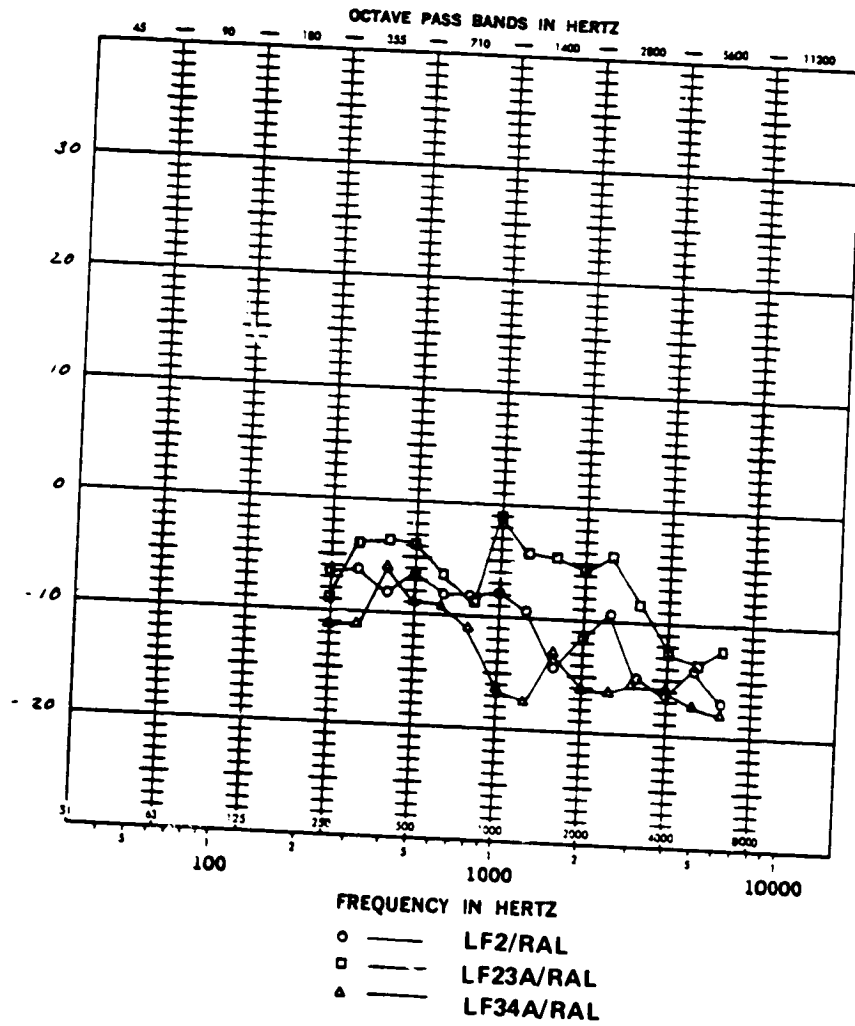


Figure 34. Variation of Vertical Transfer Function Along the Main Longitudinal Frame for RAL Excitation.

ORIGINAL RECORD
OF POOR QUALITY

ACOUSTIC DATA - OCTAVE SPECTRUM

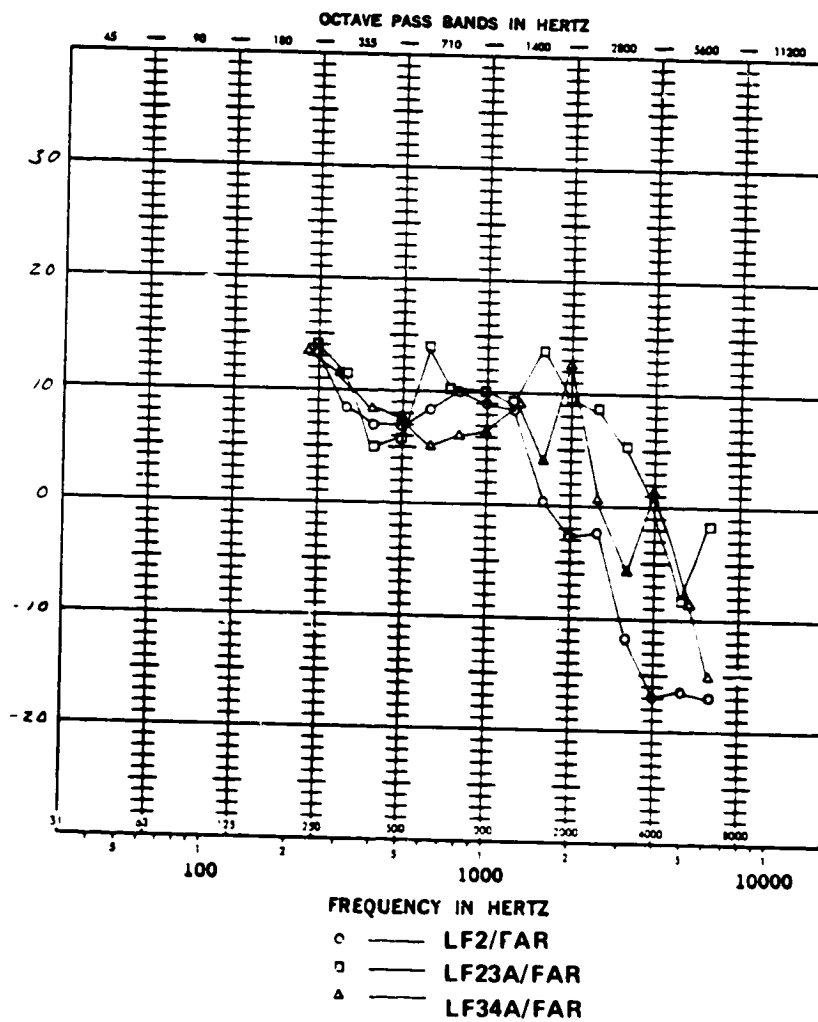


Figure 35. Variation of Vertical Transfer Function Along the Main Longitudinal Frame for FAR Excitation.

ACOUSTIC DATA - OCTAVE SPECTRUM

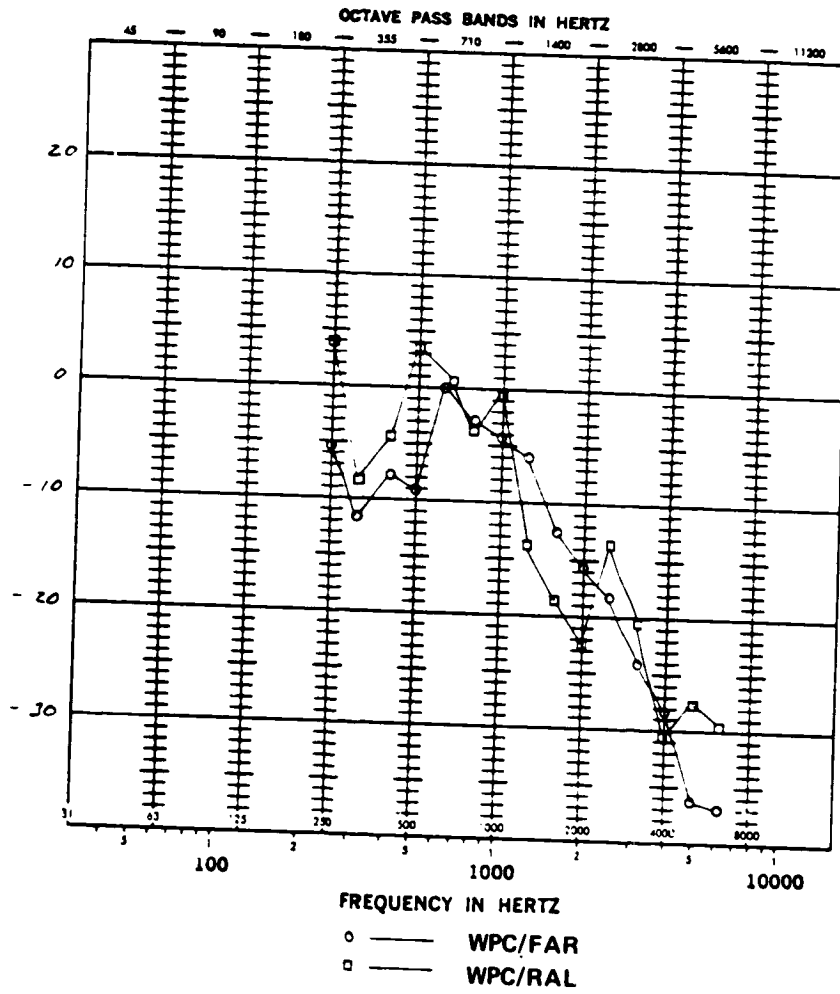


Figure 36. Effect of Excitation Point on Window Post Center Transfer Function.

The flight test measurements are primarily intended to provide source level data for both acoustic and vibration sources. The measured source levels will be used to scale the inputs to the overall model. Recently developed partial coherence techniques will be applied to in-flight data to determine the contribution of each source to cabin levels. This will provide an independent check of the overall model prediction.

An important additional objective of in-flight measurements is to provide detailed descriptions of the cabin noise environment for different flight operating conditions. The descriptions involve detailed measurements of cabin pressure levels at the different passenger/crew locations including an evaluation of spacial variations in level near the different passenger locations and in the vicinity of important radiating panels. It also includes extensive measurements on panels radiating directly into the cabin including overhead panels, the webs of main frames, door panels and windows, etc. Vibration and acoustic levels will be measured at intermediate locations on the airframe and in intermediate acoustic spaces, for example the luggage compartment. The measurements in the cabin and at intermediate locations provide distributions of levels throughout the helicopter for comparison with the model predictions.

Several flight operating conditions will be evaluated during the measurements, including:

- 75 meters per second level flight
- level flight at most efficient forward speed (longest range)
- hover

Other details of the flight condition as regards weight, weight distribution, etc., will be consistent with standard flight test requirements.

Initial survey measurements will be performed by moving a single microphone or accelerometer from location to location. A reference location will be monitored to verify that the operating conditions have remained stable. This reference location will be monitored during the fully instrumented flight tests to verify the consistency of flight condition. Analysis of this initial survey data will be used to select specific in-flight measurement locations for the detailed data acquisition required for the analytic model verification.

The fully instrumented flight test measurements will involve a large number of acoustic and vibration sensors located throughout the helicopter with simultaneous recordings on a 14 channel tape recorder. Since the Phase III isolator design is likely to involve materials with temperature sensitive characteristics, temperature measurements near the isolator locations will be obtained. A total of approximately 36 sensor locations is estimated for these flight test measurements.

Statement of Work For Ground and Flight Test Measurements

Task 1.0 ground test measurements. - These ground test measurements are primarily intended to determine SEA parameter values and verify several postulates.

- 1.1 Instrument model S-76 aircraft (without gearbox) with accelerometers along the frames and panels. Shaker to be mounted at successive gearbox attachment points. Repeat measurements at hydraulics attachment points. Acquire acoustic measurements in acoustic spaces as well as acceleration data while monitoring source strengths. Perform near-field probe sweep of selected panels for radiation efficiency.
- 1.2 Install two shakers at gearbox attachment points and conduct coherence test with 1) one shaker, 2) the other shaker and 3) both shakers operating.
- 1.3 Install impedance head on shaker at airframe/gearbox attachment point on gearbox and measure impedance looking into gearbox at each foot. Repeat for attachment looking into airframe.
- 1.4 Instrument airframe without panels to measure accelerations along the framing members and obtain data with a shaker successively at the attachment points.
- 1.5 Install shaker at locations several substructures removed from the gearbox area to obtain excited subsystem decay and total loss factor data.
- 1.6 Instrument individual key model subassemblies (such as windshield and junctions) in separate laboratory tests with shaker and accelerometers to obtain loss factor data.
- 1.7 Install speakers in each of the six acoustic spaces (gearbox, turbine inlet, turbine, luggage compartment, ECU, nose compartment) and measure acoustic levels in adjoining spaces and cabin operating one speaker at a time. Use a complete aircraft with gearbox for this acoustic transmission test.
- 1.8 Locate speaker outside complete aircraft and measure transmission characteristics for windows and side panels with intensity probe.

Task 2.0 flight test measurements. - These flight test measurements are primarily intended to determine source strength levels.

- 2.1 Instrument model S-76 aircraft with accelerometers at key locations (gearbox, hydraulics, frames, windshield, etc.)
- 2.2 Perform 1 hr. preliminary vibratory/acoustic survey to identify additional in-flight hot spots
- 2.3 Acquire approximately 6 hours of flight data in various conditions measuring vibration and acoustic levels at approximately 36 locations
- 2.4 Acquire approximately 3 hours of flight data (subsequent to SEA model modification). Measurement locations will be chosen to verify model modifications and refinements.

Model Comparisons and Refinements

The primary objective of Phase II is the validation of the cabin interior noise model developed in Phase I. The development of a noise model for a system with the complexity of a helicopter necessitates an iterative process in order to establish confidence in the model. Measured data for a representative helicopter is compared with preliminary model predictions in order to identify weaknesses in the model which require additional refinements.

The validation process involves comparisons of the reduced flight and ground test data with predictions from the model. The model is exercised for original estimates of parameter values in making an initial comparison with measured data. Subsequently, additional predictions are generated to determine the sensitivity of the predicted results to variations in key parameter values. This also involves comparisons between predicted values for individual parameter values, for example, coupling loss factors for specific structural connections with the results from specially designed laboratory experiments on structural subsections.

The intended end result of the Phase II measurements and comparisons is a cabin noise model that has been thoroughly validated and which is readily applicable for evaluating the effectiveness of a variety of noise control treatments.

SUMMARY AND CONCLUDING REMARKS

Dynamic mesh forces within the gearboxes of modern civilian/commercial helicopters are the dominant source of cabin noise. The cabin airframe is a complex structure with the potential for many highly interconnected structureborne and airborne transmission paths from the gearbox to the cabin. The high frequency nature of the mesh forces, with tonal harmonics throughout the important audio bands, excites a multitude of structural and acoustic resonances.

Classical modal analysis procedures and finite element methods are applicable for modeling the cabin noise environment at great cost because of the structural complexity of the airframe and the large number of resonances that are excited. Statistical methods are appealing as alternatives in that the response is described statistically in terms of groups of resonant modes having similar dynamic behavior. The number of degrees of freedom (dof) in the model are greatly reduced over other approaches.

A model of the helicopter airframe and cabin noise environment has been developed for the Sikorsky S-76 based on Statistical Energy Analysis (SEA). The number of degrees of freedom is 180 in the full SEA model and 106 in a reduced model when there is symmetry in the airframe structure and gearbox excitation. Though large, the dof are significantly smaller than for the comparable finite element models of the airframe in the same frequency range.

The physics of the vibration transmission problem are described by SEA in the form of a coupling loss factor for power flow across junctions between attached subsections of the airframe and a damping loss factor for power dissipated internally within a group of modes including the effects of added damping treatments.

The model developed for the S-76 represents an important extension of the application of SEA to larger, more complicated transmission problems. SEA procedures for setting up and solving the system equations are not any more complicated for larger systems. Of importance is how assumptions made in characterizing the resonant behavior of individual airframe subsections and the dynamics of the junctions that connect them affect the overall prediction of vibration transmission. Specific areas for potential further refinement of the model include the modeling of frame member dynamics and the coupling between panel subsections across intervening frames. There is potential concern for the effects of resonant cross-sectional deformation in frames and the effects of non-resonant frame motion in coupling between panels.

As with any modeling approach, confidence in the model improves with increasing familiarity with the particular problem. Insights gained from measured data on the actual system, in the lab, or

under operational conditions, contribute importantly to one's past experience in initially developing the model and subsequently in refining it. The second model verification phase of the NASA program will provide important measurement inputs in demonstrating the usefulness of a Statistical Energy Analysis approach for the complicated problem of modeling the cabin noise environment of helicopters.

APPENDIX A

Details of Source/Path Identification Techniques

Path identification by temporal discrimination. - The most direct method of identifying transmission paths of a non-dispersive system is by exciting the system with impulses (using either an externally applied signal or internal impulsive sources within the system). One monitors the response at a point and detects the arrival time of the impulse. Since the wavespeed is constant, then a measurement of the travel time leads to an estimate of the propagation distance between the points if the wavespeed is known, or an estimate of the wavespeed if the spatial path separation between the points is known. Examination of later impulses received gives information on the first few reflections within the system. Thus, various paths can be identified and their relative amplitudes measured.

Problems arise with all time delay methods when the arrival times for successive propagation paths become closely spaced relative to the pulse or tone burst duration. For vibration transmission in a helicopter airframe this may constitute a serious limitation because the structure is relatively compact and path length differences are small. The technique would involve exciting the gearbox attachment points with tone bursts or impulses and monitoring the received acoustic signals at different passenger locations. Vibration levels on different panel surfaces of the cabin interior may also be monitored.

Temporal discrimination: correlation analysis - A second method of temporal discrimination involves the use of correlation analysis. The cross-correlation function is computed between the source and the response point if the source location is known, or between the two response points. If the source excitation is white noise or band-limited noise, then the cross-correlation function is a maximum at a delay time which is equal to the time delay for propagation between the two response points. The most important difference between the time delay measurement method and the correlation analysis method is that the time delay technique is useful for pulse excitation, whereas the correlation technique is useful for steady-state, random excitation. If the source excitation is broad-band and produced within the system, then correlation analysis is often the more appropriate technique.

Suppose the excitation is band-limited white noise between the lower frequency f_L and upper frequency f_U . Then the cross-correlation function $R_{xy}(\tau)$ between the responses $x(t)$ and $y(t+\tau)$ whose path length difference is d is

$$R_{xy}(\tau) = XY \cos[\pi(\tau-d/c)(f_L+f_U)] \frac{\sin[\pi(\tau-d/c)(f_U-f_L)]}{\pi(\tau-d/c)(f_U-f_L)} \quad (143)$$

where X and Y are the signal amplitudes. The cross-correlation function is a maximum at $\tau=d/c$, the propagation time between the two response points, and the envelope of the peak is more sharply defined as the noise bandwidth (f_U-f_L) increases. Therefore, determination of the peaks in the spatial cross-correlation function enable a measurement of the time delay between the signals.

Now suppose we have a system with N paths such that the path length d_i ($i = 1, 2, \dots, N$) is different for each path. The resulting cross-correlation function between the input and output has N peaks as shown in Figure 37. The peaks in the cross-correlation function have exactly the same form as in Equation (143), so that the delay time for each path corresponds to the time at which each peak of the cross-correlation function is located. The amplitudes of each peak depend upon the relative magnitudes of the transmission coefficients of the various paths.

Figure 37 illustrates that various transmission paths can be identified only if the delay times between any pair of paths are sufficiently different that the peaks can be distinguished. Let τ_1 and τ_2 be the delay times for two of the transmission paths between the two response points. The criterion [27] such that these paths may be distinguished using correlation analysis is that the difference in these delay times satisfy the following inequality:

$$|\tau_2 - \tau_1| (f_U - f_L) > 1 \quad (144)$$

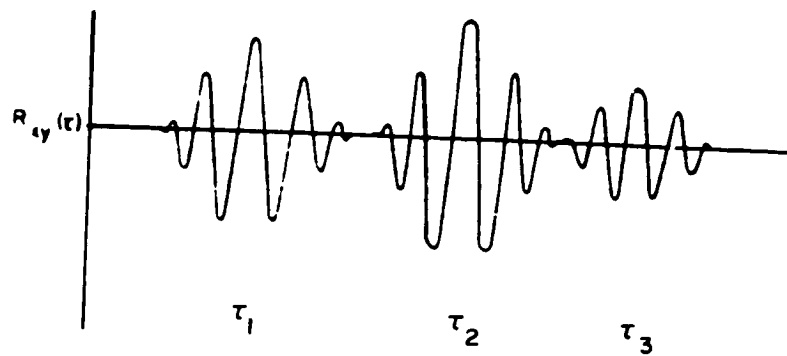
The normalized correlation coefficient $C_{xy}(\tau)$ is defined to be,

$$C_{xy}(\tau) = R_{xy}(\tau) / [R_{xx}(0) R_{yy}(0)]^{1/2} \quad (145)$$

where R_{xy} is defined in Equation (143) and R_{xx} and R_{yy} are the input and output autocorrelation functions. The correlation coefficient for the time delay between transmission paths is given by Equation (143) with the signal magnitudes X and Y set equal to unity. Thus, the correlation coefficient evaluated at the delay time is equal to

$$C_{xy}(\tau=d/c) = 1 \quad (146)$$

ORIGINAL PAGE IS
OF POOR QUALITY



Cross correlation in multiple-path system.

Figure 37. Cross Correlation in Multiple-Path System.

It is important to note that the amplitude of the correlation coefficient is independent of the transmission path characteristics for non-dispersive systems. This is not the case for dispersive systems. Figure 38 shows the correlation coefficient for a dispersive system. The time width Δt between the adjacent zeros of the correlation coefficient on either side of the central peak is illustrated on the figure, and this time width is equal to

$$\Delta t = 1/(f_U - f_L) = 1/\Delta f \quad (147)$$

where Δf is the frequency bandwidth of the excitation. The correlation coefficient peak is most clearly resolved by increasing the frequency bandwidth of the excitation. Equation (147) also helps illustrate why the condition expressed in Equation (144) must be satisfied for multiple transmission path systems in order to resolve individual transmission paths.

Temporal discrimination: the frequency domain. - The time delay between various transmission paths also may be measured in the frequency domain. A common method is to use the cross-spectral density function. Consider a signal s impinging on each of two response points with excitations $x(t)$ and $y(t)$ such that a noise signal is present at each response point as follows:

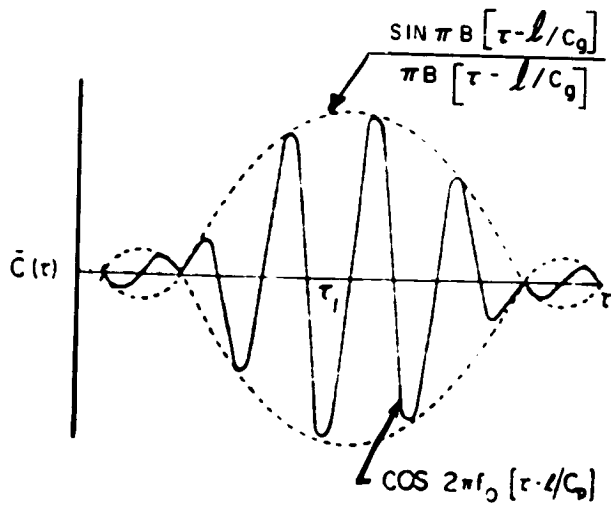
$$x(t) = s(t) + m(t) \quad (148)$$

$$y(t) = s(t+\tau) + n(t) \quad (149)$$

There is a time delay τ of the signal at y relative to x . The noise signals $m(t)$ and $n(t)$ are presumed to be uncorrelated with $s(t)$ and with respect to each other. The cross-spectral density $G_{xy}(f)$ between x and y is

$$G_{xy}(f) = G_{ss}(f) e^{j\omega\tau} \quad (150)$$

ORIGINAL PAGE 19
OF POOR QUALITY



Cross correlation
of dispersive waves.

Figure 38. Cross Correlation of Dispersive Waves.

The autospectral (power) density of signal s is G_{ss} , and it is a real non-negative quantity. Therefore, the phase ϕ_{xy} of G_{xy} is,

$$\phi_{xy} = \omega\tau \quad (151)$$

The delay time between the transmission paths is simply obtained as the average slope of the graph of phase versus angular frequency.

It is sometimes possible to improve the resolution of the delay time measurement by use of the coherence function. The complex coherence function γ_{xy} between the response at x and y is defined to be

$$\gamma_{xy}(f) = \frac{G_{xy}}{\sqrt{G_{xx} G_{yy}}} \quad (152)$$

The squared magnitude of the complex coherence function is the coherence function previously discussed. The complex coherence function for the system defined by Equations (148) and (149) is

$$\gamma_{xy}^2(f) = \frac{G_{ss} e^{j\omega\tau}}{\sqrt{(G_{ss} + G_{mm})(G_{ss} + G_{nn})}} \quad (153)$$

where G_{mm} and G_{nn} are the noise autospectral densities. The phase of the complex coherence function is precisely equal to the phase defined in Equation (151), so that the complex coherence function or the cross-spectral density function may be used to estimate the path length difference.

The main distinction between the two frequency domain methods occurs when the noise sources are partially correlated with the signal s . The signal s in practice may not be a white noise signal. It may, for example, be a signal with noise components as well as a few strong sinusoidal components. Such a signal will not be statistically independent relative to a noise signal. Thus the phase of such a cross-spectral density is not proportional to

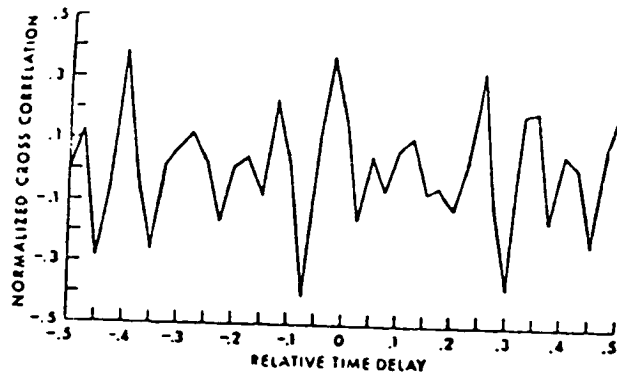
the delay time, but includes phase error terms due to the correlation of the signal with the "noise sources" - noise in any practical measurement situation meaning any background signal which is not of interest. The cross-spectral density function and the complex coherence function differ only in their magnitude response. The complex coherence function is the ratio of the cross-spectral density to the square root of the product of the autospectral densities of the two signals. This division by the autospectral densities has the effect of "whitening the spectrum" since the frequencies at which the autospectral densities are small are boosted in the complex coherence function relative to the cross-spectral density. Conversely, Equation (153) shows that if the noise at either measurement point is large relative to the signal autospectral density G_{ss} , then the complex coherence function is reduced in magnitude. It is possible to weight the complex coherence function by appropriate low, high, or band-pass filtering to eliminate points where the coherence is low.

The inverse Fourier transform of the complex coherence function γ_{xy} weighted by a smooth weighting function $W(f)$ is the smoothed coherence transform (SCOT) defined as follows:

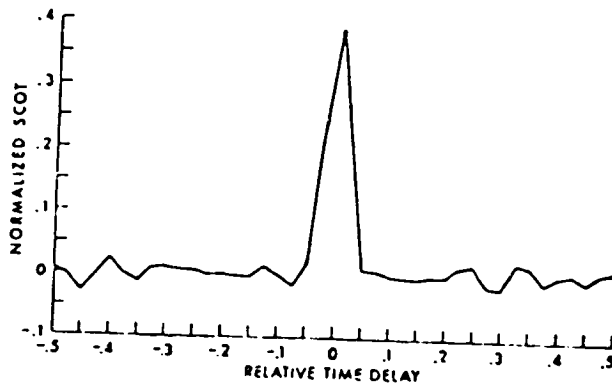
$$C_{xy}(\tau) = \int_{-\infty}^{\infty} W(f) \gamma_{xy}(f) e^{-2\pi j f \tau} df \quad (154)$$

The frequency domain weighting function is used to filter out frequencies at which the magnitude of the complex coherence is small relative to unity. As with the cross-correlation function a peak in the SCOT occurs at a time equal to the time delay between the two signal paths. An advantage of the SCOT over the cross-correlation function is that the peak in the SCOT is often times sharper. Figure 39 is an example from Reference [28] which illustrates the potential benefit of the SCOT. The signal $s(t)$ is a source with broad band noise and three sinusoids. The cross-correlation function, which is the inverse Fourier transform of the cross-spectral density, is illustrated in Figure 39. A delay between two broad band noise signals produces a peak in the cross-correlation at a time equal to the delay time. The presence of the sinusoids in addition to the noise leads to a complicated cross-correlation such that no dominant transmission path delay times are discernible. Figure 39 also shows the SCOT. There is a clear peak at the correct delay time, normalized to zero on the horizontal axes of both plots. This figure clearly shows that the SCOT is a useful estimator of delay time for certain types of complex signals.

CROSS CORRELATION
OF POOR QUALITY



Cross correlation of $x(t)$ and $y(t)$.



Normalized SCOT of $x(t)$ and $y(t)$.

Figure 39. Normalized SCOT.

Path identification for dispersive systems. - The identification of transmission paths in dispersive systems such as flexural waves in structures is complicated by the fact that the phase speed of the wave excitation is not constant with frequency. As a result, different frequency components of a disturbance in the system propagate at different speeds so that the shape of the disturbance smears out and is difficult to follow in space. For flexural waves in structures, the phase speed increases as the square root of frequency. An immediate consequence of dispersion is that there is not a well-defined delay time between transmission paths.

This factor affects each of the methods used for non-dispersive systems as previously discussed. In order to relate measured travel times with the path length difference it is necessary to know the propagation speed. Since this changes with frequency in dispersive systems it is necessary to look at various narrow frequency bands individually. This prevents the use of the impulse technique since it is applicable only for broad band transient signals.

Cross-correlation analysis for a dispersive system. - There are significant differences between the cross-correlation analysis of dispersive versus non-dispersive systems. The limitations of time-bandwidth considerations must be clearly recognized. It was remarked that the dispersive effects can be minimized by choosing a sufficiently small frequency bandwidth Δf in which the phase velocity is nearly constant. Such a system is nearly indistinguishable from a non-dispersive system. However, the discussion of the cross-correlation in non-dispersive systems notes that the time width of the peak of the cross-correlation function is inversely proportional to the frequency bandwidth (see Equation (147)). As the frequency bandwidth is narrowed, the peak in the cross-correlation function or correlation coefficient becomes spread out. Since the delay time is estimated by measurement of the time for which the cross-correlation function has its peak value, then it becomes difficult to estimate the delay time for excitations with a narrow frequency bandwidth. To summarize the difficulty, narrowing the frequency bandwidth to lessen the effects of dispersion increases the uncertainty in estimating the delay time.

This problem becomes more pronounced in a system such as a helicopter airframe with multiple transmission paths, since the individual peaks in the cross-correlation function corresponding each to a single transmission path delay time cannot be resolved as the frequency bandwidth is diminished.

Suppose that the system is excited by band-limited noise with lower and upper cutoff frequencies f_L and f_U , respectively. The system is dispersive and is composed of a single transmission path. An example of such a system might be the propagation of (dispersive) bending waves on an aircraft fuselage from a source excitation point to a distant point on the fuselage. The cross-correlation coefficient $C_{xy}(\tau)$, defined below as the normalized cross-correlation function, is

$$\begin{aligned} C_{xy}(\tau) &= R_{xy}(\tau) / [R_{xx}(0) R_{yy}(0)]^{1/2} \\ &= (1/\Delta f) \int_{f_L}^{f_U} \cos[2\pi f(\tau - d/c_p(f))] df \end{aligned} \quad (155)$$

where d is the transmission path length difference, Δf is the frequency bandwidth, and $c_p(f)$ is the dispersive phase velocity which varies with frequency.

Equation (155) has been investigated [27, 29] for bending waves. The phase velocity for a bending wave on a plate of thickness h and longitudinal phase velocity c_L is

$$c_p(f) = [whc_L/\sqrt{12}]^{1/2} \quad (156)$$

Define the center frequency f_0 of the frequency band as follows:

$$f_0 = (f_L + f_U)/2 \quad (157)$$

For this choice of phase velocity, the cross-correlation coefficient in Equation (155) is found to be

$$\begin{aligned} C_{xy}(\tau) &= [2f_0/(\Delta f^2 \tau_p)] \{ \cos[\beta(Ci(z_U) - Ci(z_L))] \\ &\quad + \sin[\beta(Si(z_U) - Si(z_L))] \} \end{aligned} \quad (158)$$

where

$$\beta = 2\pi f_0 \tau_p [(\tau/\tau_p - 3/4)^2 + 3/8] \quad (159)$$

$$z = (8f_0 \tau_p)^{1/2} [f/(4f_0) - \tau/\tau_p - 3/4] \quad (160)$$

and the term z is evaluated at the upper and lower band frequencies in Equation (158). The Fresnel cosine and sine integrals [30] are $Ci(z)$ and $Si(z)$, respectively.

The main features of the analysis do not require a detailed evaluation of the Fresnel integrals. The peak in the cross-correlation function (or cross-correlation coefficient) occurs at a time τ_g equal to the group delay defined as follows:

$$\tau_g = d/c_g \quad (161)$$

The group velocity c_g is the velocity at which energy propagates. The group delay is the time interval for energy to travel a distance d . The group velocity is not equal to the phase velocity in a dispersive system; it is given by

$$c_g = \partial\omega/\partial k \quad (162)$$

For dispersive flexural waves in structures, the phase velocity is given in Equation (156) and the group velocity is

$$c_g = 2c_p \quad (163)$$

The peak of the cross-correlation function occurs at a time equal to the group delay time for a dispersive system. The peak for a non-dispersive system occurs at a time equal to d/c_p , but this phase delay time is equal to the group delay since the phase and group velocities are equal in a non-dispersive system.

The time width Δt of the cross-correlation function (as well as the cross-correlation coefficient) for a dispersive system is given by

$$\Delta t = \tau_p \Delta f / 4f_0 > 1/\Delta f \quad (164)$$

The center frequency of the excitation is f_0 , and the phase delay τ_p is defined in terms of the phase velocity c_p and path length difference d by,

$$\tau_p = d/c_p = 2\tau_g \quad (165)$$

The width of the time window in Equation (164) has been defined to be the time interval in which the cross-correlation coefficient in Equation (158) is greater than or equal to one-half of its peak value. There are two differences between the width of the time window for dispersive and non-dispersive systems. The width of the cross-correlation peak for a non-dispersive system is independent of the delay time whereas for the dispersive system it depends on the phase delay time. Secondly, the peak width of the cross-correlation function is more spread out in a dispersive system than a non-dispersive system.

The peak amplitude of the cross-correlation coefficient for a non-dispersive system is equal to unity independent of time delay or frequency bandwidth. This is not the case for dispersive systems. The mean amplitude of the cross-correlation coefficient for a dispersive system within the window width corresponding to a single peak is

$$\overline{c_{xy}} = 2 (f_0 \tau_p)^{-1/2} (f_0 / \Delta f) \quad (166)$$

This demonstrates that the cross-correlation coefficient can have a value much larger than unity, particularly for narrow bandwidth signals. Equation (166) is valid when the path length difference is large relative to a flexural wavelength. As the path length difference becomes small relative to a wavelength the cross-correlation peak value approaches unity.

The results of this section are summarized in the statement that the cross-correlation coefficient contains information on the dispersive system transmission path characteristics with respect to the time at which the peak occurs, the time width of the peak, and the mean amplitude of the peak. The cross-correlation coefficient contains information on a non-dispersive system only with respect to the time at which an individual peak occurs.

Cepstral analysis. - This section describes a nonlinear filtering technique known as cepstral analysis. Due to the advent of small computers with extensive computational power, practical applications of cepstral analysis for filtering and signal recovery in the laboratory have become possible. Cepstral techniques have

advantages over the more traditional linear signal processing techniques in the areas of dereverberation or spectral smoothing, the analysis of periodic signals, source identification, and transmission path analysis.

Cepstral analysis may be used to detect and/or remove echoes from a signal, and can thus be employed to compute the free-field response from the measured reverberant field response. Of particular interest as regards helicopter applications are the capabilities of cepstral analysis for periodic signals. The periodic components of the spectrum produced by harmonics of a particular gearbox rotation rate is one such periodic signal. All of the harmonics corresponding to a particular rotation rate are mapped by the cepstrum into a single peak. Filtering in the cepstral domain thus isolates the source characteristics of the various gearbox sources. The cepstrum may under certain conditions be used to separate source and transmission path effects. This is because the cepstrum converts the convolution of source/path characteristics in the time domain into simple addition in the cepstral domain.

Future cepstral applications to systems, such as a helicopter frame exhibiting both dispersion and reverberation, depend upon the development of more powerful techniques than exist at present. If the dispersive characteristics of the structure can be adequately modeled, then a combination of cepstral techniques with inverse filtering (used to remove dispersive effects) can be employed to study structural transmission paths.

The complex cepstrum $k_y(q)$ of a signal $y(t)$, whose Fourier transform is $Y(f)$, is the inverse Fourier transform of the logarithm of $Y(f)$. Since the transform $Y(f)$ is a complex quantity, then the appropriate logarithm is the complex logarithm.

The transform $Y(f)$ is written in terms of its magnitude and phase as follows:

$$Y(f) = |Y(f)| e^{j\phi} \quad (167)$$

and the complex logarithm of $Y(f)$ is

$$\log Y(f) = \log |Y(f)| + j\phi \quad (168)$$

The real part of the above involves the logarithm of a real number, and this is well-defined. The imaginary part is not uniquely defined since addition of 2π radians to the phase of $Y(f)$

does not alter the complex value of $Y(f)$. Thus, it is necessary to restrict the range of the phase to 2π . Under this condition the complex cepstrum $k_y(q)$ is defined to be the inverse Fourier transform of the logarithm of $Y(f)$ as follows:

$$k_y(q) = \int_{-\infty}^{\infty} \log Y(f) e^{j2\pi fq} df \quad (169)$$

The parameter q plays a role analogous to that of time in the conventional Fourier transform. During the computation of the cepstrum it is necessary to unwrap the phase; i.e., the phase must be a continuous function of frequency. Information on the computation of the complex cepstrum is found in the references.

The power cepstrum $c_p(q)$ is defined to be the inverse Fourier transform of the logarithm of the autospectral density $G_{yy}(f)$ of the signal $Y(f)$ as follows:

$$c_p(q) = \int_{-\infty}^{\infty} \log[G_{yy}(f)] e^{j2\pi fq} df \quad (170)$$

Since the autospectral density is a real, non-negative function, then the logarithm in Equation (170) is the real logarithm.

It is important to note that both the power and complex cepstrum are real quantities. This is obvious in the case of the power cepstrum, but the fact that the complex cepstrum is real depends upon the symmetry properties of Equation (169) [31].

The complex cepstrum is more general since the original time domain signal may be completely reconstructed, whereas this reconstruction is not possible with the power cepstrum.

Cepstral analysis has usefully been applied to signal deconvolution. Consider the single input, single output linear system. The input and output time domain signals $x(t)$ and $y(t)$, respectively, are related by the following convolution:

$$y(t) = h(t) * x(t) \quad (171)$$

$$y(t) = \int_{-\infty}^{\infty} h(\tau) x(t-\tau) d\tau \quad (172)$$

Equation (171) is a short-hand notation for Equation (172). The impulse response function of the system is $h(t)$.

Convolution in the time domain becomes addition in the cepstral domain. It is this property which makes cepstral analysis useful. One may filter in the cepstral domain to focus attention on either the source ($x(t)$) or transmission path ($h(t)$) characteristics. A periodic source excitation produces a cepstrum with a peak at a single value of q which is directly related to the repetition rate of the time domain signal.

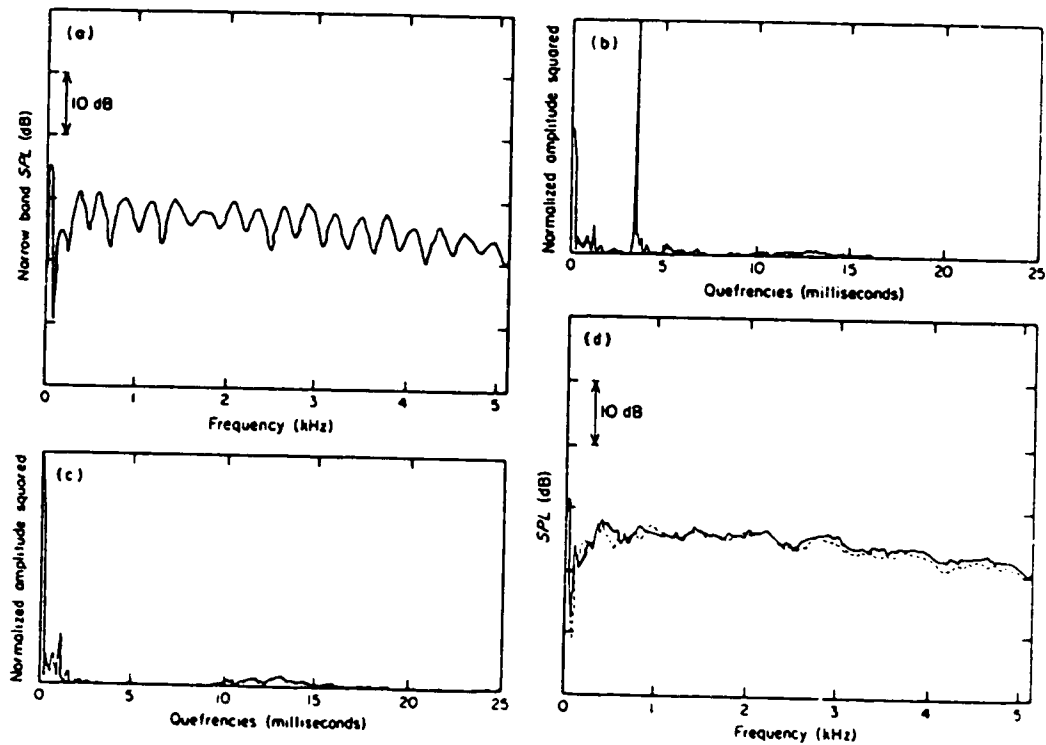
One may thus use the same filtering techniques in the cepstral domain that are used in the frequency domain. For example, assume that the input $x(t)$ to the single input, single output system is a repetitive pulse such as is produced by gearbox noise. Assume also that the impulse response function of the system is slowly varying relative to the repetition rate of the pulse. The convolution of this pulse with the impulse response function produces a cepstrum whose high q values are predominantly due to the pulse, and whose low q values are due to the transfer function. Application of a low-pass filter in the cepstral domain isolates the transfer function contribution.

The time domain signal $x'(t)$, after filtering in the cepstral domain, may be recovered by use of the inverse cepstrum. Computation is strongly affected by phase considerations and the details of the filtering in the cepstral domain.

Cepstral analysis can be used to isolate transmission paths by isolating the direct signal from the first few reflections, or from the reverberant field as a whole. The main property of the cepstrum which allows this is that a periodic time signal produces a cepstrum with a single peak. This method has been applied [32] to open air tests on the radiated sound from a jet engine. Since that study was interested in estimates of radiated power rather than reconstruction of the temporal waveform, the power cepstrum was used.

Figure 40a illustrates the radiated power spectrum, and the ripples in this spectrum are due to ground reflection. The power cepstrum corresponding to this signal is in Figure 40b, and the ground reflection is represented by the very strong peak in the cepstrum. This peak has been filtered out of the cepstrum in Figure 40c, and the resulting inverse cepstrum leads to the modified power spectrum shown in Figure 40d. This power spectrum is compared to the power spectrum measured under anechoic conditions (i.e., when measured in a special test facility which virtually eliminates all reflections in the bandwidth of interest), and the agreement is excellent. Syed et al. [32] remark that the cepstral technique is applicable even in the presence of wind, turbulence, or temperature gradients near the ground. They found it useful in both narrow-band and third octave averaging.

ORIGINAL PAGE IS
OF POOR QUALITY



Application of the cepstrum method in the removal of ground reflection. ARL data, 0.02 m nozzle microphone in position 1. (a) Log power spectrum showing reflection ripple. (b) normalized power cepstrum of 3(a) showing the peak due to the reflected signal; (c) modified power cepstrum with the ground reflection filtered out; (d) free field power spectrum from 3(c) (—) compared with free field power spectrum under anechoic conditions (----).

Figure 40. Application of the Cepstrum Method in the Removal of Ground Reflection.

APPENDIX B

Frame Junction Transmission Model

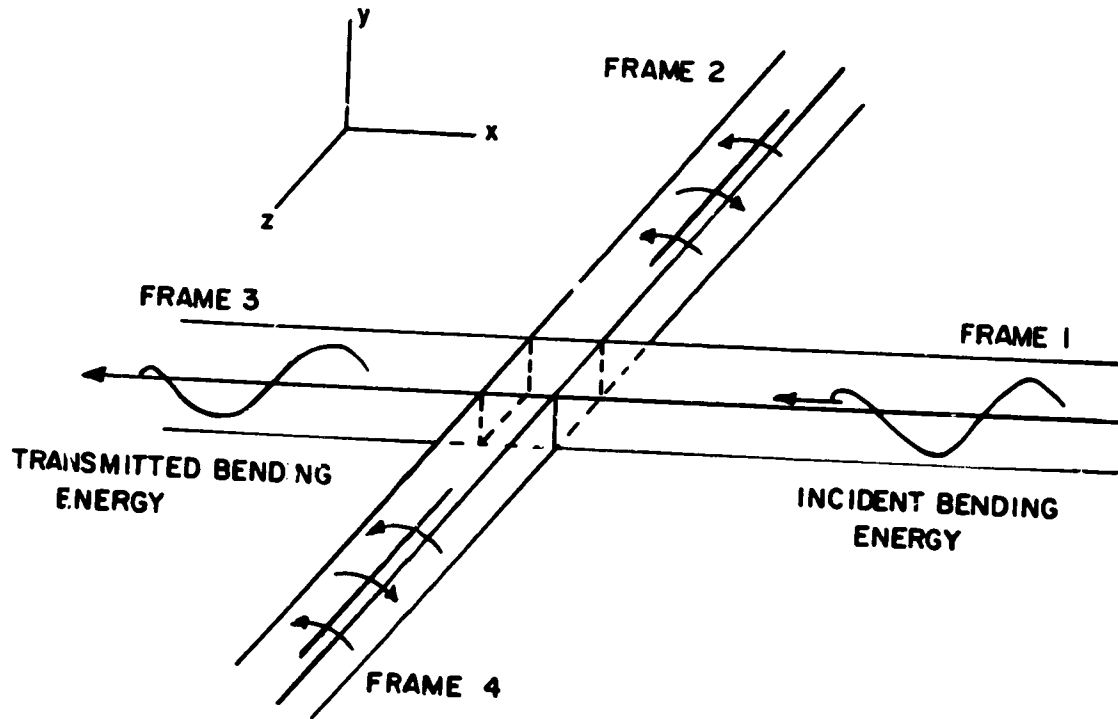
The SEA model of the helicopter airframe is an important, integral part of the overall model of the interior cabin noise environment. The fundamental feature of the airframe model is the vibration transmission through the framing including the gearbox support structure and the skeletal framework of the cabin. On the Sikorsky S-76, the framing consists of two main fore/aft frames with wrap-around transverse frames that extend between the door and side panels of the cabin. This section presents the analytical model describing the vibration transmission between frame sections joined at right angles.

Frame junction geometry. - A sketch of the S-76 airframe showing the framing is shown in Figure 2. At low frequencies the frames are treated as beams that deform in bending about the two axes perpendicular to the frame axis and in torsion about the frame axis. For both bending and torsional motions the frame cross-section does not deform. At higher frequencies cross-sectional deformation occurs and the dynamic behavior becomes more like that of flat plates. Longitudinal motion in the axis of the frame is not included in the model at present in that it is considerably stiffer than bending or torsion and is not, therefore, expected to contribute significantly to the overall vibration transmission.

A sketch of the junction between frames is shown in Figure 41. It is treated as a point connection at low frequency. Vibration transmission through the junction occurs as a result of junction motions. The exclusion of longitudinal motion from the model restricts the allowed junction motions to include the rotations about the three coordinate axes and only the translational motion perpendicular to the plane formed by the frames. The in-plane translations are suppressed by the large in-plane impedance for longitudinal motion in the frames.

A consideration of the junction motions illustrates the coupling which can occur between frames. A rotation at the junction about the Z axis induces bending deformation in frames 1 and 3 that are aligned perpendicular to the Z axis and torsional motion in frames 2 and 4 which lie along the Z axis. An out of plane translation in the Y direction induces bending deformation in all four attached frames.

ORIGINAL PAGE 19
OF POOR QUALITY



Junction Displacements

- η_y — out of plane translation
- θ_x } rotations about the coordinate axes
- θ_y }
- θ_z }

Figure 41 Sketch of Frame Junction Showing Coordinate System

Incident bending motion in frame 1 involves both vertical motions and rotational motions about the Z axis. The induced junction motions couple the incident bending motion directly into bending motion in frames 1 and 3 and torsion and bending motions in frames 2 and 4. In addition, if frames 2 and 4 are not identical, junction asymmetries result in a coupling of the out of plane junction motion into a rotation about the X axis and torsional motions of frames 1 and 3. The coupling due to junction asymmetry is the result of unbalanced reaction moments in frames on opposite sides of the junction.

Incident torsional motion in frame 1 couples directly into torsion of frame 3 and bending of frames 2 and 4. Junction asymmetries complete the coupling of the incident torsional motion into all the possible transmitted motions, as is generally the case.

In-plane bending about the Y axis couples only into in-plane bending of the attached frames.

Transmission coefficient description of junction dynamics. - The SEA model quantifies the coupling considerations described above in terms of a set of coupling loss factors. A convenient way of analytically modeling the coupling loss factors is in terms of energy transmission coefficients between the incident and transmitted motions. The transmission coefficient is defined as the ratio of transmitted to incident powers for the types of motion under consideration.

The transmission coefficient is analytically evaluated for the case where the attached frames are infinitely extended in length. The dynamic behavior at the junction is the same, but this simple formalism removes the need to consider reflected energy from other junctions in the attached frames. Multiply reflected energy leads to the build up of a reverberant vibrational energy field which is accounted for in the SEA model in the difference between the coupling loss factor and transmission coefficient.

As shown in Figure 41, incident bending or torsional energy propagates towards the junction where it is either transmitted or reflected. The solutions for the transmitted and reflected energies are obtained by considering the superposition of blocked and radiated cases as shown in Table 5. In the blocked case the junction is prohibited from undergoing both rotational and translational motions. The blocked forces and moments, which would be required to balance the effects of the incident wave and prohibit any motion at the junction, are given in Table 6 for both bending and torsional wave incidence. By definition in the blocked case, no vibration is transmitted to the other frames.

In the radiated case, the incident motion is removed and the junction motions equal those for the full problem. The non-zero junction motions result in bending and torsional waves in the attached frames. For bending two types of wave motion occur: one is localized to the region near the junction and decays exponentially while the other propagates unattenuated, in the absence of damping, away from the junction. The latter determines the power which is transmitted into the frame.

Junction impedance matrix. - Input impedances for each frame and type of motion relate the junction motions to forces and moments at the junction. For bending motion the impedances relate shear forces and moments to transverse motions and angular rotations. For torsional motions the relationship involves only moments and angular rotations. Analytic expressions for the impedances are given in Table 7.

An overall junction impedance matrix is formed by appropriately summing the moments and forces defined by the impedance matrices for each attached frame:

$$\begin{pmatrix} M_z \\ M_x \\ F_y \\ M_y \end{pmatrix} = [Z^j] \begin{pmatrix} \dot{\theta}_z \\ \dot{\theta}_x \\ \dot{\eta}_y \\ \dot{\theta}_y \end{pmatrix} \quad (173)$$

where $[Z^j]$ is the junction impedance matrix:

$$[Z^j] = \begin{bmatrix} Z_{m_z}^j & 0 & Z_{m_z, \dot{\eta}_y}^j & 0 \\ 0 & Z_{m_x}^j & Z_{m_x, \dot{\eta}_y}^j & 0 \\ Z_{m_z, \dot{\eta}_y}^j & Z_{m_x, \dot{\eta}_y}^j & Z_{f_y}^j & 0 \\ 0 & 0 & 0 & Z_{m_y}^j \end{bmatrix} \quad (174)$$

where

$$Z_{m_z}^j = Z_{m_z}^{(1)} + Z_{m_z}^{(3)} + Z_t^{(2)} + Z_t^{(4)} \quad (175)$$

$$Z_{m_x}^j = Z_t^{(1)} + Z_t^{(3)} + Z_{m_x}^{(2)} + Z_{m_x}^{(4)} \quad (176)$$

$$Z_{m_y}^j = Z_{m_y}^{(1)} + Z_{m_y}^{(2)} + Z_{m_y}^{(3)} + Z_{m_y}^{(4)} \quad (177)$$

$$Z_{f_y}^j = Z_{f_y}^{(1)} + Z_{f_y}^{(2)} + Z_{f_y}^{(3)} + Z_{f_y}^{(4)} \quad (178)$$

$$Z_{m_z, \dot{\eta}_y}^j = Z_{m, \eta}^{(1)} - Z_{m, \eta}^{(3)} \quad (179)$$

$$Z_{m_x, \dot{\eta}_y}^j = Z_{m, \eta}^{(2)} - Z_{m, \eta}^{(4)} \quad (180)$$

where the superscript denotes the frame number.

The matrix is symmetric where the main diagonal is the sum of terms from each frame that directly contribute to the particular force/moment. The off diagonal terms describe the cross coupling due to asymmetries in the junction. If opposing frames are identical, the cross coupling terms in the impedance matrix are zero.

Total moments and forces at the junction are determined by summing those due to the junction motions from the radiated case which involve the above junction impedances, with the moments/forces from the blocked case due to the incident motion. The total moment and force are equal to zero in the case with no lumped blocking masses or isolating compliances at the junction. This results in a solution for the junction motions in terms of the incident motion.

Incident and transmitted power. - The remaining step in evaluating the transmission coefficient is to relate the junction motions to the power which is radiated into the attached frames. The power radiated into a structure is given in terms of the forces/moments and transverse and angular velocities at the junction by the following:

Bending motion

Power associated with shear forces/transverse velocity

$$P_f = \frac{1}{2} \operatorname{Re} (F \dot{\eta}^*) \quad (181)$$

Power associated with moment/angular velocity

$$P_m = \frac{1}{2} \operatorname{Re} (M \dot{\theta}^*) \quad (182)$$

where * denotes the complex conjugate and Re refers to the real part.

The forces/moments are related to the velocities by the impedance expression for the individual frames as given in Table 6. The total power is the sum of terms due to forces and moments:

$$P_{\text{total}}^{\text{bend}} = \frac{1}{2} \operatorname{Re} (Z_f) |\dot{\eta}|^2 + \frac{1}{2} \operatorname{Re} (Z_m) |\dot{\theta}|^2 + \frac{1}{2} \operatorname{Re} (Z_{m,\dot{\eta}}) (\dot{\theta} \dot{\eta}^* + \dot{\eta} \dot{\theta}^*) \quad (183)$$

For torsional motion the expression involves only the moment term where the torsional impedance relating the junction moment and angular velocity is given in Table 6.

$$P_{\text{total}}^{\text{tors}} = \frac{1}{2} \operatorname{Re} (Z_t) |\dot{\theta}|^2 \quad (184)$$

The incident power can be evaluated from the above expressions. For an incident bending wave with transverse velocity amplitude ζ_{inc} the rotational angular velocity at the same cross section on the frame is given by

$$\dot{\theta}_{\text{inc}} = ik \zeta_{\text{inc}} \quad (185)$$

This relationship between the angular and transverse velocity amplitudes yields the following expression for the power incident on the junction:

$$P_{inc} = \frac{1}{2} \{ \text{Re}(Z_f) + k^2 \text{Re}(Z_m) \} |\dot{\zeta}_{inc}|^2 \quad (186)$$

Sample evaluation of transmission coefficient. - To illustrate the process of evaluating the transmission coefficient consider the case of an incident bending wave in frame 1. The bending involves rotations about the Z axis and transverse motions out of the plane of the frames. To simplify the algebra opposing frames (1,3) and (2,4) are identical so that off diagonal terms in the junction impedance matrix are zero.

Summing the moments/forces due to the junction motions with the blocked forces/moments and setting the sums equal to zero yields the following:

$$M_z : \quad \dot{\theta}_z = - \frac{C_m^{bl}}{Z_{m_z}^j} \dot{\zeta}_{inc} \quad (187)$$

$$F_y : \quad \dot{\eta}_y = - \frac{C_f^{bl}}{Z_{f_y}^j} \dot{\zeta}_{inc} \quad (188)$$

$$M_x : \quad \dot{\theta}_x = 0 \quad (189)$$

$$M_y : \quad \dot{\theta}_y = 0 \quad (190)$$

The incident power is given by:

$$P_{inc} = \frac{1}{2} \{ \text{Re}(Z_f^{(1)}) + k^2 \text{Re}(Z_m^{(1)}) \} |\dot{\zeta}_{inc}|^2 \quad (191)$$

The power transmitted to frame 2 is obtained from the following equations for bending and torsional motion, respectively:

$$P_{bend}^{(2)} = \frac{1}{2} \text{Re}(Z_f^{(2)}) |\dot{\eta}_y|^2 = \frac{\frac{1}{2} \text{Re}(Z_f^{(2)}) |C_f^{bl}|^2}{|Z_{f_y}^j|^2} |\dot{\zeta}_{inc}|^2 \quad (192)$$

$$P_{\text{tors}}^{(2)} = \frac{\frac{1}{2} \text{Re}(Z_t^{(2)}) |C_m^{bl}|^2}{|Z_{m_z}^j|^2} |C_{\text{inc}}^z|^2 \quad (193)$$

The transmission coefficients between bending in frame 1 and bending and torsion in frame 2 are determined from the ratios of transmitted to incident powers:

$$\tau_{\text{bend,bend}}^{(1,2)} = \frac{\text{Re}(Z_f^{(2)}) |C_f^{bl}|^2}{\{\text{Re}(Z_f^{(1)}) + k^2 \text{Re}(Z_m^{(1)})\} |Z_{m_z}^j|^2} \quad (194)$$

and

$$\tau_{\text{bend,tors}}^{(1,2)} = \frac{\text{Re}(Z_t^{(1)}) |C_m^{bl}|^2}{\{\text{Re}(Z_f^{(1)}) + k^2 \text{Re}(Z_m^{(1)})\} |Z_{m_z}^j|^2} \quad (195)$$

With the frame impedance expressions from Table 7 and the blocked force/moment expressions from Table 6, these become:

$$\tau_{\text{bend,bend}}^{(1,2)} = \frac{4 \text{Re}(Z_f^{(2)}) \text{Re}(Z_f^{(1)})}{|Z_{f_y}^j|^2} \quad (196)$$

and

$$\tau_{\text{bend,tors}}^{(1,2)} = \frac{4 \text{Re}(Z_t^{(2)}) \text{Re}(Z_m^{(1)})}{|Z_{m_z}^j|^2} \quad (197)$$

These expressions have a relatively simple form in terms of impedances for the individual frames. It should be noted that the expressions involve only moment or force impedance and not combinations of both.

The final step involves evaluating the coupling loss factor in terms of the transmission coefficient. The coupling loss factor is

$$\eta_{\text{bend,bend}}^{(1,2)} = \frac{2}{\pi \omega n_1} \frac{\text{Re}(Z_f^{(2)}) \text{Re}(Z_f^{(1)})}{|Z_{f_y}^j|^2} \quad (198)$$

$$\eta_{\text{bend,tors}}^{(1,2)} = \frac{2}{\pi \omega n_1} \frac{\text{Re}(Z_t^{(2)}) \text{Re}(Z_m^{(1)})}{|Z_m^j|^2} \quad (199)$$

where n_1 = mode density of frame 1 in bending.

These expressions illustrate the use of the generalized coupling loss factor equation. Identical expressions are obtained for the coupling loss factors between frames 1 and 4 because the junction is symmetric and the frames identical.

The result for the coupling into frame 3, which is in line with frame 1, is more complicated. The transmitted power includes only bending motion for the symmetric junction case. Both non-zero junction motions, η_y and θ_z contribute to the bending energy which propagates away from the junction into frame 3. The transmitted power now includes terms due to both η_y and θ_z .

The expression for the transmission coefficient will contain both moment and force impedances. The non-zero correlation between η_y and θ_z results in a power contribution associated with the cross term. The expressions provided still allow for a determination of the transmission coefficient, but the final result is not as simply presented in terms of frame impedances.

Allowing for junction asymmetries in the form of non-identical frames also results in more complicated expressions for the transmission coefficients. In addition, the incident motion now couples into motions that it did not couple into for the symmetric case. These effects are fully described by the expressions given, though the algebra is more involved.

TABLE 5. Blocked and Radiated Cases for Frame Junction Vibration Transmission

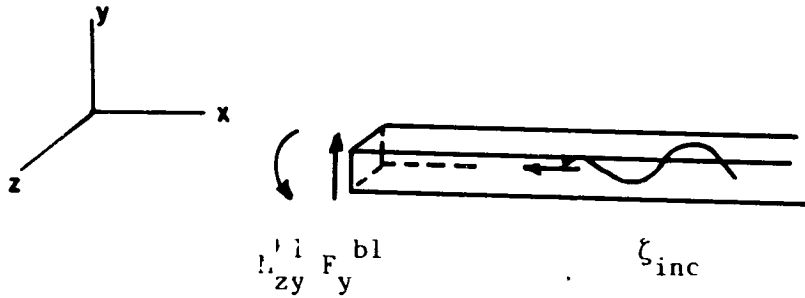
		Superposition of:	
Full Problem	=	1) Blocked Case	plus 2) Radiated Case
(Incident Energy) (Junction Motion)		(Incident Energy) (No Junction Motion)	(No Incident Energy) (Junction Motion)

Junction Motions		Zero Junction Motions	Non Zero Junction Motions
Translation η_y		$\eta_y = 0$	η_y
Rotation $\theta_x, \theta_y, \theta_z$		$\theta_x = \theta_y = \theta_z = 0$	$\theta_x, \theta_y, \theta_z$
		Blocked Forces/Moments at Junction	

Transmitted and Reflected Waves		Reflected Wave in Source Frame	Transmitted Waves into all Frames
		No Transmitted Waves	

Table 6. Blocked Force/Moment Expressions

Incident Bending Wave: $\zeta_{inc} e^{-i(kx + \omega t)}$

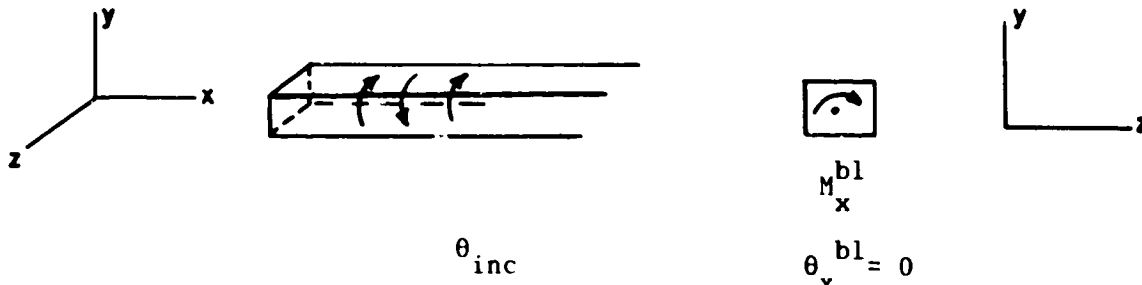


$$\theta_z^{bl} = \eta_y^{bl} = 0$$

$$M_{zy}^{bl} = 2 \frac{Bk^2}{\omega} (i - 1) \dot{\zeta}_{inc} = C_m^{bl} \dot{\zeta}_{inc}$$

$$F_y^{bl} = 2 \frac{Bk^3}{\omega} (i - 1) \dot{\zeta}_{inc} = C_m^{bl} \dot{\zeta}_{inc}$$

Incident Torsional Wave: $\theta_{x,inc} e^{i(kx + \omega t)}$



$$M_x^{bl} = -2 Z_t \dot{\theta}_{x,inc} = C_t^{bl} \dot{\theta}_{x,inc}$$

$$\theta_x^{bl} = 0$$

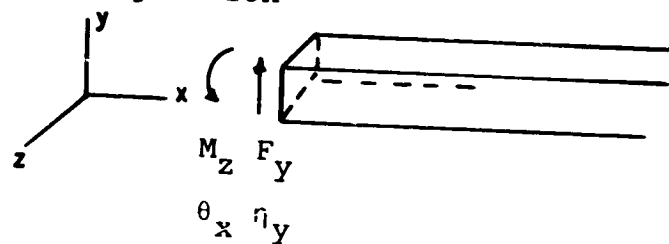
See Tables 7 and 8 for definition of parameters.

C-3

ORIGINAL PAGE IS
OF POOR QUALITY

Table 7. Impedance Expressions for Torsional and Bending Motions

Bending Motion



M_z, θ_z - moment, angular rotation about Z axis

F_y, η_y - shear force, traverse displacement

$$\begin{matrix} F_y \\ M_z \end{matrix} = \begin{matrix} Z_f & Z_{m, \dot{\eta}} \\ Z_{m, \dot{\eta}} & Z_m \end{matrix} \begin{matrix} \dot{\eta}_y \\ \dot{\theta}_z \end{matrix}$$

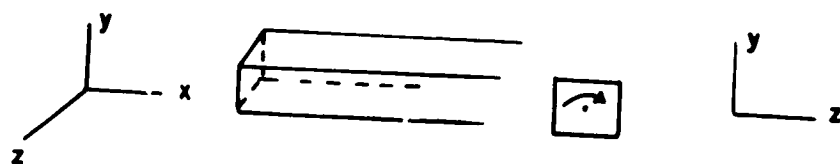
dot above symbol denotes time derivative

$$Z_f = \frac{Bk^3}{\omega} (1 - i)$$

$$Z_{m, \dot{\eta}} = \frac{Bk^2}{\omega}$$

$$Z_m = \frac{Bk}{\omega} (1 + i)$$

Torsional Motion



M_x, θ_x moment about axis angular rotation about axis

$$M_x = Z_t \dot{\theta}_x$$

$$Z_t = \rho I_p C_t$$

See Table 8 for definition of parameters.

See Reference [21] for descriptions of general procedures for evaluating impedances of mechanical systems.

Table 8. Dynamics Parameters for Torsion and Bending of Frame

Bending Wave Motion

$$C_b = \left(\frac{EI}{\rho A} \right)^{\frac{1}{2}} \sqrt{\omega}$$

$$k = \omega / C_b$$

$$B = EI$$

C_b - bending wave speed

B - bending rigidity

k - bending wave number

ω - radian frequency

E - Young's modulus

ρ - density

A - cross-sectional area

I - moment of inertia of cross-section about bending axis

Torsional Wave Motion

$$C_t = \left(\frac{GJ}{\rho I_p} \right)^{\frac{1}{2}}$$

C_t - torsional wave speed

G - shear modulus

J - torsional stiffness of cross-section

I_p - polar moment of inertia of cross-section

ρ - density

S-76 frame junction vibration transmission characteristics. -
 Transmission characteristics were computed for a right angle frame function representative of the overhead framing on the Sikorsky S-76. The framing is a riveted construction with upper and lower T section flanges connected by web plating. The overall height is approximately .2 m, and the width of the flanges is approximately .05 m. Plate thicknesses vary from approximately .8 to 1.5 mm. The calculated frame inertias, torsional stiffness, etc., are given in Table 9. For simplicity all four frames at the junction were taken to be identical. The resulting symmetry at the junction reduces the number of non-zero transmission coefficients and coupling loss factors.

Transmission coefficient values are shown in Figure 42 for the coupling between incident out-of-plane bending motion in the source frame and bending and torsional motions in the receiving frames. Bending motion for the symmetric junction couples only into bending motion of the in-line frame on the other side of the junction and both bending and torsional motions in the right angle frames.

The coupling into bending motion of the in-line frame is significantly greater than the coupling into either bending or torsional motions of the right angle frames. This result is related to the large bending rigidity of the frames. The bending rigidity of the overhead framing is of considerable structural importance in supporting the gearbox and cabin. The frames are quite stiff for out-of-plane bending motion in comparison with torsional motion. The coupling across a right angle junction is large because the cross frame impedance in torsion does not constitute a significant impedance discontinuity for the incident bending motion.

For frame sections the coupling loss factor is related to the transmission coefficient according to the following:

$$\eta_{1,2} = \frac{c_g}{2\omega L} \tau_{1,2} \quad (200)$$

- c_g = group velocity for incidental motion
 - = $2 c_b$ for bending (c_b -bending wavespeed)
 - = c_t for torsion
- L = length of source frame
- ω = frequency (rad/sec)

Coupling loss factors corresponding to the transmission coefficient values in Figure 42 are shown in Figure 43. The different frequency dependencies in Figure 43 are the result of the factor, ω , and the frequency dependence of c_g in Equation (200).

The coupling loss factor is important in quantifying the power flow out of the source frame algebraically in the same way as the damping loss factor. The significance of the coupling loss factor values can be understood in comparison with typical damping loss factors. For riveted structures damping loss factor values near .01 are common. On a dB basis this value is -20 dB, which is small in comparison with the coupling loss factor for bending motion into the in-line frame. The comparison is not exact because the energy which transmits back into the source frame due to reflection and reverberation in the receiving frame is not accounted for in this calculation. That energy is accounted for in solving the SEA matrix equations for the subsystem energies.

Other coupling loss factors involving incident in-plane bending and torsional motions are shown in Figures 44 and 45. Torsional motion is only weakly coupled through the junction. In-plane bending motion is equally coupled into the right angle and in-line receiving frames though less strongly than for out-of-plane bending motion.

Table 9 Representative S-76 Frame Parameter Values

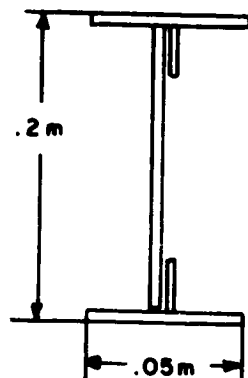
Material - Aluminum

$$E = 7.2 \times 10^{10} \text{ n/m}^2$$

$$G = 2.7 \times 10^{10} \text{ n/m}^2$$

$$\rho = 2700 \text{ kg/m}^2$$

Frame Geometry



Upper T Flange

Lower T Flange

Parameter Values

Moments of Inertia of the cross-section

$$I_x = 3.2 \times 10^{-6} \text{ m}^4$$

$$I_y = 4.29 \times 10^{-8} \text{ m}^4$$

Torsional stiffness of the cross-section

$$J = 1.69 \times 10^{-7} \text{ m}^4$$

Cross-Sectional Area

$$A_c = 4.43 \times 10^{-4} \text{ m}^2$$

Length of source frame between cross frame locations 2 and 3

$$L = .84 \text{ m}$$

ORIGINAL DRAWING
OF POOR QUALITY

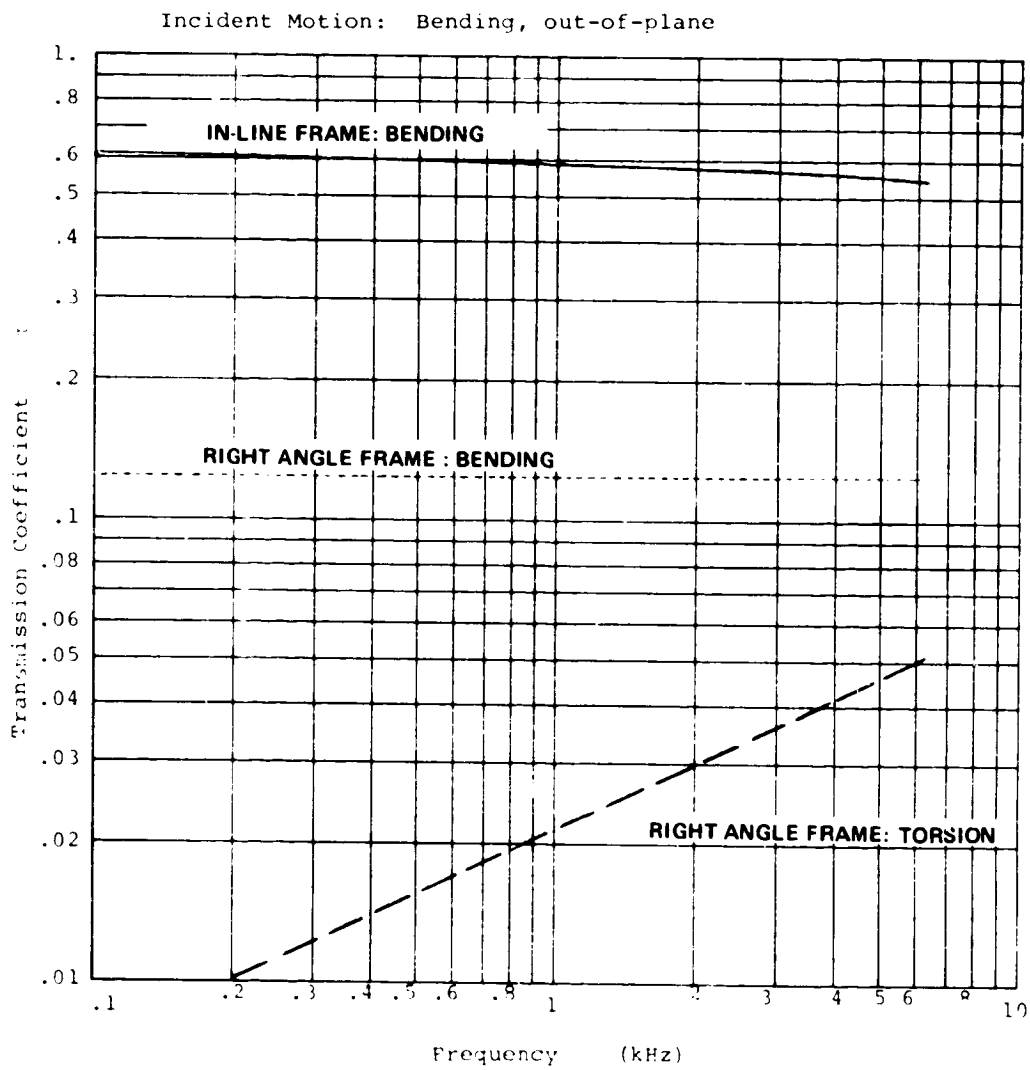


Figure 42. S-76 Frame Junction: Transmission Coefficients for Out-of-Plane Bending.

ORIGINAL
OF POWER QUALITY

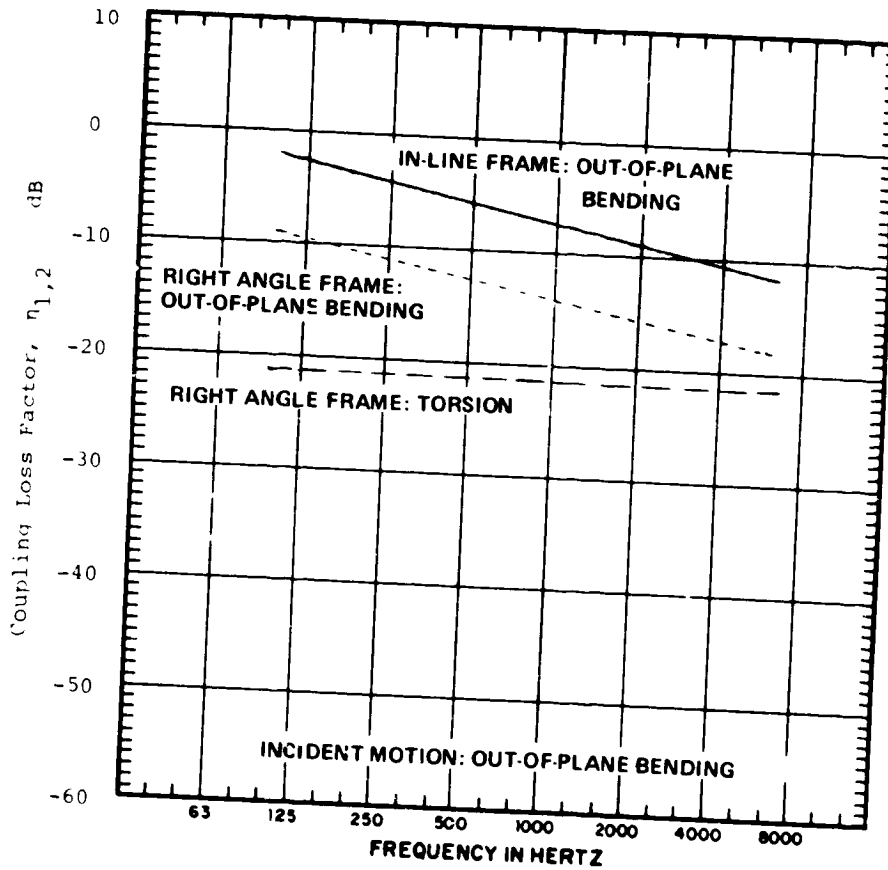


Figure 43. S-76 Frame Junction: Coupling Loss Factors for Out-of-Plane Bending.

6
OF POOR QUALITY

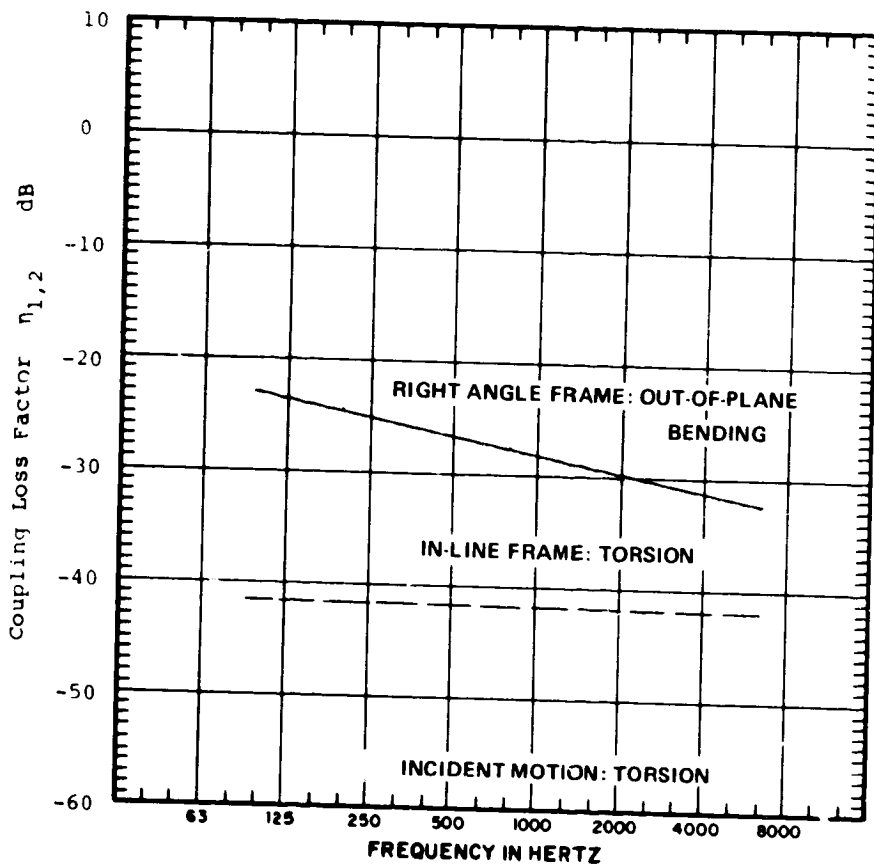


Figure 44. S-76 Frame Junction: Coupling Loss Factors for Torsional Motion.

COUPLING LOSS FACTOR
FOR AOKI QUALITY

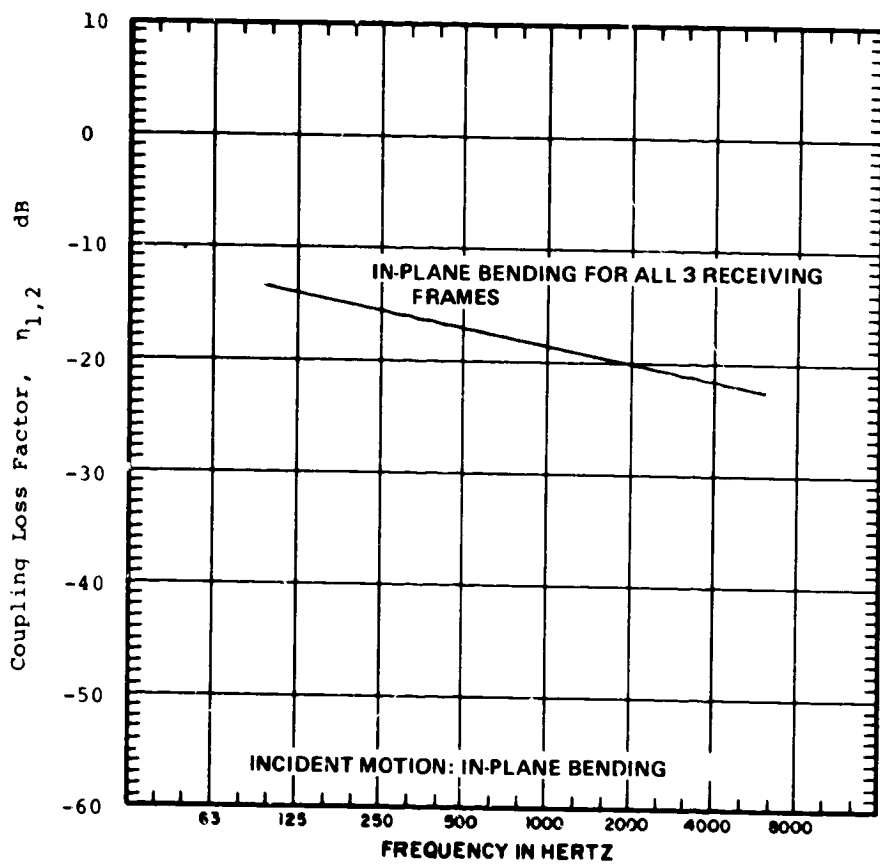


Figure 45. S-76 Frame Junction: Coupling Loss Factors for In-Plane Bending.

APPENDIX C

Acoustic Intensity Method

The acoustic intensity method involves scanning over a vibrating and radiating surface with a transducer which generates outputs that can be processed to give the acoustic intensity or power. The net acoustic power from the surface is obtained from an average of the intensity evaluated at close distances to the surface and at a sufficient number of locations over the radiating area. This method does not generate information characterizing the directivity of the acoustic power.

It is important to distinguish between the intensity and pressure or velocity variables which are used as inputs and outputs. The intensity is a flow variable describing a net flow of energy through a surface in space. It is obtained as a time average of the product of in-phase components of pressure and velocity on the surface. For different surfaces which have coherent components of velocity an additional factor is involved in assessing the influence of that coherence on the radiated intensity. This factor is that there is a mutual coupling between the radiation impedances of the two surfaces. That is, the pressure at surface one is influenced by the motion of surface one, but it is also influenced by the motion of surface two as well as any other vibrating surfaces.

The definition of acoustic intensity in terms of acoustic pressure and flow is now introduced. The acoustic pressure p and particle velocity u_r in the r direction are related by

$$u_r = - (1/\rho) \int dt \partial p / \partial r \quad (201)$$

where the equilibrium density of air is ρ and the integration is over time. Thus measurement of the pressure gradient $\partial p / \partial r$ in the r direction enables a computation of the flow in that direction. The acoustic intensity I_r in the r direction is defined to be the time-average of the product of pressure and flow as follows:

$$I_r = \langle pu_r \rangle \quad (202)$$

where the brackets ' $\langle \dots \rangle$ ' denote a time average.

Acoustic intensity is measured using two pressure-sensing microphones spaced a distance Δr apart as illustrated in Figure 46. The component of the acoustic intensity parallel to the line joining the microphones is measured. Let the pressure time

history from the microphone closest to the source be $p_1(t)$ and that from the microphone farthest from the source be $p_2(t)$. The pressure p and pressure gradient $\partial p/\partial r$ at the midpoint between the microphones may be estimated using the finite difference approximation by,

$$p = (p_1 + p_2)/2 \quad (203)$$

$$\partial p/\partial r = (p_2 - p_1)/\Delta r = \Delta p/\Delta r \quad (204)$$

so that Equation (201) for u_r becomes

$$u_r = -(1/(\rho\Delta r)) \int (p_2 - p_1) dt \quad (205)$$

The acoustic intensity may be written in terms of the two microphone pressures by,

$$I_r = \langle (-1/(2\rho\Delta r)) (p_1+p_2) \int dt (p_2-p_1) \rangle \quad (206)$$

The time domain approach using analog methods is to construct the sum and difference of the pressure signals histories, integrate the pressure difference and carry out the necessary multiplication of the signals. Time-averaging of the resultant product leads to the acoustic intensity.

With the widespread acceptance of digital signal processing techniques, it is more convenient to estimate the acoustic intensity using a frequency domain approach constructed using the sampled time series of the two pressure signals. Fahy [33] shows that the acoustic intensity spectrum $I_r(f)$ may be expressed in terms of the imaginary part of cross-spectral density function $G_{12}(f)$ by,

$$I_r(f) = - \text{Im}(G_{12}(f))/(2\pi f \rho \Delta r) \quad (207)$$

Ensemble averaging is used in conjunction with Equation (207) to estimate the cross-spectral density. Ensemble averaging is equivalent to time averaging in most practical applications. The total acoustic intensity over all frequencies is obtained by integrating Equation (206) over all frequencies in the measurement bandwidth.

The main potential obstacle in applying Equation (207) to acoustic intensity measurements is to ensure that the phases of the instrumentation are matched between the two channels. Chung [34] has developed a technique which bypasses the need for phase calibration between the channels. Figure 47 shows the relevant instru-

mentation needed for a measurement. The i -th channel pressure signal p_i ($i=1,2$) is sensed by a microphone with a microphone sensitivity transfer function H_{Ti} , and this signal is amplified by an amplifier with a transfer function H_{Ai} . Thus the total transfer function $H_i(f)$ associated with each channel is

$$H_i(f) = |H_i(f)| e^{j\phi_i(f)} = H_{Ai}(f) H_{Ti}(f) \quad (208)$$

It follows that the cross-spectral density $G_{p_1 p_2}(f)$ between the actual pressure signals is related to the measured $G_{12}(f)$ by

$$G_{p_1 p_2}(f) = G_{12}(f) / [H_2(f) H_1^*(f)] \quad (209)$$

Suppose now that the channels are switched and the measured cross-spectral density is denoted $G_{12}^{(s)}(f)$. The cross-spectral density function $G_{p_1 p_2}(f)$ is given under these new test conditions by

$$G_{p_1 p_2}(f) = G_{12}^{(s)}(f) / [H_1(f) H_2^*(f)] \quad (210)$$

Multiplying the above two equations and taking the square root of the resulting expression leads to

$$G_{p_1 p_2}(f) = [G_{12}(f) G_{12}^{(s)}(f)]^{1/2} / \{|H_1(f)| |H_2(f)|\} \quad (211)$$

so that the acoustic intensity may be estimated by

$$I_r(f) = \text{Im}\{[G_{12}(f) G_{12}^{(s)}(f)]^{1/2}\} / [2\pi f \rho \Delta r |H_1(f)| |H_2(f)|] \quad (212)$$

Thus the microphone switching technique requires two ensemble averages of a cross-spectral density function, that the sound field remain stationary over both measurements, and it requires taking the square root of a complex quantity -- namely, the product of the cross-spectral densities in Equation (212). In addition, the magnitude of the instrumentation transfer function must be measured for each channel.

The switching technique requires interchanging all of the instrumentation associated with each channel, the microphone, pre-amplifier, and amplifier, in addition to any other possible filters and recording devices. If one uses a pair of microphones and pre-amplifiers which are phase-matched, then it is only necessary to switch the remaining instrumentation.

This instrument switching technique has the advantage of eliminating errors due to phase calibration uncertainties. Other sources of error remain including random and bias errors in the estimation of the cross-spectral density functions and those due to limitations in the finite difference approximation and microphone interaction effects.

ORIGINAL DRAWING
OF POOR QUALITY

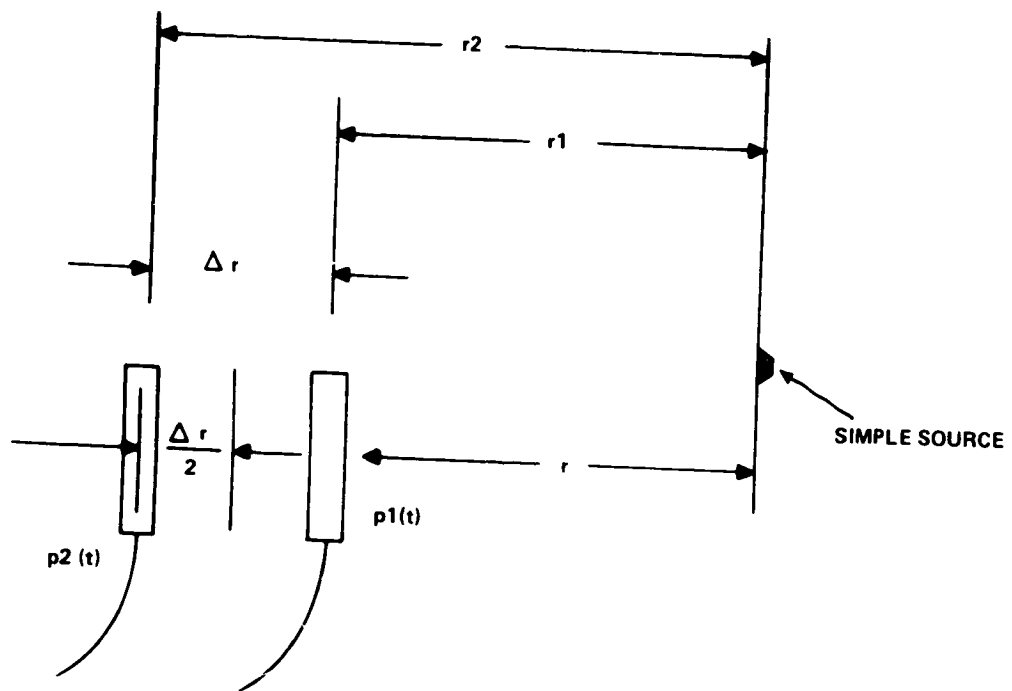


Figure 46. Typical Intensity Probe Schematic.

CONFIDENTIAL
REF ID: A66117

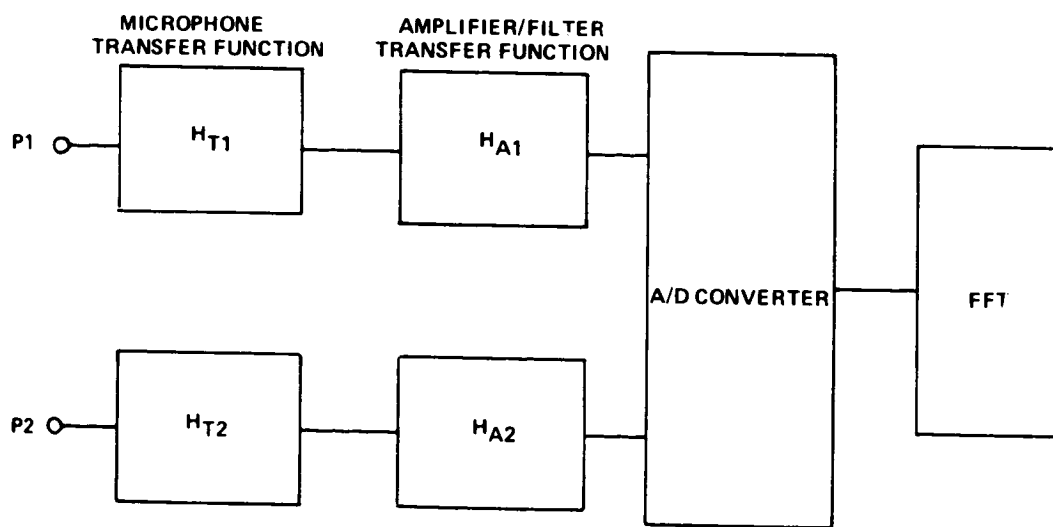


Figure 47. Typical Intensity Measurement Instrumentation.

REFERENCES

1. Levine, L.S.; and DeFelice, J.J.: Civil Helicopter Research Aircraft Internal Noise Prediction. Sikorsky Aircraft, NASA CR-145146, April 1977.
2. Leverton, J.W.: The Influence of the Noise Environment on Crew Communications. Proceedings of an International Specialists Symposium, NASA Langley Research Center, Hampton, VA, May 22-24, 1978.
3. Murray, B.S.; and Wilby, J.F.: Helicopter Cabin Noise - Methods of Source and Path Identification and Characterization. Proceedings of an International Specialists Symposium, NASA Langley Research Center, Hampton, VA, May 22-24, 1978.
4. Marze, H.J.; and d'Ambra, F.: Helicopter Internal Noise Reduction Research and Development Application to the SA360 and SA365 Dauphin. Proceedings of an International Specialists Symposium, NASA Langley Research Center, Hampton, VA, May 22-24, 1978.
5. Levine, L.S.; and DeFelice, J.J.: A Practical Approach to Helicopter Internal Noise Prediction. Proceedings of an International Specialists Symposium, NASA Langley Research Center, Hampton, VA, May 22-24, 1978.
6. Edwards, B.D.; and Cox, C.R.: Helicopter Internal Noise Control - Three Case Histories. Proceedings of an International Specialists Symposium, NASA Langley Research Center, Hampton, VA, May 22-24, 1978.
7. Bossler, R.B.; and Bowes, M.A.: An Analytical Method for Designing Low Noise Helicopter Transmissions. Proceedings of an International Specialists Symposium, NASA Langley Research Center, Hampton, VA, May 22-24, 1978.
8. Bellavita, P.; and Smullin, J.: Cabin Noise Reduction for the Agusta A-109 Helicopter. Paper No. 61, Fourth European Rotorcraft and Powered Lift Aircraft Forum, September 1978, Stresa, Italy.
9. Vaicaitis, R.; and Slazak, M.: Cabin Noise Control for Twin Engine General Aviation Aircraft. NASA CR-165833, February 1982.

10. Vaicaitis, R.; and Slazak, M.: Noise Transmission Through Stiffened Panels. *Journal of Sound and Vibration*, Vol. 70, No. 3 1980, pp. 413-426.
11. Roskam, J.; Grosveld, F.; and Van Aken, J.: Summary of Noise Reduction Characteristics of Typical General Aviation Materials. SAE Technical Paper 79-0627, Business Aircraft Meeting and Exposition, Century II, Wichita, Kansas, April 1979.
12. Pope, L.D.; Wilby, E.G.: Analytical Prediction of the Interior Noise for Aircraft Fuselages for Prescribed Exterior Noise Fields. NASA CR-165869, April 1982.
13. Oppenheim, A.V.; Schafer, R.W.: *Digital Signal Processing*. Prentice Hall, 1975.
14. Bendat, J.S.; and Piersol, A.G.: *Engineering Applications of Correlation and Spectral Analysis*. Wiley Interscience, 1980.
15. Richards, E.J.; and Mead, D.J., ed.: *Noise and Acoustic Fatigue in Aeronautics*. John Wiley & Sons, Inc., 1968.
16. Powell, A.: On the Response of Structures to Random Pressures and to Jet Noise in Particular. *Random Vibration*, S.H. Crandall, ed.; Technology Press of MIT and John Wiley & Sons, Inc., 1958, Chapter 8.
17. Lyon, R.H.: *Statistical Energy Analysis of Dynamical Systems: Theory and Applications*. MIT Press, 1975.
18. Timoshenko, S.P.; and Goodier, J.N.: *Theory of Elasticity*. Third ed. McGraw-Hill, 1970.
19. Beranek, L.L.: *Noise and Vibration Control*. McGraw-Hill, 1971.
20. Maidanik, G.: Energy Dissipation Associated with Gas-Pumping in Structural Joints. *J. Acoust. Soc. America*, Vol. 40, No. 5, November 1966, pp 1064-1072.
21. Cremer, L.; Heckl, M.; Ungar, E.E.: *Structure-Borne Sound*. Springer Verlag, 1973.
22. Smith, P.W.; and Lyon, R.H.: *Sound and Structural Vibration*. NASA CR-160, March 1965.

23. Moore, J.A.; Sound Transmission Loss Characteristics of Three Layer Composite Wall Constructions. Ph.D. Thesis, MIT, May 1975.
24. Morse, P.M.; and Ingard, K.U.: Theoretical Physics. McGraw-Hill, 1968.
25. McGary, M.C.: Noise TL of Aircraft Panels Using Acoustic Intensity Methods. NASA TP-2046, August 1982.
26. McGary, M.C.: A New Measurement Method for Separating Airborne and Structureborne Noise Radiated by Aircraft-Type Panels, NASA TP-2079, September 1982.
27. White, P.H.: Cross-Correlation in Structural Systems: Dispersion and Nondispersion Waves. J. Acoust. Soc. America, Vol. 45, 1969, p. 1118.
28. Carter, G.C.; Nuttal, A.H.; and Cable, P.G.: The Smoothed Coherence Transform. Proc. IEEE 61, 1973, pp. 1497-1498.
29. Barger, J.E.: Noise Path Diagnostics in Dispersive Structural Systems Using Cross-Correlation Analysis. Noise Control Engineering, Vol. 6, 1976, pp. 122-129.
30. Abramowitz, M.; and Stegun, I.: Handbook of Mathematical Functions. National Bureau of Standards, 1964.
31. Oppenheim, A.V.; and Schaefer, R.W.: Digital Signal Processing. Prentice Hall, 1975.
32. Syed, A.A.; Brown, J.D.; Oliver, M.J.; and Hills, S.A.: The Cepstrum: A Viable Method for the Removal of Ground Reflections. J. Sound. & Vib., Vol. 71, 1980 pp. 299-313.
33. Fahy, F.J.: Measurements of Acoustic Intensity Using the Cross-Spectral Density of Two Microphone Signals. J. Acoust. Soc. Vol. 62, Letter to the Editor, 1977.
34. Chung, J.Y.: Cross-Spectral Method of Measuring Acoustic Intensity Without Error Caused by Instrument Phase Mismatch. J. Acoust. Soc. America, Vol. 64, 1978, pp. 1613-1616.
35. Smullin, J.I.: Gear Isolation for Reducing Noise in Single Rotor Helicopters, Paper F3, Symposium on Internal Noise in Helicopters, Univ. of Southampton, 1979.

END

DATE

FILMED

OCT 22 1984